

OXYGEN PERMEABILITY PROPERTIES OF ZWITTERIONIC POLYMER COATINGS

OXYGEN PERMEABILITY PROPERTIES OF ZWITTERIONIC POLYMER
POLYTETRAFLUOROETHYLENE COATINGS FOR LONG-TERM SURFACE WATER
MONITORING WITH INDIGENOUS COMMUNITIES

By ERIK FRÉCHETTE, B.Eng.Biosci.

A Thesis Submitted to the School of Graduate Studies in Partial Fulfilment of the Requirements
for the Degree Master of Applied Science

McMaster University © Copyright by Erik Fréchette, December 2023

MASTER OF APPLIED SCIENCE (2023)
Chemical Engineering, McMaster University
1280 Main St W, Hamilton, Ontario L8S 4L7

TITLE: Oxygen Permeability Properties of Zwitterionic Polymer Coatings

Oxygen Permeability Properties of Zwitterionic Polymer Polytetrafluoroethylene Coatings for Long-Term Dissolved Oxygen Surface Water Monitoring with Indigenous Communities

AUTHOR: Erik Fréchette
B.Eng.Biosci. (McMaster University, Canada)

SUPERVISOR: Dr. Charles-François de Lannoy

NUMBER OF PAGES: xiii, 142

Abstract

Indigenous communities in Canada have long suffered from poor water security due to a combination of political, environmental, and social factors. Concerns regarding the health of community waters in the Six Nations of the Grand River reserve prompted the desire for a solution which provided a qualitative assessment of these waters. A distributed network of water quality monitoring stations (WQMSs) measuring five common water quality parameters was installed along the McKenzie Creek around an area the community found to need monitoring. Since monitoring any aquatic environment leads to the attachment of microorganisms and macromolecules to instrumentation, which can disrupt the flow of analyte, it is essential to reduce these foulants to prevent sensor signal bias. However, some antifouling (AF) coatings can reduce transmembrane analyte flow. As such, a series of zwitterionic polymer coatings was developed to assess the permeability of oxygen through a dissolved oxygen (DO) sensor membrane to determine its data collection integrity. Zwitterionic coatings were found to slow the oxygen transfer rate significantly but without compromising the rapidity of field readouts. WQMSs were able to collect and relay live data, but errors in accuracy and consistency need to be fixed before more widespread implementation of these systems can be adopted. Finally, a framework was developed to guide scientists and engineers researching Indigenous lands and resources, drawing from existing literature and firsthand experiences collaborating with Indigenous communities.

Acknowledgements

I have been extremely fortunate to have participated in such a unique project combining such diverse academic disciplines. Support for this project has come from many sources, and I can only list some of the many who have all dearly touched my life in their own distinct ways.

First and foremost, I'd like to thank Dr. Charles de Lannoy. Charles has been a tremendous influence in furthering my personal and professional growth, and it is thanks to his guidance, commitment, trust, and, above all, patience, I have been able to make it as far as I have. I am incredibly thankful for him keeping me on track amid a constantly evolving project despite the many fascinating research side paths that always seemed to emerge. Thank you to Dawn Martin-Hill for her instrumental work leading the Ohneganos Ohnegahde:gyo team, without whose efforts, none of this project would have been possible. Thank you to Rod Whitlowe for his intimate knowledge and tireless commitment to providing community resources and for his willingness to spend long hours in the bush, in rain or shine, in sweltering heat and near-freezing temperatures, and doing maintenance on these pesky sensor boxes. Thank you to Chris Marin for his commitment to education and for mobilizing students from STEAM Academy to become stewards of the nature found in their communities. Thank you to the Six Nations of the Grand River for your trust in allowing me to build a relationship with your community.

Thank you to those at the CCEM, notably Chris Butcher and Jhoynner Martinez, for their help in utilizing the JEOL 7000 microscope. Thank you to João Firmino and Mouhanad Babi for their support in using the various CALM facilities, especially the Atomic Force Microscope. Thank you to Peter Brodersen at OCCAM for his help with XPS characterization and Xiaodong Hu from Element for his help in gas permeability characterization. Thanks to Heera Marway and Afshin Abrishamkar for further assistance in membrane characterization.

Thank you to Emil Sekerinski and Tianyu Zhou for their immense contributions throughout the development of the WQMS electronics. Thanks also to Varshan Srivasanthakumar for his preliminary work on configuring the devices. Thank you to Paul Gatt, Justin Bernar, and Mike Clarke for their help designing and building the WQMSs. Thanks to Tim Stephens for his guidance throughout my time as a teaching assistant for the third- and fourth-year lab courses and for his assistance in providing equipment that made installing the WQMSs so much easier. Thank you to Jake Nease for his direction in producing working MATLAB code.

Thank you to Hannah Grewal, Colin Gibson, and Sheel Ayachi, the FN research group, for your friendship and collaboration and for being there for each other as we started our research journeys in the middle of the pandemic. Thank you to members of the de Lannoy lab, Yichen Wu, Scott Laengert, Nan Zhang, Mohamed Elganzoury, Abdelrahman Awad Babiker, Nathan Mullins, and also those outside the lab including Todd Hoare, Sarah Dickson-Anderson, Marta Princz, Ryan Larue, Abhishek Premachandra, Jamie Rose and Nahieli Preciado, for their advice and support throughout the scope of my lab and fieldwork. Thanks also to Lina Liu, Hyejin Lee, Mohamad Amin Halali, Parviz Shahbazikhah, Riccardo Checchetto, and Zeynel Bayindir for their help on work that ultimately did not form part of this manuscript. Thank you to Brandon Theriault and Raimo Veniläinen for their help as I was finishing writing this thesis. Finally, thank you to my parents, sister, mummu, and pappa for being my biggest supporters.

Table of Contents

Abstract.....	iii
Acknowledgements.....	iv
Table of Contents.....	vi
List of Figures.....	viii
List of Tables.....	xi
Abbreviations and Terms.....	xii
1. Literature Review.....	1
1.1. Water Security.....	1
1.1.1. Water Security in Indigenous Communities.....	2
1.2. Indigenous Peoples in Canada.....	3
1.2.1. Terminology.....	4
1.2.2. Indigenous-Academic Relations.....	4
1.2.3. Case Study Community: Six Nations of the Grand River.....	5
1.3. Water Management at SNGR.....	6
1.4. Surface Water Monitoring.....	8
1.4.1. Water Temperature.....	9
1.4.2. Dissolved Oxygen.....	9
1.4.3. pH.....	9
1.4.4. Conductivity.....	10
1.4.5. Turbidity.....	10
1.5. Dissolved Oxygen Monitoring.....	11
1.5.1. Galvanic DO Sensors.....	11
1.6. Membrane Technologies.....	12
1.6.1. Porous Membranes.....	12
1.6.2. Dense Membranes.....	12
1.7. Biofouling.....	14
1.8. Antifouling Strategies.....	16
1.8.1. Zwitterionic Coatings.....	18
1.9. Thesis Outline.....	20
1.10. References.....	21
2. Gas Diffusion Properties of Zwitterionized Galvanic Dissolved Oxygen Sensor Membranes.....	29

2.1.	Introduction.....	29
2.2.	Materials and Methods.....	31
2.2.1.	Surface Preparation.....	31
2.2.2.	Physical Characterization Techniques	35
2.2.3.	Chemical Characterization Techniques.....	36
2.2.4.	Oxygen Permeability Techniques	37
2.3.	Results and Discussion	41
2.3.1.	Surface Preparation.....	41
2.3.2.	Surface Hydrophilicity.....	42
2.3.3.	Scanning Electron Microscopy	44
2.3.4.	Atomic Force Microscopy	45
2.3.5.	Elemental Analysis	48
2.3.6.	X-Ray Photoelectron Spectroscopy	51
2.3.7.	Oxygen Permeability Tests	60
2.3.8.	Simulating Oxygen Transfer.....	70
2.4.	Conclusions.....	71
2.5.	References.....	72
3.	Real-time Water Quality Monitoring Stations (WQMSs)	76
3.1.	Introduction.....	76
3.2.	Materials & Methods	77
3.2.1.	Live Monitoring WQMSs	77
3.2.2.	Spot Sampling.....	79
3.2.3.	Sample Site Selection and Monitoring.....	81
3.3.	Results and Discussion	81
3.3.1.	WQMS Troubleshooting.....	81
3.3.2.	Water Temperature	87
3.3.3.	Dissolved Oxygen.....	89
3.3.4.	pH.....	91
3.3.5.	Conductivity.....	93
3.3.6.	Turbidity	94
3.3.7.	Chemical Oxygen Demand & Total Organic Carbon	96
3.3.8.	Cost	97
3.4.	Conclusions.....	99

3.5.	References.....	100
4.	Co-Creative Practices in Reconciling Traditional Indigenous Knowledge and Western Science	103
4.1.	Introduction.....	103
4.2.	Methods: Co-Creative Framework.....	104
4.2.1.	Wheel 1: Core Principles	106
4.3.	Results: Implementing the Co-Creative Framework.....	108
4.3.1.	Community Engagement.....	108
4.3.2.	Project Design.....	112
4.3.3.	Data Collection & Analysis	114
4.3.4.	Dissemination	117
4.4.	Discussion: Reflecting on Implementing the Framework.....	120
4.5.	Conclusions.....	121
4.6.	References.....	122
5.	Conclusions and Recommendations	124
5.1.	References.....	126
Appendix A: Supplemental Information.....		127
Appendix A.1: Chapter 2 Supplementary Information.....		127
Appendix A.2: Chapter 3 Supplementary Information.....		138
Appendix A.3: Appendix References		142

List of Figures

Figure 1. McKenzie Creek and Boston Creek watersheds, including water treatment sites and locations of previously collected survey data [46-48]. FN boundary data collected from [49]. Hydrology layers processed from [50]. Created in ArcGIS Pro 3.1.0.	8
Figure 2. Foulants such as macromolecules, bacteria, diatoms, or even larger organisms such as mussels attach to sensors, preventing accurate data transmission and inducing data drift.	16
Figure 3. Non-toxic AF coatings usually seek to maximize or minimize the water contact angle, θ , depending on the application. The surface energies (γ) between solid, liquid, and vapour states can be calculated using $\gamma_{sv} = \gamma_{sl} + \gamma_{lv}\cos\theta$ [83].	18
Figure 4. AF capabilities of the PGS copolymer help reduce foulant attachment via a thick hydration layer.	34
Figure 5. Primary relevant molecules in the formation of AF coatings on PTFE.....	34
Figure 6. LOC test prior to first use of the device, showing OP tank (no dye) and OR tank (pink dye). The dye test was performed to confirm no passage of micromolecules through the membrane.	39
Figure 7. Selected coating WCA measurements. A single typical measurement is shown here.	43

Figure 8. FESEM micrographs of the bare PTFE membrane and each of the nine coated samples. Images were taken at 3000x magnification. Scale bar represents 10 μm 44

Figure 9. AFM scans on select coating surfaces: a) +PDA b) +PDA/PEI c) +Z10-Mid. d) Average coating thicknesses of all nine polymer coatings. Error bars are the standard deviation of height differences across three cross sections, averaged across three membrane samples (nine total cross sections per data point). 46

Figure 10. Elemental composition of samples by mass percent listed for nitrogen, carbon, hydrogen, and sulfur. Error bars represent standard deviation. 49

Figure 11. Carbon 1s spectra of +PDA, +PDA/PEI, and +PDA/PEI+SBMA samples. 55

Figure 12. Normalized carbon 1s spectra of ZL coatings. A representative deconvolution is shown for the +Z20-24hr sample. Inconsistent peaks around 292 eV represent C-F bonds from underlying PTFE. 56

Figure 13. Fluorine F 1s from bare PTFE showing a single C-F₂ peak, and +PDA+PGS showing a C-F₂ peak and a C-F₂ peak with non-bonding interactions with other highly electronegative atoms. 57

Figure 14. Normalized nitrogen 1s spectra showing a characteristic SBMA signal for ZL coatings. A representative deconvolution is shown for the +Z20-24hr sample. 58

Figure 15. Normalized oxygen 1s spectra showing a characteristic SBMA signal for ZL coatings. A representative deconvolution is shown for the PGS powder sample. 60

Figure 16. Profile of a typical LOC test for bare PTFE, showing the initially OR tank (black) and OP tank (red). 61

Figure 17. LOC tests for three coating samples, namely PTFE (blue), +PDA (red), and +Z10-24hr (green), taken at averaged 10-minute intervals. Shaded regions represent the standard deviation of three trials. 64

Figure 18. Permeability coefficients as calculated via Equation (8). Uncertainty measurements represent standard deviations of triplicate experiments. 66

Figure 19. 2D and 3D models of diffusion profiles across a theoretical coating profile consisting of a 10 μm -thick PTFE substrate, a 2 μm -thick GL, a 1 μm -thick ZL, and a 2 μm -thick FL. 70

Figure 20. A finalized interior of one of the WQMSs (a), pinging the WQMSs to ensure proper functionality before deployment (b), deploying a WQMS (c), community partner retrieving a WQMS with a dinghy (d), website portal for accessing real-time water quality measurements (e). 85

Figure 21. Cell tower locations in the vicinity of SNGR, July 2021. Blue markers represent Bell Canada towers, while towers marked in red are owned by Rogers Communications [10]. Red dots indicate the initial WQMS installation sites. 86

Figure 22. Locations of gateway 3G signal test sites (green, yellow, red squares) and locations at which WQMS were ultimately installed during this study (blue circles). Created in ArcGIS Pro 3.1.0. 87

Figure 23. Water temperature data obtained from McKenzie Creek WQMS at points M4 (●), M4.5 (●), and M5 (●). Spot data obtained from the same locations M4 (◆), M4.5 (◆), and M5 (◆) are also shown, along with spot data from 2010-2021 (◆) taken from the PWQMN McKenzie Creek site. Uncertainties are standard deviations for triplicate measurements. 88

Figure 24. DO data obtained from McKenzie Creek WQMS at points M4 (●), M4.5 (●), and M5 (●). Spot data obtained from the same locations M4 (◆), M4.5 (◆), and M5 (◆) are also shown, along with spot data from 2010-2021 (◆) taken from the PWQMN McKenzie Creek site. Uncertainties are standard deviations for triplicate measurements. 90

Figure 25. Abrasions on a DO membrane fouled for two weeks in the McKenzie Creek between October 6 and 20, 2022. 91

Figure 26. pH data obtained from McKenzie Creek WQMS at points M4 (●), M4.5 (●), and M5 (●). Spot data obtained from the same locations M4 (◆), M4.5 (◆), and M5 (◆) are also shown, along with spot data from 2010-2021 (◆) taken from the PWQMN McKenzie Creek site. Uncertainties are standard deviations for triplicate measurements.	92
Figure 27. Conductivity data obtained from McKenzie Creek WQMS at points M4 (●), M4.5 (●), and M5 (●). Spot data obtained from the same locations M4 (◆), M4.5 (◆), and M5 (◆) are also shown, along with spot data from 2010-2021 (◆) taken from the PWQMN McKenzie Creek site. Uncertainties are standard deviations for triplicate measurements.	94
Figure 28. Turbidity data obtained from McKenzie Creek WQMS at points M4 (●), M4.5 (●), and M5 (●). Spot data obtained from the same locations M4 (◆), M4.5 (◆), and M5 (◆) are also shown, along with spot data from 2010-2021 (◆) taken from the PWQMN McKenzie Creek site. b) shows lower magnitude data at a different scale for clarity. Uncertainties are standard deviations for triplicate measurements.	95
Figure 29. COD (a) and TOC (b) data obtained from sample sites M4, M4.5, and M5. Uncertainty is calculated as the standard deviation of two COD samples. No uncertainty is available for TOC.	97
Figure 30. The developed co-creative framework.	106
Figure 31. Pamphlet sent out to alert community members of the upcoming activities on the McKenzie Creek in the first year of WQMS operation.	112
Figure 32. Students and staff members from STEAM, as well as SNGR community partners, in various stages of setting up a WQMS (a-c), STEAM staff (community partner Chris Martin) and students learning about the workings of a WQMS (d), selfie with community partner Rod Whitlow following successful installation of a WQMS (e).	116
Figure A.1. Triplicate AFM scans for all coated samples.	127
Figure A.2. Example OCT scan of an uncoated sample (left) with +Foul60 (right).	128
Figure A.3. Mass % Normalized to C.	128
Figure A.4. Mol composition as normalized to carbon.	129
Figure A.5. Normalized XPS survey spectra for all samples.	130
Figure A.6. N 1s spectra of +PDA, +PDA/PEI, +PDA/PEI+SBMA, and PGS powder.	133
Figure A.7. O 1s spectra of +PDA, +PDA/PEI, +PDA+PGS samples.	133
Figure A.8. Typical presentations of sulfur 2p and silicon 2p.	134
Figure A.9. Additional individual LOC tests not shown in Figure 17: a) +Foul14, b) +Foul60, c) +Z10-12hr, d) +Z10-48hr, e) +Z20-24hr, f) +Foul14, g) +Foul60. Shaded area represents standard deviation of three trials.	134
Figure A.10. Concentration profiles monitoring a sudden change in DO for modified and unmodified PTFE.	135
Figure A.11. Component damage due to high humidity conditions within WQMS, high creek flow conditions which may have caused water to seep into the WQMS.	138
Figure A.12. Example DO data from site M4 over a period from November 24 to December 2, 2022 (top), with a selection of data that can be easily exported for community members of the curious public.	139
Figure A.13. PWQMN grab sample sites for conductivity, DO, pH, turbidity, and temperature from 2010-2021. McKenzie Creek samples (crossing Haldimand Road 9, MOE ID: 16018412902) are in orange and York samples (at York Bridge, MOE ID: 16018409202) are in blue [1].	140

List of Tables

Table 1. Index of characterized samples.	32
Table 2. Relative elemental percentage concentrations of bare PTFE, coated PTFE, and PGS powder samples as determined by XPS after removal of PTFE background from coated PTFE samples.	53
Table 3. Permeability (Q), diffusivity (D), and solubility coefficients (S) of oxygen through PTFE adjusted to the experimental run temperature [19]. Adjustments were made using Equation (5) and parameters from [18]. Uncertainty measurements are for the standard deviations of two measurements..	65
Table 4. Permeability, diffusion, and solubility coefficients of measured samples, as calculated via concentration models obtained from Equation (9).....	67
Table 5. Individual layer permeabilities.	70
Table 6. Price list for constructing a single WQMS.	98
Table A.1. Original relative elemental percentage concentrations of bare PTFE, coated PTFE, and PGS powder samples as determined by XPS.	129
Table A.2. Carbon XPS position data.	130
Table A.3. Fluorine XPS position data.	130
Table A.4. Nitrogen XPS position data.....	131
Table A.5. Oxygen XPS position data.	131
Table A.6. Relative percentages of carbon bonds.....	131
Table A.7. Relative percentages of fluorine bonds.....	131
Table A.8. Relative percentages of nitrogen bonds.	132
Table A.9. Relative percentages of oxygen bonds.....	132
Table A.10. Model constants for concentration profile over time in OP tanks (time in hours).....	134
Table A.11 Model constants for concentration profile over time in OR tanks (time in hours).	135
Table A.12. Gas permeation results as originally tested at 30°C.....	135
Table A.13. The following code produces the 2D and 3D concentration profiles shown in Figure 19....	135
Table A.14. E. coli and TCF data obtained from M5. * indicates RDL of 100 CFU/100mL, ** indicates RDL of 2 CFU/100mL.....	141
Table A.15. Anion data obtained from M5. * indicates RDL of 0.05 mg/L, ** indicates RDL of 0.1 mg/L.	141

Abbreviations and Terms

AANDC	Aboriginal Affairs and Northern Development Canada
AF	Anti-Fouling
AFM	Atomic Force Microscopy
AIBN	Azobisisobutyronitrile
ATRP	Atom Transfer Radical Polymerization
BE	Binding Energy
BI	Biointerfaces Institute (Hamilton, Canada)
CALM	McMaster Centre for Advanced Light Microscopy (Hamilton, Canada)
CBPR	Community Based Participatory Research
CCEM	Canadian Centre for Electron Microscopy (Hamilton, Canada)
CD	Coating Density
CFU	Colony Forming Units
COD	Chemical Oxygen Demand
D	Diffusion coefficient (m^2/s)
DA	Dopamine
DI	Deionized
DWSN	Distributed Wireless Sensor Network
EAL	Effective Attenuation Length
FESEM	Field Emission Scanning Electron Microscopy
FL	Foulant Layer
GA	Glutaraldehyde
GIS	Geographic Information System
GL	Grafting Layer
GMA	Glycidyl Methacrylate
GRCA	Grand River Conservation Authority
IC	Inorganic Carbon
IK	Indigenous Knowledge
IPA	Isopropyl alcohol
J	Diffusion flux ($\text{km}/\text{m}^2/\text{s}$)
LNM	Loose Nanofiltration Membranes
LOC	Liquid Oxygen-Carrier
MCFN	Mississaugas of the Credit First Nation (Ontario, Canada)
MOE	Ministry of the Environment
MW	Molecular Weight
OC	Organic Carbon
OCAP	Ownership, Control, Access, and Possession
OCCAM	Open Centre for the Characterization of Advanced Materials (Toronto, Canada)
OCT	Optical Coherence Tomography
OLI	Omniphobic Liquid-Infused
OP	Oxygen-Poor
OR	Oxygen-Rich
PDA	Polydopamine
PDMS	Polydimethylsiloxane
PEG	Polyethylene Glycol

PEI	Polyethylenimine
PES	Polyethersulfone
PGS	poly(GMA-co-SBMA)
PMMA	Polymethyl Methacrylate
ppO ₂	Oxygen Partial Pressure
PTFE	Polytetrafluoroethylene
PVA	Polyvinyl alcohol
PVC	Polyvinyl Chloride
PVP	Polyvinylpyrrolidone
PWQMN	Provincial Water Quality Monitoring Network
Q	Permeability coefficient (mol/m/s/Pa)
QA	Quaternary Ammonium
RDL	Relative Detection Limit
S	Solubility coefficient (mol/m ³ /Pa)
SBMA	Sulfobetaine Methacrylate
SLA	Sealed Lead Acid
SNGR	Six Nations of the Grand River (Ontario, Canada)
SNP	Six Nations Polytechnic (Ohsweken, Ontario, Canada)
STEAM	Science, Technology, Engineering, Arts, & Math Academy (Brantford, Canada)
STP	Standard Temperature and Pressure (IUPAC definition: 0°C, 100 kPa)
TBT	Tributyltin
TC	Total Carbon
TCF	Total Coliform
TEK	Traditional Ecological Knowledge
TOC	Total Organic Carbon
USEPA	United States Environmental Protection Agency
WCA	Water Contact Angle
WQMS	Water Quality Monitoring Station
WQSS	Water Quality Sampling Site
WS	Western Science
WTP	Water Treatment Plant
XPS	X-Ray Photoelectron Spectroscopy
ZL	Zwitterionic Layer

1. Literature Review

1.1. Water Security

Ensuring global water security is one of humanity's most important initiatives for the 21st century. While the previous century saw a four-fold increase in population, global water consumption has increased by a factor of seven [1]. By 2050, over 40% of the global population will live in areas affected by severe water stressor conditions [2]. Anthropogenic activities have resulted in increased pressure on aquatic ecosystems. Excessive resource consumption has led to the depletion of animal habitats, the pollution of waterways, and the depletion of groundwater reserves. Industrial discharge, agricultural runoff, and improper waste disposal introduce excessive nutrient loading into waterways, enabling the proliferation of harmful bacteria and rendering water sources undrinkable. Climate change exacerbates problems related to extreme weather events, migration, and conflict, intensifying the frequency and severity of such events and leading to resource scarcity, population displacement, and heightened competition for water resources [3].

While many large-scale technologies, such as desalination plants and membrane bioreactors, have emerged offering to reduce water strain, these technologies are expensive and energy-intensive. Thus, they can often not be relied upon to support water scarcity needs in poorer or rural communities. Local renewable sources of energy, such as geothermal, wave, or wind, may fill an energy need for some communities, but this relies on the geography of a community and cannot be used as a general solution while also requiring additional capital expenditure that the community cannot afford [4]. Existing urban treatment infrastructure has also been acknowledged as insufficient in dealing with changing climate and population dynamics [3]. Therefore, global water security issues will need to be addressed not only by technological improvements but through a comprehensive and integrated approach unique to each region, involving different

sectors, such as water resource management, agriculture, energy, and industry, as well as effective governance and policy frameworks [3].

1.1.1. Water Security in Indigenous Communities

Although Canada's freshwater reserves are among the world's largest, many Indigenous communities lack reliable means to access clean water. Drinking water advisories (DWAs) are common throughout Indigenous communities, with 70% of First Nations (FN) communities in Canada suffering from a DWA in a 10-year period [5]. A majority of these DWAs were present in communities with aged or malfunctioning infrastructure or inexperienced treatment system operators [5]. Boil water advisories are 2.5 times more prevalent in FN communities than non-FN communities, and the incidence of waterborne infections is 26 times greater in FN communities than in their non-FN counterparts [6]. Additionally, Canadians are served by provincial water regulations, while FN communities fall under federal regulations that are not legally enforceable, contributing to a fragmented water security framework [7, 8]. Health, education, and economic disparities have resulted from colonial policies giving limited control over land and water resources [9-11].

Despite a recent allocation of \$1.8 billion in 2021 for enhancing water treatment plants (WTPs), it is widely acknowledged that exclusively and singularly investing in WTPs is deemed ineffective for solving long-term water quality issues [5, 6, 12, 13]. Relying on costly urban-focused technologies like treatment plants constitutes a long-term, economically detrimental decision for predominantly rural Indigenous communities [6]. Therefore, multi-pronged approaches to improving water security, such as source water protection plans, decentralized wastewater treatment facilities, and the introduction of water-sharing agreements with nearby communities, are being incorporated into water security plans [6, 8]. Indigenous Knowledge (IK)

and Traditional Ecological Knowledge (TEK), emphasizing relationship and responsibility to care for water as a living being, are now beginning to be appreciated by Western audiences as valid epistemology that can provide crucial water security insights even in non-Indigenous contexts [12, 13]. Allowing for the promotion of IK and TEK will continue to further Western understanding of the human connection to water in both natural and built environments and promote the sovereignty and resilience of Indigenous communities in the face of changing environmental conditions.

1.2. Indigenous Peoples in Canada

According to the 2021 census, Indigenous peoples in Canada number some 1.8 million, with some 330,000 living in Indigenous communities [14, 15]. Indigenous identity is often associated with biological heritage and cultivating an enduring relationship with the land that they have long inhabited [16]. FN people are highly diverse, with widely varying cultural symbols, practices, and languages [17]. Following European contact, Indigenous sovereignty gradually diminished until the establishment of policies such as the Indian Act of 1876, which placed Indigenous peoples across Canada in a legal framework which allowed for their control by the federal government [10]. This act officially dispossessed Indigenous peoples from the vast majority of the land they had inhabited for millennia, depriving them of their identity and culture, limiting economic opportunities, restricting their movement, and forcing them into Western social paradigms [10, 18]. Arguably, the most well-known effect of the act was the establishment of Residential Schools, which removed children from their communities to schools that were deliberately underfunded, rife with disease, abuse, and neglect, in an effort to assimilate Indigenous peoples [10, 19, 20]. These policies have been widely labelled as constituting genocide [11, 19]. The Indian Act, as well as numerous other treaties signed between Indigenous nations and federal, provincial, and

territorial governments throughout the past two centuries, continue to underscore settler-Indigenous relations.

1.2.1. Terminology

In Canada, the terms Indigenous, First Peoples, or less commonly, Native American, are colloquially synonymous with Aboriginal, a legal term referring to three groups of people differentiated by the federal government under the Constitution Act of 1982 [21]. The largest group is that of the First Nations (FN). It is common but erroneous to refer to all Indigenous peoples as FN. However, these diverse peoples are grouped under the vague FN designation primarily for political reasons, as the relationship of FN peoples with the federal government is uniquely overseen by the Indian Act of 1876 [18]. The Métis, people of mixed Indigenous and European ancestry, and the Inuit, who primarily inhabit Canada's Arctic regions, comprise the other two groupings of Indigenous peoples [22, 23].

1.2.2. Indigenous-Academic Relations

Relations between Indigenous peoples and academics have been rooted in an unequal colonial power dynamic [24]. This dynamic has allowed for the development of helicopter research, or neo-colonial science, where WS practitioners enter a community to collect samples or data and leave, publishing research without the involvement of the studied community beyond minor participation [25]. This practice is not limited to Indigenous communities in Canada and is still globally prevalent, especially in developing countries [25, 26]. Studies on Indigenous peoples in Canada were conducted with white supremacist attitudes, often under the guise of 'civilizing' the populations and often without the consent of the community [27, 28]. Unethical research included the deliberate promotion of starvation and disease, theft of cultural artifacts, misuse of tissue samples and genetic information, and forced sterilization. In many instances, residential school

students were subjected to these experiments [10, 27-30]. Canadian museums additionally retain the remains of Indigenous peoples despite calls for their repatriation and reburial in the communities from which they were removed [30, 31]. This historical precedent has clearly positioned Indigenous peoples as mere objects for academic study rather than humans.

More recently, many other complaints have been levelled against researchers. Some of these include choosing research topics with little or no community benefit, producing data inaccessible to the community, interpreting data without consulting Indigenous knowledge holders, and blatantly ignoring community protocols [30, 32]. It is against this backdrop that Indigenous communities express continued skepticism against interacting with academics.

1.2.3. Case Study Community: Six Nations of the Grand River

The Six Nations of the Grand River (SNGR) is Canada's most populated FN community, with some 12,892 inhabitants as of 2019, but with 27,559 registered band members [33]. Notably, it is the only Indigenous community comprising significant populations of all six Haudenosaunee (Iroquois) nations [34]. SNGR is governed by the traditional Haudenosaunee Confederacy, as well as a federally administered Elected Council [35]. The traditional homeland of the Haudenosaunee is located in upstate New York, constituting the Seneca, Cayuga, Onondaga, Oneida, Mohawk, and later the Tuscarora nations [33, 36]. Following the British defeat in the American Revolutionary War, many Haudenosaunee were relocated to the Haldimand Tract, reserved for the Haudenosaunee along the Grand River in what is now Ontario [37]. Land transfers of this tract to settlers, the legality of which is still debated, eventually resulted in the reduction of SNGR territory to 5% of the original tract of land granted by the Haldimand Proclamation [37, 38].

1.3. Water Management at SNGR

The Grand River watershed is a source of water for about a million people, and a repository of wastewater from 30 treatment plants which collects from 600,000 people [39]. Over 95% of the watershed's population lies upstream of SNGR, including the urban centres of Kitchener-Waterloo, Guelph, Cambridge, and Brantford. Each treatment plant removes 95% of pollutants, allowing the remainder to be managed by environmental processes [39]. The watershed is managed by the Grand River Conservation Authority (GRCA). Surface water sources constitute less than 30% of the watershed's drinking water supply [40]. While upstream communities can use groundwater and surface water sources, SNGR is one of the few communities relying heavily on surface water [40]. The river has suffered from water quality stressors for over a century. Population growth and agricultural production strain the natural assimilative capacity of the river, leading to high nutrient concentrations, notably phosphorus and nitrogen [39, 40]. Water quality is further reduced with the presence of drugs and artificial sweeteners emanating from water treatment plants [41, 42]. Effluents from treatment plants have been shown to cause increased intersex characteristics and altered gut microbiome in fish [43, 44]. Because of these factors, there is a noted downstream deterioration of water quality.

SNGR operates a water treatment facility that sources its water from the Grand River but services 17% of households [35]. Nonetheless, this low coverage has been sufficient to circumvent assigning a community-wide DWA, the primary metric for assessing FN water security [5, 11]. For those not connected to the treatment facility, bottled water is a primary source of drinking water, but may also be used for most other water requirements. Cisterns are usually filled using bulk water deliveries. Wells are common, but community members are often disinclined to use them due to the water's unpleasant odour and discolouration. Some households use bleach, water

softeners, or filtration systems to treat domestic water [45]. Fauna has also been found in wells and cisterns [45]. Many of these observations are anecdotal but are otherwise consistent across various researchers who sampled wells and interacted with the community. As such, many suspect adverse health effects due to the water they consume.

The McKenzie Creek and Boston Creek are the primary Grand River tributaries on SNGR, with their subwatersheds covering 80% of the community (Figure 1). As these streams are used for both recreation and utilitarian purposes, there is concern that illegal non-point source dumping, pollution from local industries, as well as frequent effluent discharges from wastewater lagoons near the main settlement of Ohsweken are affecting water quality. Agricultural runoff in the McKenzie-Boston subwatershed has induced eutrophication, triggering algal blooms [46]. While GRCA has live monitoring stations along the Grand River which monitor water temperature, dissolved oxygen (DO), pH, conductivity, and turbidity, there is no live station on the McKenzie Creek. The Provincial Water Quality Monitoring Network (PWQMN) takes spot samples of the McKenzie Creek downstream of SNGR every one or two months using these same parameters. These substantial time gaps preclude the identification of rapid water quality changes, which may be detrimental to human health.

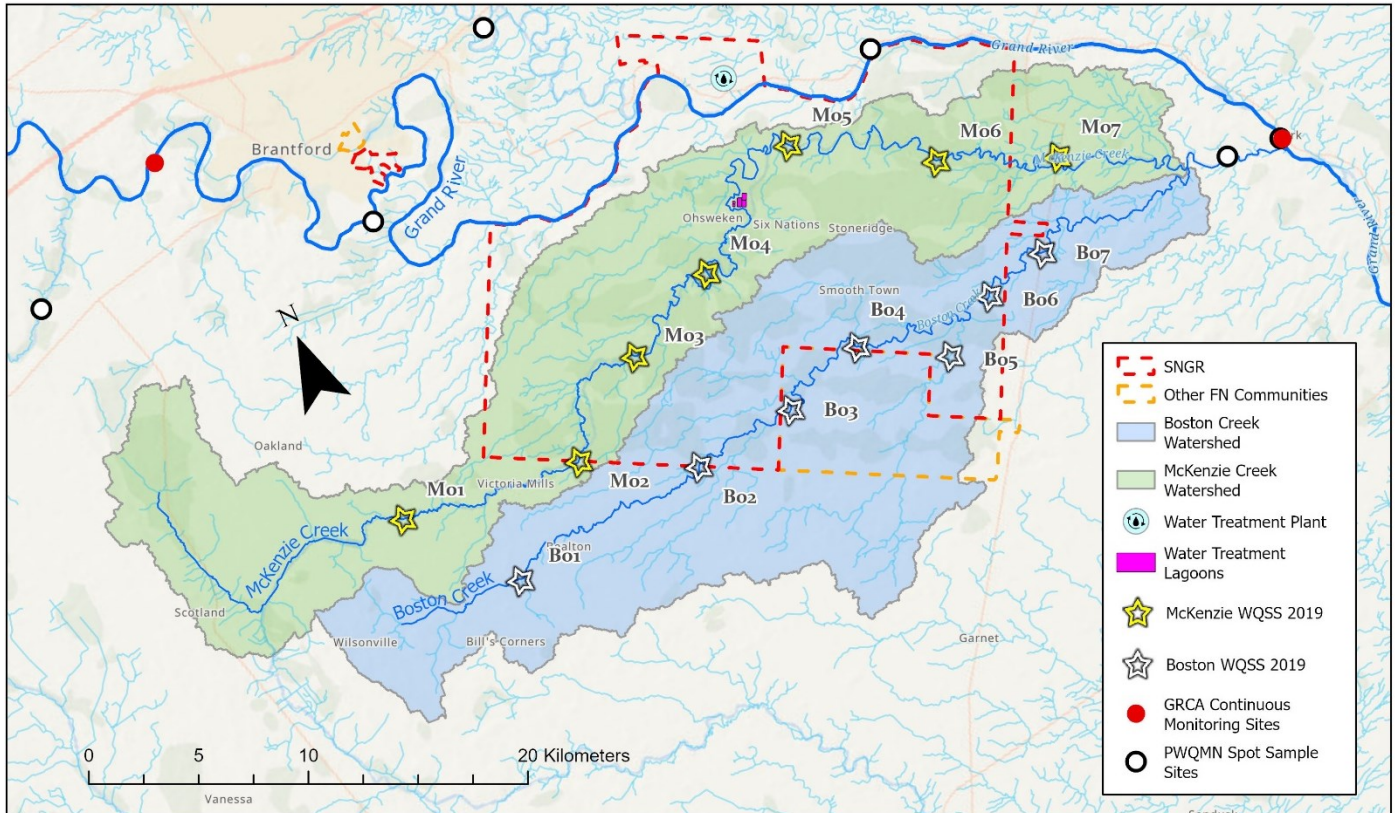


Figure 1. McKenzie Creek and Boston Creek watersheds, including water treatment sites and locations of previously collected survey data [46-48]. FN boundary data collected from [49]. Hydrology layers processed from [50]. Created in ArcGIS Pro 3.1.0.

1.4. Surface Water Monitoring

Environmental water quality monitoring typically involves laboratory-based analysis and on-site sampling, including immediate analysis or transporting samples to a laboratory for subsequent analysis. In-situ analysis allows for faster turnaround time, eliminates sample degradation, and reduces sample bias, making its use in continuous environmental monitoring solutions possible. Distributed wireless sensor networks (DWSNs) are one such real-time solution implemented for water monitoring and other applications, allowing for remote sensing with limited human impact [51-53]. A typical setup involves a dispersed series of sensor nodes which wirelessly transmit data to the closest gateway/base station. Each gateway then uploads the received data to a web server in real time [51-53].

Water quality monitoring is accomplished using a wide variety of physical, chemical, and biological parameters, helping to elucidate natural environmental dynamics or investigate anthropogenic effects on ecosystems. Several commonly used parameters are discussed below. While individual parameter deviations may not singularly signify cause for concern, deviations in multiple can be employed to identify localized waterway issues.

1.4.1. Water Temperature

Water temperature directly affects several other indicators of water quality. An increase in temperature leads to a decrease in DO, a decrease in pH, and an increase in conductivity. High turbidity can increase temperatures due to the absorption of solar radiation and subsequent heat distribution back into the aquatic environment. Changes in water temperature can affect metabolic processes, such as algal photosynthesis, the mating or migratory patterns of fish, and the uptake of toxins. The release of industrial effluent may also raise the temperature of small waterways.

1.4.2. Dissolved Oxygen

DO levels directly affect the survivability of fish and other aquatic life. DO increases with decreasing temperature and decreasing salinity. At 20°C, aquatic ecosystems with DO at 8-9 mg/L are considered healthy, while concentrations below 4 mg/L are fatal to most fish [54]. Under atmospheric conditions, DO levels reach their maximum around 14 mg/L at 0°C [55]. The predominant factors influencing DO levels are atmospheric dissolution and photosynthetic processes [55]. Eutrophication and stagnant waters lead to decreases in DO due to its consumption by bacteria and algae on the water's surface, starving marine life below.

1.4.3. pH

Normal freshwater pH readings are considered between 6.5-9 [56]. Larger diurnal pH fluctuations suggest high biodiversity [57]. pH below 6.5 can result in reduced growth and reproductive

abilities, while pH below 5 is fatal to much flora and fauna. It can also cause irritation to eyes, skin, and mucosal membranes in humans. Low pH may be caused naturally due to increases in temperature, geological factors (notably local carbonate or sulfate deposits), or the decomposition of organic matter. Anthropogenic causes of low pH include effluents from mines, WTPs, and agricultural sites [56, 57]. pH above 9 is less common but may be influenced by proximity to coastal waters, basic effluents, or geological factors [56, 57].

1.4.4. Conductivity

Conductivity, or specific conductance, is directly correlated with an increase of dissolved ions in a body of water, most commonly inorganics such as calcium, magnesium, sodium, potassium, carbonates, sulfates, and chloride [58]. Freshwater conductivities range from 50-1500 $\mu\text{S}/\text{cm}$, but the conductivity can increase in areas with hard water, which contain a high concentration of minerals [58, 59]. Similarly, increased conductivity also lowers DO levels [60]. Soil composition influences conductivity, with higher clay content in riverbeds leading to increased conductivity relative to denser and less permeable substrates [61].

1.4.5. Turbidity

Turbidity is a measurement of the optical clarity of water. Suspended and dissolved solids both affect turbidity measurements and can include sand, silt, microorganisms, or dyes [62, 63]. Rivers usually have higher turbidity than lakes as their high flow enables them to transport larger particles. High turbidity may be caused by natural silty riverine substrates, such as clay, but may also be indicative of agricultural nutrient runoff, especially nitrates or phosphates. Increased runoff, and thereby increased nitrates and phosphates, cause bacterial proliferation, which leads to increased turbidity. Increased turbidity can smother fish and their young, reduce photosynthesis, encourage

excessive microbial growth, allow for the further dispersion of contaminants, and even reduce the effectiveness of WTPs [5, 62].

1.5. Dissolved Oxygen Monitoring

DO sensors can be divided into optical and electrochemical sensors. Optical DO sensors measure the change in luminescence of a dye coating on their membrane, which reduces in response to increased DO concentration [64]. Optical sensors exhibit little data drift and require less maintenance than electrochemical sensors. Electrochemical sensors can be further divided into polarographic and galvanic varieties. Polarographic sensors operate via oxygen reduction through a pre-polarized cathode after passing through an oxygen-permeable membrane. As such, operating the instrument requires a warm-up period which may take up to an hour before use. While more accurate, both optical and polarographic sensors are much more expensive and have much greater power requirements when compared to galvanic sensors.

1.5.1. Galvanic DO Sensors

Galvanic DO sensors, also known as Clarke electrodes, comprise an electrolyte chamber housing an anode and a cathode, with the electrolyte chamber sealed from the external environment by an oxygen-permeable membrane. Oxygen passes through the membrane, where it is reduced on the cathode according to the following equation:



The hydroxide ions react with a monovalent halide salt electrolyte, the product of which reacts at the anode [65]. The electron density is directly proportional to the amount of DO in the bulk fluid, converting measured current to DO concentration. A membrane is required to regulate the diffusion of oxygen to the cathode. While other gases can permeate the PTFE membrane, their presence is not observed in significant quantities, except for nitrogen, which necessitates

considerable activation energy to outcompete the oxygen reduction reaction. PTFE is used due to its excellent chemical and mechanical strength, though it has a moderate response time compared to high density polyethylene (HDPE), another commonly used DO membrane material. As the electrochemical reduction depletes the cathode of its local oxygen supply, proper sensor functioning requires some bulk fluid current to ensure a constant oxygen flow to the sensor. Membranes must usually be replaced within one year of use.

1.6. Membrane Technologies

1.6.1. Porous Membranes

Porous membranes have interconnected pores or channels to allow the passage of specific molecules based on their size, charge, or other properties. These membranes are commonly categorized as microfiltration having the largest pore size (pores on the order of 100 nm – 1 µm), followed by ultrafiltration (pores on the order of 5 – 100 nm), nanofiltration (pores on the order of 1 – 10 nm), and finally, reverse osmosis (a non-porous dense membrane) [66]. These membranes provide a great range of separation capabilities but a less effective physical barrier than dense membranes, especially in gas separation.

1.6.2. Dense Membranes

Dense membranes do not contain any visible pore structure. Dense membranes are not permeable to most substances, as matter passes solely via diffusion and solubility mechanisms. As such, dense membranes can provide a greater level of selectivity and can act as more effective barriers compared to porous membranes. Mass transfer is most commonly modelled using solution-diffusion [67]. The ease at which molecules pass through a membrane is known as membrane permeability and can be generally calculated by Equation (2):

$$Q = DS \quad (2)$$

where Q is the membrane permeability coefficient (in mol/m/s/Pa), D is the diffusion coefficient (in m²/s), and S is the gas solubility coefficient (in mol/m³/Pa) [68, 69]. D is likened to the ease by which material travels through the bulk of the membrane, while S measures the ease of adsorption and desorption of material to and from the membrane's surface. These mass transfer parameters are commonly found by gas permeation experiments, as outlined in [70]. Q is determined by Equation (3):

$$Q = \frac{V_c * d}{R * T * A * p_h} \frac{dp}{dt} \quad (3)$$

where V_c is the volume of the low-pressure side of the test cell, d is the membrane thickness in m, R is the gas constant at 8.314 J/mol/K, T is the temperature in K, A is the membrane area in m², p_h is the pressure in the high-pressure cell in Pa, and dp/dt is the rate of pressure change in the low-pressure cell, in Pa/s. Signal dead time, the time between the occurrence of a detection event and the time at which the sensor processes it, can be used to calculate D :

$$D = \frac{d^2}{6\theta} \quad (4)$$

where d is the membrane thickness (in m), and θ is the dead time (in s) [68, 70, 71]. Clarke electrodes have a short dead time, usually measured in seconds.

According to the Arrhenius equation, all three mass transfer parameters in Equation (2) are highly dependent on temperature [68]. Thus, for example, the correction factor for Q is:

$$Q = Q_0 \exp\left(-\frac{\Delta E_q}{RT}\right) \quad (5)$$

where Q_0 is the reference permeability at STP, denoted by IUPAC to be at 0°C and 100 kPa [72], and ΔE_q is the activation energy of permeability in J/mol. This equation can also be expanded to D and S by replacing Q_0 with D_0 and Q^*H_0 (H_0 being the standard enthalpy), respectively, and

ΔE_q with ΔE_d and ΔH_s (the enthalpy of solution), respectively. Individual permeabilities can be calculated from the overall permeability using:

$$\frac{1}{Q} = \sum_{i=1}^n \frac{d_i}{Q_i} \quad (6)$$

where n is the number of layers, and d_i and Q_i are thicknesses and permeabilities for the i th layers [68].

Fick's laws govern the functionality of dense membranes, the first of which states that the solute flux (J , in $\text{kg}/\text{m}^2/\text{s}$) is proportional to the diffusion coefficient of the solute through the membrane (D , in m^2/s), and the concentration difference (dc , in kg/m^3) over the thickness of the membrane (dx , in m), as per Equation (7) [67-69]:

$$J = -D \frac{dc}{dx} \quad (7)$$

This relationship applies to diffusion across dense membranes made of a single uniform material but can also be expanded to model the overall flux of multilayered membranes. Near atmospheric pressures, dissolved gas concentration is directly related to the partial pressure of that gas in the adjacent atmosphere, according to Henry's Law [69]. Similarly, S is dependent on partial pressure, while D is independent [69].

1.7. Biofouling

Biofouling refers to the undesirable colonization of solid surfaces by biological agents in aquatic media. Adding nearly any solid object to a liquid biotic environment will result in the attachment of foulants, as shown in Figure 2. Biofouling is pervasive across many industries, such as shipping, aquaculture, power generation, water treatment, and environmental monitoring. Fouling is estimated to cost tens to hundreds of billions of US dollars to the global shipping industry alone [73, 74]. For example, fouling on maritime vessels leads to increased hull roughness, causing

greater fuel consumption and greenhouse gas emissions. Fouling also accelerates corrosion or loss of structural integrity, increasing maintenance costs [74]. Invasive species transplanted through biofouling, such as quagga and zebra mussels in the Great Lakes, have further exacerbated environmental damage by destroying local fish populations and causing wide fluctuations in water quality [75]. Fouling alters instrument sensitivity, leading to reduced data reliability caused by signal drift and is estimated to be the single largest factor affecting their upkeep [65, 74, 76].

The mechanisms of biofouling are complex and traditionally described as occurring in a series of sequential stages but can also occur simultaneously. Initiated by ionic concentration polarization, a conditioning film consisting of carbohydrates, proteins, and other macromolecules is formed within minutes of immersion. This film provides both an electrostatic and nutritional attraction for succeeding biotic foulants. Bacteria then attach to the surface and begin to cement their presence with the secretion of an extracellular matrix. This denser biofilm offers protection from predation and a greater robustness against changing environmental conditions. Finally, larger foulants such as molluscs and macroalgae may colonize the space within weeks or months [73, 74, 76, 77]. As such, mature biofilms are more challenging to remove than freshly attached organisms. Apart from local biotic populations, the rapidity and severity of foulant accumulation are dependent on environmental factors including temperature, pH, DO, nutrient concentration, and marine currents [78].

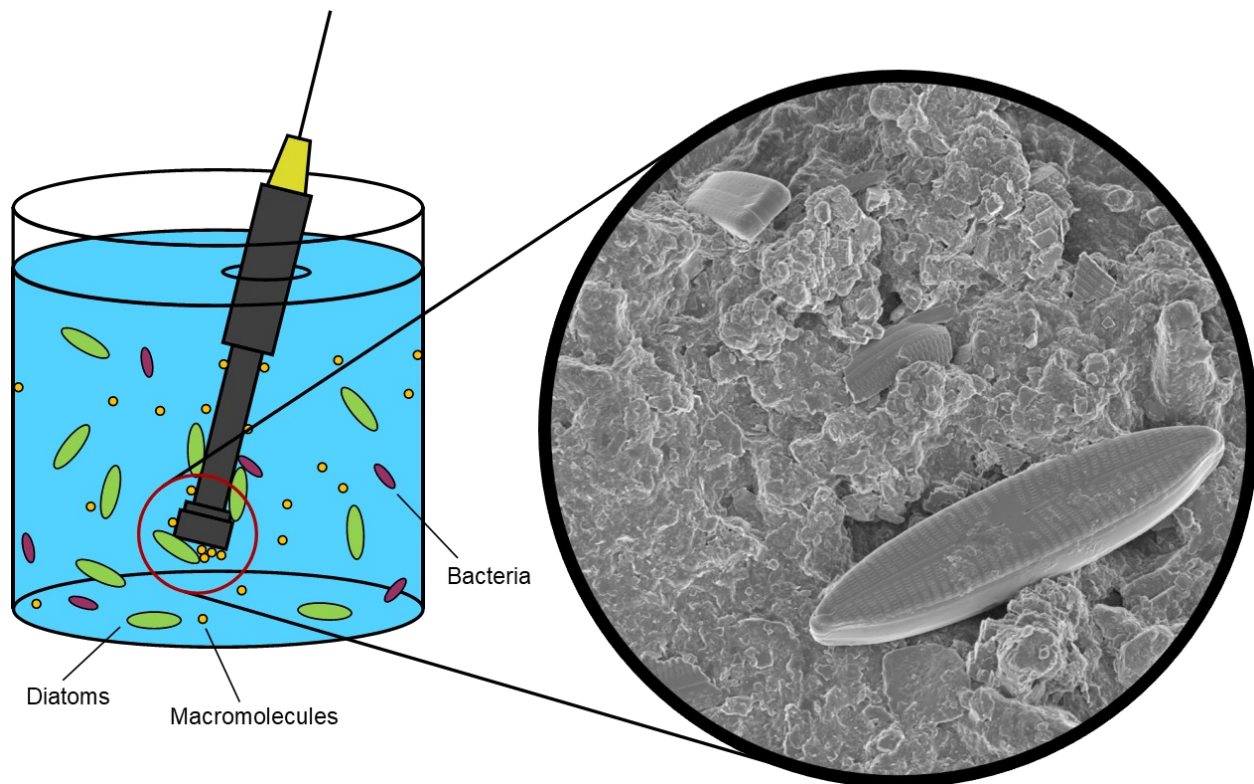


Figure 2. Foullants such as macromolecules, bacteria, diatoms, or even larger organisms such as mussels attach to sensors, preventing accurate data transmission and inducing data drift.

1.8. Antifouling Strategies

Antifouling (AF) agents have been used for millennia and have included pitch, tar, wax, and heavy metals and their associated paints (notably copper, arsenic, and lead) [77, 79]. The utilization of tributyltin (TBT) in the mid-20th century was revolutionary for AF coatings as it was cheap to produce and lasted up to five times longer than other methods. Still, its broad-spectrum biocidal characteristics resulted in its banning as an AF agent [74, 77, 79]. This resulted in a reemergence of copper-based paints, offering a comparatively reduced toxicity [80]. However, implementing biocidal AF solutions is difficult as it requires navigating a delicate balance between their biocidal potency, sufficient to deter adhesion from over 4,000 recorded foulant species in biofilms, and minimizing potential harm to non-attached local biota [73]. These challenges have prompted increased interest in the development of non-toxic AF coatings.

Non-toxic AF coatings can be divided into fouling-release and fouling-resistant coatings. Fouling-release coatings are characterized by superhydrophobicity and function by lowering the surface energy of the surface for easy removal of foulants by convection or agitation (hence the material is fouled yet quickly released) [77]. These may also rely on specialized surface topographies to resist fouling [81]. Fouling-resistant coatings are usually superhydrophilic and work by preventing fouling entirely due to the creation of a wet and slippery layer at the surface interface [82]. Many plants and animals have been the source of inspiration for antistick and self-cleaning coatings. Arguably, the most notable is the “Lotus Effect” derived from lotus leaves, where microscopic ridges and a waxy surface aid in creating a superhydrophobic surface by maintaining the surface tension of water droplets, allowing them to roll easily from the plant [83]. The *Nepenthes* pitcher plant, whose leaves have a unique microtextured liquid-infused surface, can exhibit both superhydrophobic and superoleophobic properties. This distinct biology has single-handedly inspired a field of antistick technology known as slippery liquid-infused porous surfaces (SLIPS) [82, 83]. AF surface topologies on sharkskin have also inspired several fouling-release coatings [81].

For AF to be viable, the change in Gibbs free energy of a potential foulant to the surface must be positive, as such an attachment will be energetically unfavourable, as described in Figure 3. Morphology is one of many important considerations when developing non-toxic AF solutions. Patterned morphologies may reduce adhesion, while nonpatterned rough surfaces may increase it [84]. Many coatings work better when thicker, but thicker coatings may impede the passage of solutes [85]. The enhancement in coating performance can be linked to the accumulation of foulant, as greater foulant build-up results in increased ease of removal through agitation due to enhanced inertial effects. Coatings prepared for environmental monitoring applications may fare poorly in

biological applications. For example, coatings prepared in environmental field tests exhibit a notable reduction in AF efficacy compared to laboratory assessments [86, 87]. Hydrophilic materials have been noted to be more effective in reducing macromolecule fouling [88]. Silicon polymers and fluoropolymers, such as polydimethylsiloxane (PDMS) and PTFE, are common synthetic materials used as foul-release coatings [86, 87, 89, 90]. Fouling-resistant coatings have included the use of polyethylene glycol (PEG), polyvinyl alcohol (PVA), and zwitterions [91-93].

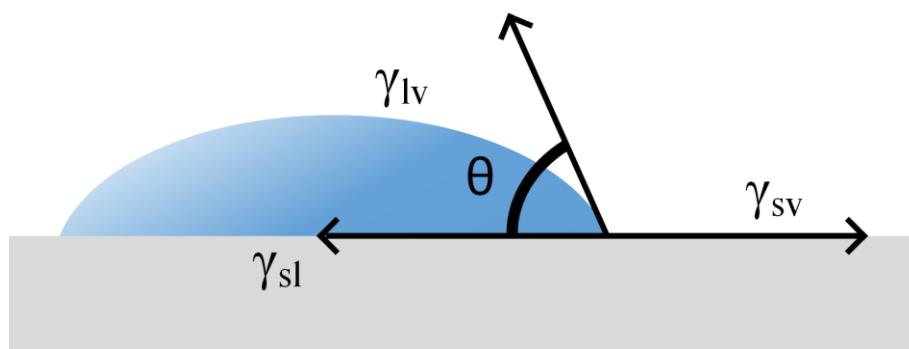


Figure 3. Non-toxic AF coatings usually seek to maximize or minimize the water contact angle, θ , depending on the application. The surface energies (γ) between solid, liquid, and vapour states can be calculated using $\gamma_{sv} = \gamma_{sl} + \gamma_{lv}\cos\theta$ [83].

1.8.1. Zwitterionic Coatings

Zwitterions are molecules which exhibit an equal number of positive and negatively charged moieties, rendering a molecule with an overall neutral charge [94]. Zwitterions are fouling-resistant materials that work by creating a thick hydration shell due to their polar moieties. Consequently, foulants are thermodynamically disinclined to approach the zwitterionized surface [74, 95]. This same mechanic also increases water retention at the coating surface. Betaines are a zwitterion category characterized by a quaternary ammonium cation and, as such, cannot isomerize into a charge-neutral molecule [96]. Betaines are naturally abundant in both prokaryotes and eukaryotes, where they aid in water retention to mitigate the effects of environmental stressors [96]. Some non-zwitterionic molecules, such as amino acids, may become zwitterions due to

changes in environmental conditions, notably pH [97, 98]. Zwitterionic polymers are often classified according to their anionic functional group backbone, with carboxybetaines, phosphobetaines, and sulfobetaines representing the most used zwitterions in coatings and hydrogels [92, 99, 100].

Zwitterions show great promise in a wide array of emerging technologies. Zwitterion AF research has been examined in a variety of technologies, including in membranes and desalination devices [101-103], drug delivery vehicles [104, 105], pollutant adsorption [106], orthopedic implants [84] or devices such as in catheters [107], sensors [108], contact and intraocular lenses [109, 110], and in firefighting [111] and marine industries [74, 112]. Zwitterions have been noted for their low cytotoxicity [105]. The hydrophilicity of zwitterions makes them hygroscopic, which can be helpful in self-healing applications, further preventing substrate damage [92]. However, this is less helpful when good mechanical properties are desired, as introducing and trapping microorganisms and macromolecules to the substrate may result in their proliferation, causing damage or loss of function of the coating [92].

Zwitterionic polymer grafts have been produced by various methods, such as atom-transfer radical polymerization (ATRP), UV-initiated radical polymerization, addition fragmentation chain transfer, and click chemistry [103, 113, 114]. Zwitterions have also been introduced directly into hydrophobic surfaces to improve their hydrophilicity [88].

Zwitterions may need scaffolding when attaching to their substrates, also known as a tie-coat [77]. Polydopamine (PDA) has been extensively studied as a zwitterionic tie-coat. Derived from the catechol secretions of mussels, it was first reported in 2007 and is noted for its adhesive abilities, chemical stability, simplicity of use, versatility, and good secondary activity [89, 115]. PDA attaches to surfaces using a variety of interactions, including covalent and hydrogen bonds,

but the precise nature of its aggregation remains controversial [116, 117]. Polyethylenimine (PEI) has also been shown to improve adhesion, and like PDA, both are known for being environmentally friendly [118, 119]. PDA/PEI scaffolding complexes can be used on a wide array of surfaces with little acknowledgement of the surface's initial chemistry [120]. This is crucial for grafting zwitterions, as the mismatch between the hydrophilicity of zwitterions and the substrates onto which they are coated can result in coating removal [94].

1.9. Thesis Outline

The first chapter presents an overview of the three main areas of study, as expanded upon in Chapters 2 to 4. The second chapter focuses on fabricating and characterizing a series of zwitterionic AF coatings. Apart from physical and chemical characterizations, mass transfer properties of oxygen through dense zwitterionized PTFE membranes were studied to gauge the effectiveness of DO transfer during water quality parameter monitoring in real surface waters. Using these parameters, a model was developed for the passage of oxygen through bare PTFE, as well as PTFE coated in PDA/PEI, zwitterion copolymer (PGS), and foulant layers. The third chapter focuses on designing, fabricating, and using a series of WQMSs for dissemination on the McKenzie-Boston subwatershed in the SNGR community. The fourth chapter examines a framework created for scientists and engineers to guide natural sciences research in partnership with Indigenous communities. It provides examples of the framework in action by relating examples from the co-creation of WQMSs with SNGR. The final chapter summarizes the contributions and conclusions presented in this work and reflects on future research directions.

1.10. References

- [1] U. N. D. Programme, "Human Development Report," Palgrave Macmillan, New York, NY, 2006.
- [2] B. P. F. Braga, "Preface II," in *Global Water Security: Lessons Learnt and Long-Term Implications*, W. W. Council Ed.: Springer, 2018, ch. xi.
- [3] J. G. Hering, T. D. Waite, R. G. Luthy, J. E. Drewes, and D. L. Sedlak, "A changing framework for urban water systems," *Environ Sci Technol*, vol. 47, no. 19, pp. 10721-6, Oct 1 2013, doi: 10.1021/es4007096.
- [4] A. Shokri and M. Sanavi Fard, "A sustainable approach in water desalination with the integration of renewable energy sources: Environmental engineering challenges and perspectives," *Environmental Advances*, vol. 9, 2022, doi: 10.1016/j.envadv.2022.100281.
- [5] L. P. Galway, "Boiling over: A Descriptive Analysis of Drinking Water Advisories in First Nations Communities in Ontario, Canada," *Int J Environ Res Public Health*, vol. 13, no. 5, May 17 2016, doi: 10.3390/ijerph13050505.
- [6] R. J. Patrick, "Uneven access to safe drinking water for First Nations in Canada: connecting health and place through source water protection," *Health Place*, vol. 17, no. 1, pp. 386-9, Jan 2011, doi: 10.1016/j.healthplace.2010.10.005.
- [7] T. Latchmore, C. J. Schuster-Wallace, D. R. Longboat, S. E. Dickson-Anderson, and A. Majury, "Critical elements for local Indigenous water security in Canada: a narrative review," *J Water Health*, vol. 16, no. 6, pp. 893-903, Dec 2018, doi: 10.2166/wh.2018.107.
- [8] B. J. Deaton and B. Lipka, "Cooperation between First Nations and Municipalities: Do Water-Sharing Arrangements Improve Drinking Water Quality?," *Land Economics*, vol. 99, no. 3, pp. 433-457, 2023, doi: 10.3368/le.99.3.053022-0042R.
- [9] A. Manuel and R. M. Derrickson, *Unsettling Canada: A National Wake Up Call*. Between the Lines, 2015.
- [10] H. A. McKenzie, C. Varcoe, A. J. Browne, and L. Day, "Disrupting the Continuities Among Residential Schools, the Sixties Scoop, and Child Welfare: An Analysis of Colonial and Neocolonial Discourses," *International Indigenous Policy Journal*, vol. 7, no. 2, 2016, doi: 10.18584/iipj.2016.7.2.4.
- [11] D. Martin-Hill *et al.*, "Striving toward reconciliation through the co-creation of water research," in *Indigenous Water and Drought Management in a Changing World*, (Current Directions in Water Scarcity Research, 2022, pp. 13-40.
- [12] C. Alcantara, S. Longboat, and S. Vanhooren, "Improving First Nations water security through governance," *Canadian Public Administration*, vol. 63, no. 2, pp. 155-176, 2020, doi: 10.1111/capa.12363.
- [13] D. McGregor, "Traditional Knowledge: Considerations for Protecting Water in Ontario," *International Indigenous Policy Journal*, vol. 3, no. 3, 2012, doi: 10.18584/iipj.2012.3.3.11.
- [14] (2022). *Indigenous identity by Registered or Treaty Indian status: Canada, provinces and territories, census metropolitan areas and census agglomerations with parts*. [Online] Available: <https://www150.statcan.gc.ca/t1/tbl1/en/tv.action?pid=9810026501>
- [15] (2021). *2561-343X, Access to Safe Drinking Water in First Nations Communities*.
- [16] E. Carlson-Manathara, "Settler Colonialism and Resistance," in *Living In Indigenous Sovereignty*, E. Carlson-Manathara and G. Rowe Eds.: Fernwood Publishing, 2021.
- [17] (2017). *The Aboriginal languages of First Nations people, Métis and Inuit*. [Online] Available: <https://www12.statcan.gc.ca/census-recensement/2016/as-sa/98-200-x/2016022/98-200-x2016022-eng.cfm>
- [18] Z. Parrott, "Indian Act," in *The Canadian Encyclopedia*, ed, 2022.

- [19] L. Haskell and M. Randall, "Disrupted Attachments: A Social Context Complex Trauma Framework and the Lives of Aboriginal Peoples in Canada," *Journal of Aboriginal Health*, vol. 5, no. 3, pp. 48-99, 2009. [Online]. Available: <https://ssrn.com/abstract=1569034>.
- [20] C. Angus, "The Mission School," in *Children of the Broken Treaty: Canada's Promise and One Girl's Dream*: University of Regina Press, 2015, pp. 13-24.
- [21] (1982). *The Constitution Acts, 1867 to 1982*. [Online] Available: https://laws-lois.justice.gc.ca/PDF/CONST_TRD.pdf
- [22] A. Gaudry, "Métis," in *The Canadian Encyclopedia*, M. A. Welch and D. Gallant, Eds., ed, 2023.
- [23] M. A. Freeman, "Inuit," in *The Canadian Encyclopedia*, A.-M. Pedersen, Z. Parrott, and D. Gallant, Eds., ed, 2023.
- [24] J. Kolopenuk, "Provoking Bad Biocitizenship," *Hastings Cent Rep*, vol. 50 Suppl 1, pp. S23-S29, May 2020, doi: 10.1002/hast.1152.
- [25] B. Minasny, D. Fiantis, B. Mulyanto, Y. Sulaeman, and W. Widyatmanti, "Global soil science research collaboration in the 21st century: Time to end helicopter research," *Geoderma*, vol. 373, 2020, doi: 10.1016/j.geoderma.2020.114299.
- [26] V.-P. Lehtola, "Sámi Histories, Colonialism, and Finland," *Arctic Anthropology*, vol. 52, no. 2, pp. 22-36, 2015. [Online]. Available: <https://www.jstor.org/stable/26449413>.
- [27] I. Mosby, "Administering Colonial Science: Nutrition Research and Human Biomedical Experimentation in Aboriginal Communities and Residential Schools, 1942–1952," *Histoire sociale/Social history*, vol. 46, no. 91, pp. 145-172, 2013, doi: 10.1353/his.2013.0015.
- [28] L. Pegoraro, "Second-rate victims: the forced sterilization of Indigenous peoples in the USA and Canada," *Settler Colonial Studies*, vol. 5, no. 2, pp. 161-173, 2014, doi: 10.1080/2201473x.2014.955947.
- [29] P. Hackett, "From Past to Present: Understanding First Nations Health Patters in a Historical Context," *Canadian Journal of Public Health*, vol. 96, Supplement 1: Aboriginal Health Research and Policy: First Nations-University Collaboration in Manitoba, pp. S17-S21, 2005. [Online]. Available: <https://www.jstor.org/stable/41994444>.
- [30] B. Schnarch, "Ownership, Control, Access, and Possession (OCAP) or Self-Deetermination Applied to Research: A Critical Analysis of Contemporary First Nations Research and Some Options for First Nations Communities," *Journal of Aboriginal Health*, vol. 1, no. 1, pp. 80-95, 2004. [Online]. Available: <https://jps.library.utoronto.ca/index.php/ijih/article/view/28934/24060>.
- [31] B. W. Morse, "Indigenous human rights and knowledge in archives, museums, and libraries: some international perspectives with specific reference to New Zealand and Canada," *Archival Science*, vol. 12, no. 2, pp. 113-140, 2011, doi: 10.1007/s10502-011-9165-y.
- [32] C. Wong, K. Ballegooyen, L. Ignace, M. J. Johnson, H. Swanson, and I. Boran, "Towards reconciliation: 10 Calls to Action to natural scientists working in Canada," *Facets*, vol. 5, no. 1, pp. 769-783, 2020, doi: 10.1139/facets-2020-0005.
- [33] C. Groat, "Six Nations of the Grand River," in *The Canadian Encyclopedia*, ed, 2020.
- [34] "About: Six Nations of the Grand River." <https://www.sixnations.ca/about> (accessed December 2, 2021).
- [35] S. Duignan, T. Moffat, and D. Martin-Hill, "Be like the running water: Assessing gendered and age-based water insecurity experiences with Six Nations First Nation," *Soc Sci Med*, vol. 298, p. 114864, Apr 2022, doi: 10.1016/j.socscimed.2022.114864.
- [36] S. M. Hill, "Introduction," in *The Clay We Are Made Of: Haudenosaunee Land Tenure on the Grand River*, J. Brownlie Ed. Winnipeg, Manitoba: University of Manitoba Press, 2017, pp. 1-11.

- [37] S. M. Hill, "Shotinonhsyonnih - They Built the Longhouse Again," in *The Clay We Are Made Of: Haudenosaunee Land Tenure on the Grand River*, J. Brownlie Ed. Winnipeg, Manitoba: University of Manitoba Press, 2017, pp. 132-85.
- [38] M. Filice, "Haldimand Proclamation," in *The Canadian Encyclopedia*, ed, 2020.
- [39] "Wastewater." Grand River Conservation Authority. <https://www.grandriver.ca/en/our-watershed/Wastewater.aspx> (accessed May 5, 2023).
- [40] B. Veale and S. Cooke, "Implementing integrated water management: illustrations from the Grand River watershed," *International Journal of Water Resources Development*, pp. 1-18, 2016, doi: 10.1080/07900627.2016.1217503.
- [41] A. Rodayan, S. Afana, P. A. Segura, T. Sultana, C. D. Metcalfe, and V. Yargeau, "Linking drugs of abuse in wastewater to contamination of surface and drinking water," *Environ Toxicol Chem*, vol. 35, no. 4, pp. 843-9, Apr 2016, doi: 10.1002/etc.3085.
- [42] J. Spoelstra, S. L. Schiff, and S. J. Brown, "Artificial sweeteners in a large Canadian river reflect human consumption in the watershed," *PLoS One*, vol. 8, no. 12, p. e82706, 2013, doi: 10.1371/journal.pone.0082706.
- [43] R. N. Tanna *et al.*, "Occurrence and degree of intersex (testis-ova) in darters (*Etheostoma* spp.) across an urban gradient in the Grand River, Ontario, Canada," *Environ Toxicol Chem*, vol. 32, no. 9, pp. 1981-91, Sep 2013, doi: 10.1002/etc.2262.
- [44] V. E. Restivo, K. A. Kidd, M. G. Surette, M. R. Servos, and J. Y. Wilson, "Rainbow darter (*Etheostoma caeruleum*) from a river impacted by municipal wastewater effluents have altered gut content microbiomes," *Sci Total Environ*, vol. 751, p. 141724, Jan 10 2021, doi: 10.1016/j.scitotenv.2020.141724.
- [45] R. Plummer, D. de Grosbois, D. Armitage, and R. C. de Loë, "An integrative assessment of water vulnerability in First Nation communities in Southern Ontario, Canada," *Global Environmental Change*, vol. 23, no. 4, pp. 749-763, 2013, doi: 10.1016/j.gloenvcha.2013.03.005.
- [46] S. Makhdoom, "Assessing potability of drinking-water sources and quality of surface water on the Reserve of the Six Nations of the Grand River, Ontario (Canada)," Master of Science, Department of Biology, McMaster University, Hamilton, Ontario, 2021. [Online]. Available: <http://hdl.handle.net/11375/27030>
- [47] R. Whitlow, "Stream habitat assessment and aquatic resource inventory of the Six Nations of the Grand River watershed," Six Nations of the Grand Band Council, Unpublished, 1989.
- [48] R. Whitlow, "Six Nations of the Grand River Fisheries Project Discussion Paper," Six Nations of the Grand Band Council, Unpublished, 1990.
- [49] *Aboriginal Lands of Canada Legislative Boundaries*, Natural Resources Canada. [Online]. Available: <https://open.canada.ca/data/en/dataset/522b07b9-78e2-4819-b736-ad9208eb1067>
- [50] *Ontario Integrated Hydrology (OIH) data* [Online]. Available: <https://open.canada.ca/data/en/dataset/ef0c4387-38ce-4adc-b761-f0506b82564e>
- [51] M. Chu *et al.*, "SitkaNet: A low-cost, distributed sensor network for landslide monitoring and study," *HardwareX*, vol. 9, p. e00191, Apr 2021, doi: 10.1016/j.ohx.2021.e00191.
- [52] A. T. Demetillo, M. V. Japitana, and E. B. Taboada, "A system for monitoring water quality in a large aquatic area using wireless sensor network technology," *Sustainable Environment Research*, vol. 29, no. 1, 2019, doi: 10.1186/s42834-019-0009-4.
- [53] M. Pule, A. Yahya, and J. Chuma, "Wireless sensor networks: A survey on monitoring water quality," *Journal of Applied Research and Technology*, vol. 15, no. 6, pp. 562-570, 2017, doi: 10.1016/j.jart.2017.07.004.
- [54] G. T. Miller and S. E. Spoolman, "Water Pollution," in *Living in the Environment*, 19th ed.: Cengage Learning, 2018.

- [55] *Instruction Manual DO6: Economy Hand-held Dissolved Oxygen Meter*. (2004). Eutech Instruments Pte Ltd, Oakton Instruments. [Online]. Available: <https://cwc.com.au/cwc2/wp-content/uploads/2016/07/EC-DO6-Instruction-Manual.pdf>
- [56] G. Suter II, S. Cormier, K. Schofield, J. Gilliam, and C. Barbour. "pH." United States Environmental Protection Agency. <https://www.epa.gov/caddis-vol2/ph> (accessed December 12, 2022).
- [57] L. Radke. "pH of coastal waterways." OzCoasts: Australian Online Coastal Information. https://ozcoasts.org.au/indicators/biophysical-indicators/ph_coastal_waterways/ (accessed December 12, 2022).
- [58] "Conductivity," in *Standard Methods for the Examination of Water and Wastewater*, R. B. Baird, A. D. Eaton, and E. W. Rice Eds., 23rd ed.: American Public Health Association, American Water Works Association, Water Environment Federation, 2017.
- [59] M. Hayashi, "Temperature-Electrical Conductivity Relation of Water for Environmental Monitoring and Geophysical Data Inversion," *Environmental Monitoring and Assessment*, vol. 96, no. 8, pp. 119-128, 2004, doi: <https://doi.org/10.1023/B:EMAS.0000031719.83065.68>.
- [60] (1988). *Specific Conductance:-Theoretical Considerations and Application to Analytical Quality Control*. [Online] Available: <https://pubs.usgs.gov/wsp/2311/report.pdf>
- [61] H. S. Salem, "The Influence of Clay Conductivity on Electric Measurements of Glacial Aquifers," *Energy Sources*, vol. 23, no. 3, pp. 225-234, 2010, doi: 10.1080/00908310151133906.
- [62] R. J. Davies-Colley and D. G. Smith, "Turbidity Suspended Sediment, and Water Clarity: A Review," *Journal of the American Water Resources Association*, vol. 37, no. 5, pp. 1085-1101, 2001, doi: 10.1111/j.1752-1688.2001.tb03624.x.
- [63] "Turbidity," in *Standard Methods for the Examination of Water and Wastewater*, R. B. Baird, A. D. Eaton, and E. W. Rice Eds., 23rd ed.: American Public Health Association, American Water Works Association, Water Environment Federation, 2017.
- [64] "Oxygen (Dissolved)," in *Standard Methods for the Examination of Water and Wastewater*, R. B. Baird, A. D. Eaton, and E. W. Rice Eds., 23rd ed.: American Public Health Association, American Water Works Association, Water Environment Federation, 2017.
- [65] P. M. A. Fraher and D. W. Clarke, "Fouling Detection and Compensation in Clark-Type DOx Sensors," *IEEE Transactions on Instrumentation and Measurement*, vol. 47, no. 3, pp. 686-691, 1998, doi: 10.1109/19.744325.
- [66] M. Peter-Varbanets, C. Zurbrugg, C. Swartz, and W. Pronk, "Decentralized systems for potable water and the potential of membrane technology," *Water Res*, vol. 43, no. 2, pp. 245-65, Feb 2009, doi: 10.1016/j.watres.2008.10.030.
- [67] J. G. Wijmans and R. W. Baker, "The solution-diffusion model: a review," *Journal of Membrane Science*, vol. 107, pp. 1-21, 1995, doi: 10.1016/0376-7388(95)00102-I.
- [68] L. W. McKeen, "Chapter 1: Introduction to Permeation of Plastics and Elastomers," in *Permeability Properties of Plastics and Elastomers*, Fourth ed.: Elsevier William Andrew, 2017, pp. 1-19.
- [69] C. J. Geankoplis, "Principles of Mass Transfer," in *Transport Processes and Unit Operations*, Third ed.: Prentice-Hall International, Inc., 1993, pp. 381-425.
- [70] *Rubber, vulcanized or thermoplastic — Determination of permeability to gases Part 1: Differential-pressure methods*, 2022.
- [71] X. Hu, "Oxygen Gas Permeation Test of Films," Element, Cypress, TX, 2022.
- [72] J. G. Calvert, "Glossary of Atmospheric Chemistry Terms," *Pure & Applied Chemistry*, vol. 62, no. 11, pp. 2167-2219, 1990, doi: 10.1351/pac199062112167.
- [73] W. J. Yang, K.-G. Neoh, E.-T. Kang, S. L.-M. Teo, and D. Rittschof, "Polymer brush coatings for combating marine biofouling," *Progress in Polymer Science*, vol. 39, no. 5, pp. 1017-1042, 2014, doi: 10.1016/j.progpolymsci.2014.02.002.

- [74] D. Liu, H. Shu, J. Zhou, X. Bai, and P. Cao, "Research Progress on New Environmentally Friendly Antifouling Coatings in Marine Settings: A Review," *Biomimetics (Basel)*, vol. 8, no. 2, May 13 2023, doi: 10.3390/biomimetics8020200.
- [75] H. M. Arterburn and R. F. McMahon, "Population and Reproductive Dynamics of Zebra Mussels (*Dreissena polymorpha*) in Warm, Low-Latitude North American Waters," *Biol Bull*, vol. 242, no. 3, pp. 207-221, Jun 2022, doi: 10.1086/720151.
- [76] A. Delgado, C. Briciu-Burghina, and F. Regan, "Antifouling Strategies for Sensors Used in Water Monitoring: Review and Future Perspectives," *Sensors (Basel)*, vol. 21, no. 2, Jan 8 2021, doi: 10.3390/s21020389.
- [77] M. Lejars, A. Margailan, and C. Bressy, "Fouling release coatings: a nontoxic alternative to biocidal antifouling coatings," *Chem Rev*, vol. 112, no. 8, pp. 4347-90, Aug 8 2012, doi: 10.1021/cr200350v.
- [78] S. Kiil, K. Dam-Johansen, C. E. Weinell, M. S. Pedersen, and S. A. Codolar, "Dynamic Simulations of a Self-Polishing Antifouling Paint Exposed to Seawater," *Journal of Coatings Technology*, vol. 74, no. 929, pp. 45-54, 2002, doi: 10.1007/BF02698368.
- [79] "The History of the Prevention of Fouling," in *Marine Fouling and its Prevention*: Woods Hole Oceanographic Institute, United States. Navy Dept. Bureau of Ships, 1952.
- [80] E. Ytreberg, J. Karlsson, and B. Eklund, "Comparison of toxicity and release rates of Cu and Zn from anti-fouling paints leached in natural and artificial brackish seawater," *Science of The Total Environment*, vol. 408, no. 12, pp. 2459-2466, 2010, doi: 10.1016/j.scitotenv.2010.02.036.
- [81] J. F. Schumacher *et al.*, "Engineered antifouling microtopographies - effect of feature size, geometry, and roughness on settlement of zoospores of the green alga *Ulva*," *Biofouling*, vol. 23, no. 1-2, pp. 55-62, 2007, doi: 10.1080/08927010601136957.
- [82] K. Zhuang, X. Yang, W. Huang, Q. Dai, and X. Wang, "Efficient Bubble Transport on Bioinspired Topological Ultrasticky Surfaces," *ACS Appl Mater Interfaces*, vol. 13, no. 51, pp. 61780-61788, Dec 29 2021, doi: 10.1021/acsami.1c19414.
- [83] T. Darmanin and F. Guittard, "Wettability of conducting polymers: From superhydrophilicity to superoleophobicity," *Progress in Polymer Science*, vol. 39, no. 4, pp. 656-682, 2014, doi: 10.1016/j.progpolymsci.2013.10.003.
- [84] P. Liu, E. Domingue, D. C. Ayers, and J. Song, "Modification of Ti6Al4V substrates with well-defined zwitterionic polysulfobetaine brushes for improved surface mineralization," *ACS Appl Mater Interfaces*, vol. 6, no. 10, pp. 7141-52, May 28 2014, doi: 10.1021/am501967y.
- [85] J. Tian *et al.*, "Facile fabrication of superhydrophobic coatings with superior corrosion resistance on LA103Z alloy by one-step electrochemical synthesis," *Surface and Coatings Technology*, vol. 452, 2023, doi: 10.1016/j.surfcoat.2022.129090.
- [86] J. Sun *et al.*, "Environmentally benign smart self-healing silicone-based coating with dual antifouling and anti-corrosion properties," *Applied Materials Today*, vol. 28, 2022, doi: 10.1016/j.apmt.2022.101551.
- [87] J. Tan, J. Xu, D. Wang, J. Yang, and S. Zhou, "Seawater-responsive SiO₂ nanoparticles for in situ generation of zwitterionic polydimethylsiloxane antifouling coatings with underwater superoleophobicity," *Journal of Materials Chemistry A*, vol. 8, no. 45, pp. 24086-24097, 2020, doi: 10.1039/d0ta07617a.
- [88] L.-F. Fang *et al.*, "Improved antifouling properties of polyvinyl chloride blend membranes by novel phosphate based-zwitterionic polymer additive," *Journal of Membrane Science*, vol. 528, pp. 326-335, 2017, doi: 10.1016/j.memsci.2017.01.044.
- [89] H. J. Waite, "Adhesion à la Moule," *Integrative and Comparative Biology*, vol. 42, no. 6, pp. 1172-1180, 2002, doi: 10.1093/icb/42.6.1172.

- [90] L. Wang *et al.*, "In-vitro antibacterial and anti-encrustation performance of silver-polytetrafluoroethylene nanocomposite coated urinary catheters," *J Hosp Infect*, vol. 103, no. 1, pp. 55-63, Sep 2019, doi: 10.1016/j.jhin.2019.02.012.
- [91] V. M. Sardinha, L. L. Lima, W. D. Belangero, C. A. Zavaglia, V. P. Bavaresco, and J. R. Gomes, "Tribological characterization of polyvinyl alcohol hydrogel as substitute of articular cartilage," *Wear*, vol. 301, no. 1-2, pp. 218-225, 2013, doi: 10.1016/j.wear.2012.11.054.
- [92] J. Xie, P. Yu, Z. Wang, and J. Li, "Recent Advances of Self-Healing Polymer Materials via Supramolecular Forces for Biomedical Applications," *Biomacromolecules*, vol. 23, no. 3, pp. 641-660, Mar 14 2022, doi: 10.1021/acs.biomac.1c01647.
- [93] E. Ostuni, R. G. Chapman, E. Holmlin, S. Takayama, and G. M. Whitesides, "A Survey of Structure-Property Relationships of Surfaces that Resist the Adsorption of Protein," *Langmuir*, vol. 17, no. 18, pp. 5605-5620, 2001, doi: 10.1021/la010384m.
- [94] D. J. Miller, D. R. Dreyer, C. W. Bielawski, D. R. Paul, and B. D. Freeman, "Surface Modification of Water Purification Membranes," *Angew Chem Int Ed Engl*, vol. 56, no. 17, pp. 4662-4711, Apr 18 2017, doi: 10.1002/anie.201601509.
- [95] C. Leng, H.-C. Hung, O. A. Sieggreen, Y. Li, S. Jiang, and Z. Chen, "Probing the Surface Hydration of Nonfouling Zwitterionic and Poly(ethylene glycol) Materials with Isotopic Dilution Spectroscopy," *The Journal of Physical Chemistry C*, vol. 119, no. 16, pp. 8775-8780, 2015, doi: 10.1021/acs.jpcc.5b01649.
- [96] S. A. S. Craig, "Betaine in human nutrition," *American Journal of Clinical Nutrition*, vol. 80, no. 3, pp. 539-549, 2004, doi: 10.1093/ajcn/80.3.539.
- [97] B. Palecz, H. Piekarski, and S. Romanowski, "Studies on homogeneous interactions between zwitterions of several α -amino acids in water at a temperature of 298.15 K," *Journal of Molecular Liquids*, vol. 84, no. 3, pp. 279-288, 2000, doi: 10.1016/S0167-7322(99)00194-4.
- [98] P. Lin, T. L. Chuang, P. Z. Chen, C. W. Lin, and F. X. Gu, "Low-Fouling Characteristics of Ultrathin Zwitterionic Cysteine SAMs," *Langmuir*, vol. 35, no. 5, pp. 1756-1767, Feb 5 2019, doi: 10.1021/acs.langmuir.8b01525.
- [99] J. Xu and H. Lee, "Anti-Biofouling Strategies for Long-Term Continuous Use of Implantable Biosensors," *Chemosensors*, vol. 8, no. 3, 2020, doi: 10.3390/chemosensors8030066.
- [100] J. B. Schlenoff, "Zwitteration: coating surfaces with zwitterionic functionality to reduce nonspecific adsorption," *Langmuir*, vol. 30, no. 32, pp. 9625-36, Aug 19 2014, doi: 10.1021/la500057j.
- [101] C. Wen *et al.*, "Zwitterionic hydrogel coated superhydrophilic hierarchical antifouling floater enables unimpeded interfacial steam generation and multi-contamination resistance in complex conditions," *Chemical Engineering Journal*, vol. 421, 2021, doi: 10.1016/j.cej.2021.130344.
- [102] W. Cai *et al.*, "Cicada wing-inspired solar transmittance enhancement and hydrophobicity design for graphene-based solar steam generation: A novel gas phase deposition approach," *Applied Energy*, vol. 320, 2022, doi: 10.1016/j.apenergy.2022.119322.
- [103] M. N. Zainol Abidin, M. M. Nasef, and T. Matsuura, "Fouling Prevention in Polymeric Membranes by Radiation Induced Graft Copolymerization," *Polymers (Basel)*, vol. 14, no. 1, Jan 4 2022, doi: 10.3390/polym14010197.
- [104] A. Shimizu, E. Hifumi, K. Kojio, A. Takahara, and Y. Higaki, "Modulation of Double Zwitterionic Block Copolymer Aggregates by Zwitterion-Specific Interactions," *Langmuir*, vol. 37, no. 50, pp. 14760-14766, Dec 21 2021, doi: 10.1021/acs.langmuir.1c02809.
- [105] Y. Men *et al.*, "Biodegradable Zwitterionic Nanogels with Long Circulation for Antitumor Drug Delivery," *ACS Appl Mater Interfaces*, vol. 10, no. 28, pp. 23509-23521, Jul 18 2018, doi: 10.1021/acsami.8b03943.

- [106] H. Li, L. Li, J. Wen, G. Ye, J. Chen, and X. Wang, "Introducing self-assembly effect in adsorption process for efficient uranium extraction by zwitterion highly-functionalized fibers," *Chemical Engineering Journal*, vol. 456, 2023, doi: 10.1016/j.cej.2022.140935.
- [107] A. Vaterrodt, B. Thallinger, K. Daumann, D. Koch, G. M. Guebitz, and M. Ulbricht, "Antifouling and Antibacterial Multifunctional Polyzwitterion/Enzyme Coating on Silicone Catheter Material Prepared by Electrostatic Layer-by-Layer Assembly," *Langmuir*, vol. 32, no. 5, pp. 1347-59, Feb 9 2016, doi: 10.1021/acs.langmuir.5b04303.
- [108] S. Boonjamnian, V. Sadsri, V. P. Hoven, and P. Na Nongkhai, "Magnetic nanoparticles coated with zwitterionic copolymer as an advanced material for rapid and instrument-free biomolecular detection in human serum," *Journal of Metals, Materials and Minerals*, vol. 32, no. 4, pp. 186-193, 2022, doi: 10.55713/jmmm.v32i4.xxxx.
- [109] J. Zhang *et al.*, "Antifouling and antibacterial zwitterionic hydrogels as soft contact lens against ocular bacterial infections," *European Polymer Journal*, vol. 167, 2022, doi: 10.1016/j.eurpolymj.2022.111037.
- [110] K. Li *et al.*, "Surface modification of commercial intraocular lens by zwitterionic and antibiotic-loaded coating for preventing postoperative endophthalmitis," *Colloids Surf B Biointerfaces*, vol. 222, p. 113093, Feb 2023, doi: 10.1016/j.colsurfb.2022.113093.
- [111] K. A. Barzen-Hanson, S. E. Davis, M. Kleber, and J. A. Field, "Sorption of Fluorotelomer Sulfonates, Fluorotelomer Sulfonamido Betaines, and a Fluorotelomer Sulfonamido Amine in National Foam Aqueous Film-Forming Foam to Soil," *Environ Sci Technol*, vol. 51, no. 21, pp. 12394-12404, Nov 7 2017, doi: 10.1021/acs.est.7b03452.
- [112] H. Jin, L. Tian, W. Bing, J. Zhao, and L. Ren, "Bioinspired marine antifouling coatings: Status, prospects, and future," *Progress in Materials Science*, vol. 124, 2022, doi: 10.1016/j.pmatsci.2021.100889.
- [113] T. Xiang, L. S. Zhang, R. Wang, Y. Xia, B. H. Su, and C. S. Zhao, "Blood compatibility comparison for polysulfone membranes modified by grafting block and random zwitterionic copolymers via surface-initiated ATRP," *J Colloid Interface Sci*, vol. 432, pp. 47-56, Oct 15 2014, doi: 10.1016/j.jcis.2014.06.044.
- [114] H. Yu, Y. Cao, G. Kang, J. Liu, M. Li, and Q. Yuan, "Enhancing antifouling property of polysulfone ultrafiltration membrane by grafting zwitterionic copolymer via UV-initiated polymerization," *Journal of Membrane Science*, vol. 342, no. 1-2, pp. 6-13, 2009, doi: 10.1016/j.memsci.2009.05.041.
- [115] H. Lee, S. M. Dellatore, W. M. Miller, and P. B. Messersmith, "Mussel-Inspired Surface Chemistry for Multifunctional Coatings," *Science*, vol. 318, no. 5849, pp. 426-430, 2007, doi: 10.1126/science.1147241.
- [116] Y. Jiang, D. Choudhury, M. Brownell, A. Nair, J. A. Goss, and M. Zou, "The effects of annealing conditions on the wear of PDA/PTFE coatings," *Applied Surface Science*, vol. 481, pp. 723-735, 2019, doi: 10.1016/j.apsusc.2019.03.076.
- [117] R. A. Zangmeister, T. A. Morris, and M. J. Tarlov, "Characterization of polydopamine thin films deposited at short times by autoxidation of dopamine," *Langmuir*, vol. 29, no. 27, pp. 8619-28, Jul 9 2013, doi: 10.1021/la400587j.
- [118] Y. Lv, S. J. Yang, Y. Du, H. C. Yang, and Z. K. Xu, "Co-deposition Kinetics of Polydopamine/Polyethyleneimine Coatings: Effects of Solution Composition and Substrate Surface," *Langmuir*, vol. 34, no. 44, pp. 13123-13131, Nov 6 2018, doi: 10.1021/acs.langmuir.8b02454.
- [119] W. Xie *et al.*, "Polydopamine/ polyethyleneimine/ MOF ternary-coated poly (vinyl chloride) nanocomposite membranes based on green solvent for shale gas wastewater treatment," *Journal of Membrane Science*, vol. 665, 2023, doi: 10.1016/j.memsci.2022.121100.

- [120] P. M. P. T. Fowler *et al.*, "Surface Zwitterionization of Expanded Poly(tetrafluoroethylene) via Dopamine-Assisted Consecutive Immersion Coating," *ACS Appl Mater Interfaces*, vol. 12, no. 37, pp. 41000-41010, Sep 16 2020, doi: 10.1021/acsami.0c09073.

2. Gas Diffusion Properties of Zwitterionized Galvanic Dissolved Oxygen Sensor Membranes

2.1. Introduction

Water quality monitoring stations (WQMSs) are invaluable tools for monitoring distant, inaccessible, or otherwise inconvenient sites for water quality monitoring. Their real-time nature enables prompt responses to potential water quality issues, such as pollution events, and they can be easily customized and are scalable to suit the needs of the project and site. Additionally, WQMSs are cost-effective, eliminating the need for manual sampling and frequent laboratory analysis, as well as time and money spent getting to and from the site. However, one of the most significant problems with the use of WQMS is that their sensors are prone to biofouling. While considerable research has investigated ways to mitigate biofouling on a variety of surfaces and sensors [1-3], most of this work has not focused on investigating the ability for these antifouling (AF) coatings to allow the passage of certain molecules through the AF surface, a principle important for the functioning of galvanic dissolved oxygen (DO) sensors.

Galvanic DO sensors rely on the principle of oxygen partial pressure measurement. A dense membrane, usually polytetrafluoroethylene (PTFE) separates the measured liquid from an internal galvanic cell, known as a Clark electrode [4, 5]. As oxygen molecules diffuse through the PTFE barrier, they are electrolyzed at the noble metal cathode. Electrons generated from this reaction are then analyzed at an electronic module and are linearly correlated with oxygen concentration in the measured liquid [5]. As such, galvanic DO sensors (henceforth referred to simply as DO sensors) rely on a stable DO pathway from the measured liquid to the cathode surface. The buildup of material on the sensor will lead to inaccurate readings and sensor signal drift [6-9].

While PTFE itself exhibits passable foul-release characteristics, these properties are not sufficient for most applications [10].

Some research has been done into oxygen permeable coatings for sensing applications. Bayat et al. investigated the removal of antifoulants via phage treatment to remove developed fouling on DO membranes without damaging their delicate surface [11]. Hsu and Selvaganapathy investigated changing the permeable polymer membrane itself with PEG-functionalized PDMS, improving AF performance while eliminating the additional layer through which oxygen transfer occurred [12]. Osborne et al. showed that an omniphobic liquid-infused (OLI) coating could successfully be used for improving the AF properties of a dissolved oxygen probe, reducing fouling in an incubated yeast environment, and importantly, showing that oxygen permeability through the DO membrane remained possible with an OLI coating [13]. Zwitterionic coatings have been shown to help reduce sensor signal drift [7]. However, a scan of the literature does not yet reveal any insights into the nature of oxygen diffusion capabilities of zwitterion-coated DO membranes.

In this chapter, a series of zwitterionic poly[sulfobetaine methacrylate-co-glycidyl methacrylate] (PGS) polymers were synthesized and grafted to dense PTFE membranes. Physical characterizations of the coatings were obtained using contact angle goniometry, Field Emission Scanning Electron Microscopy (FESEM), Atomic Force Microscopy (AFM), Elemental Unicube analysis, and X-Ray Photoelectron Spectroscopy (XPS). To assess the useability of these AF membranes for dissolved oxygen (DO) environmental sensing applications, membranes underwent liquid dissolved-oxygen permeability tests using a custom-built liquid oxygen-carrier (LOC) setup. Given the elongated, spindly nature of zwitterionic moieties, it is hypothesized that a LOC device will allow for the extension of zwitterionic chains when interacting with water, which will allow

DO to pass more easily through the zwitterionic layer (ZL), and therefore, through the membrane itself when compared to traditional gas permeation measurements. A gas differential pressure sensor method was used to verify the physical parameters obtained in this characterization. The physical parameters obtained through oxygen permeability tests were then used to create a model of oxygen diffusion through coated and environmentally fouled membranes.

2.2. Materials and Methods

2.2.1. Surface Preparation

Samples were prepared according to the conditions set out in Table 1. Not all characterizations were performed for all samples listed. The leading '+' found for all samples except PTFE refers to the subsequent listed layers as being added onto the PTFE substrate. Samples consist of bare PTFE, PTFE membranes after fouling in two freshwater conditions, PTFE membranes with two different grafting layer (GL) conditions, two PTFE membranes coated with three out of four GL and zwitterionic layer (ZL) polymers or copolymers, five full GL and ZL copolymer layers produced at varying grafting concentrations of zwitterionic solution as well as varying grafting times, and zwitterionic powder. Numbers in a sample ID are either associated with fouling time, ZL graft concentration, or ZL graft time.

Table 1. Index of characterized samples.

Sample ID	PTFE	Fouling Layer	PDA	PEI	SBMA	GMA	ZL Graft Time	ZL Graft Conc.	Fouling Time
PTFE	✓	-	-	-	-	-	-	-	-
+Foul14	✓	✓	-	-	-	-	-	-	14 days
+Foul60	✓	✓	-	-	-	-	-	-	60 days
+PDA	✓	-	✓	-	-	-	-	-	-
+PDA/PEI	✓	-	✓	✓	-	-	-	-	-
+PDA/PEI+SBMA	✓	-	✓	✓	✓	-	24 hrs	10 mg/mL	-
+PDA+PGS	✓	-	✓	-	✓	✓	24 hrs	10 mg/mL	-
+Z5-24hr	✓	-	✓	✓	✓	✓	24 hrs	5 mg/mL	-
+Z10-12hr	✓	-	✓	✓	✓	✓	12 hrs	10 mg/mL	-
+Z10-24hr	✓	-	✓	✓	✓	✓	24 hrs	10 mg/mL	-
+Z10-48hr	✓	-	✓	✓	✓	✓	48 hrs	10 mg/mL	-
+Z20-24hr	✓	-	✓	✓	✓	✓	24 hrs	20 mg/mL	-
PGS Powder	-	-	-	-	✓	✓	-	-	-

2.2.1.1. Zwitterionic Surface Preparation

Polytetrafluoroethylene (PTFE) films of 10 μm (trade name Goodfellow 112-898-43) purchased from Sigma Aldrich were used for all membrane characterizations except for coating density measurements, which used 200 μm films from Sigma Aldrich, and for gas permeation tests, which instead used 762 μm sheets purchased from McMaster Carr. Sulfobetaine methacrylate (SBMA) was purchased from Sigma Aldrich under the name [2-(Methacryloyloxy)ethyl]dimethyl-(3-sulfopropyl)ammonium hydroxide with a purity of $\geq 97\%$. DA hydrochloride, branched PEI ($M_n = 600$ Da), Glycidyl methacrylate (GMA, purity of $\geq 97\%$), Tris base (THAM, purity 99.9%), azobisisobutyronitrile (AIBN, purity 98%), and 25% glutaraldehyde (GA) were obtained from Sigma Aldrich. HPLC grade methanol, isopropyl alcohol (IPA), and 1M HCl were obtained from Fischer Scientific.

Fabrication of zwitterionic coatings is partially derived from [14] and [15] in a graft-from fashion. PTFE sheets were cut into 1.5 cm x 1.5 cm squares and were washed in deionized (DI) water and IPA prior to use. PGS was synthesized using a SBMA:GMA:AIBN reaction molar ratio of 80:20:1, determined from the source literature to be an optimal ratio. Equal amounts of DI water

and methanol were mixed, to which was added SBMA and GMA. This mixture was left to stir for 10 minutes, then purged with nitrogen while mixing for a further half hour. AIBN was added and the mixture was left to stir for 15 minutes. This solution was reacted at 60°C in for 6 hours, followed by termination of the reaction by immersing the vessel in an ice bath. To aid in precipitating the polymer, the reaction contents were placed in a -4°C freezer. The supernatant was discarded, and the remaining white polymer was thrice purified by redissolving it in water and precipitating it again in methanol. The resulting polymer was lyophilized, yielding white, needle-like crystals.

Membranes were prepared according to the general scheme of Figure 4. GLs were prepared by adding 50 mM Tris base to sufficient DI water, then lowering the pH to 8.5 using HCl. DA and PEI were dissolved in concentrations of 2 mg/mL and 1 mg/mL, respectively. These concentrations were chosen as they have previously been optimized to provide a thick GL, while a low PEI M_n of 600 Da has been shown to greatly improve hydrophilicity [15, 16]. Sample GLs without PEI retained a 2 mg/mL PDA concentration. After 10 minutes of mixing, the darkening solution was poured into Petri dishes and the bare PTFE films were floated on the PDA/PEI mixture. The dishes were covered, sealed, and placed in an oven for 24 hours at 40°C to allow for the accumulation of the PDA/PEI layer. The surfaces were thrice rinsed with DI water and stored in DI water for further use.

ZLs were prepared by preheating DI water to 60°C. 5, 10, and 20 mg/mL of PGS copolymer were dissolved within. Experiments involving only SBMA ZLs used concentrations of 10 mg/mL. Each of these solutions was poured into a Petri dish, and the PDA or PDA/PEI discs were floated with the coating side submerged in the zwitterionic fluid. The dishes were covered, sealed, and

zwitterionized in an oven at 60°C for 12, 24, and 48 hours. The resulting coatings were gently rinsed with DI water and stored in DI water for further use.

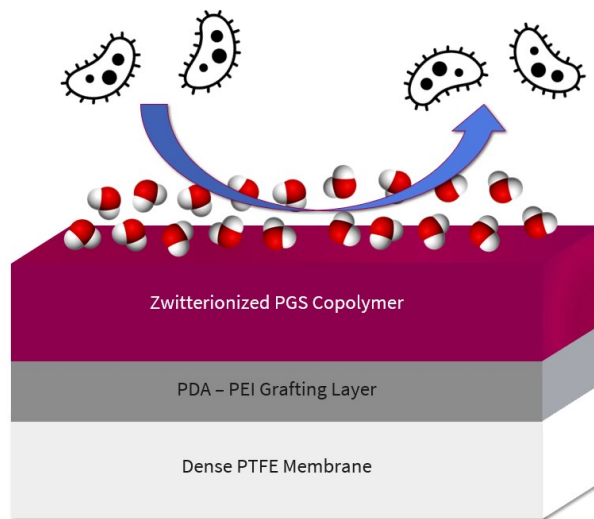


Figure 4. AF capabilities of the PGS copolymer help reduce foulant attachment via a thick hydration layer.

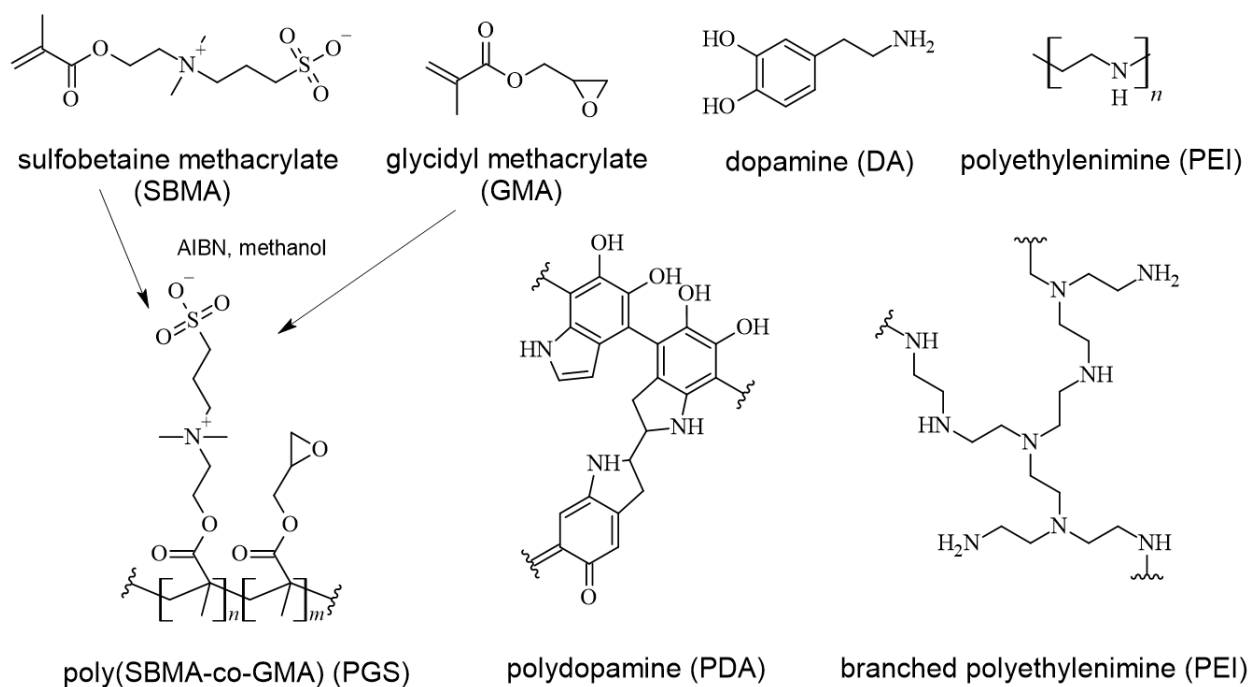


Figure 5. Primary relevant molecules in the formation of AF coatings on PTFE.

2.2.1.2. Fouling Surface Preparation

Samples were prepared for environmental fouling by cutting up the 10 μm PTFE film into 7.5 cm square slices. Each film was attached uncoated to a plastic scaffold, which was then fixed to 30 cm of fishing wire on a small buoy to allow for complete submersion of each sample. Membranes were fouled in Cootes Paradise, Lake Ontario. Samples were fouled for 14 days and 60 days in pentaplicate to allow for damage or mishandling.

2.2.2. Physical Characterization Techniques

2.2.2.1. Surface Hydrophilicity

A contact angle goniometer was used to measure the dynamic contact angle of the surface samples. 4 μL droplets of deionized water were dropped onto each surface and the WCA was measured for 6 seconds. Data was collected using Drop Shape Analyzer software. Measurements were performed in triplicate, but the cleanest of each measurement was displayed.

2.2.2.2. Scanning Electron Microscopy

Images were acquired CCEM's JEOL JSM-7000F instrument. Images were taken using a beam strength of 3.0kV and at a magnification of 3000x. Samples were prepared by cutting them into pieces about 5 mm x 5 mm in size, then affixed to a copper conductive tape in place on the sample mount. Given the highly insulating nature of the samples, a nickel paste was dotted around the perimeter of each sample. This application additionally prevented the thin, delicate samples from moving in the vacuum of the instrument without pressing them to the conductive tape. Finally, the samples were coated with 5 nm Pt.

2.2.2.3. Atomic Force Microscopy

Membrane morphologies were acquired using CALM's Bruker Dimension iCon AFM instrument in tapping mode, using an RTESPA-300-125 tip. Before preparing the surface coatings, a piece of

scotch tape was attached to the PTFE. Following the completion of the coating process, this piece of tape was removed, leaving a thin “cliff” between the coated and uncoated sections of the sample. Coated PTFE slices were fixed with GA before imaging. Each slice was fully immersed in a 3% GA solution for one hour at 4°C, followed by a series of three-minute 25°C baths at 50%, 70%, 90%, and 100% ethanol to dehydrate the samples. The samples were then left to dry overnight. Sample sites were scanned at a width of 20 µm with an aspect ratio of 3, with the coated half on the left side of the scan and the uncoated half on the right. Images were processed in Gwyddion, a free AFM analysis software. After correcting for any horizontal scars, a three-point level was applied to the coating-free half and its height was set to zero. The points for the three-point level were selected to form a wide area, with each point situated approximately 1 µm from the edge of the uncoated surface. For each sample, three images were scanned, and three cross-sectional slices were analysed for a total of nine cross-sections per sample coating. The mean height of all points along each of the coated and uncoated halves was calculated, and the mean uncoated section’s height was subtracted from the mean coated section’s height to yield a final coating thickness. The mean and standard deviations of these nine thicknesses were then calculated. A Thorlabs Optical Coherence Tomography (OCT) instrument was additionally used to determine the thickness of environmentally fouled layers. Triplicate scans for each +Foul14 and +Foul60 were analyzed using ThorImageOCT v. 5.5.

2.2.3. Chemical Characterization Techniques

2.2.3.1. *Elemental Analysis*

Elemental Analysis was performed using an Elementar Unicube configured to measure nitrogen, carbon, hydrogen, and sulfur. Samples of uncoated and coated slices of 10 µm-thick pieces of PTFE were used, as well as samples of PGS powder. 2 ± 0.2 mg of each sample was analyzed at

least thrice, and the standard deviation was taken. Each sample is heated to 1,200 °C, and the emittent gases are sent through a chromatography column to analyze the four constituent elements above [17]. The remaining elements, fluorine and oxygen, could be deduced from the mass percentage results. While hydrogen characterization on samples was not crucial, an absence of hydrogen was used to discard unusable or nonsensical results.

2.2.3.2. X-Ray Photoelectron Spectroscopy

XPS data was acquired using OCCAM's ThermoFisher K-Alpha instrument. Measurements were performed using a 1486.6 eV monochromatic Al K_α x-ray source with an elliptical spot size of 400 μm x 200 μm. The source beam was run at 6mA and 12kV. Charge neutralization was accomplished using an electron/argon ion flood source. Survey spectra were acquired using a pass energy of 200 eV (1 eV/step), with higher resolution elemental scans acquired at 50 eV (0.1 eV/step). High-resolution scans were acquired for C 1s, F 1s, N 1s, O 1s, S 2p, and Si 2p regions, with relative scaling factors (RSF) of 1.0, 4.43, 1.8, 2.93, 1.667, and 0.817, respectively. The dwell time for these spectra was 50 ms. Data analysis was performed using CasaXPS 2.3.25. The effective attenuation length (EAL) escape depth correction factor was used, and the magic angle was used as the angular distribution correction factor. The Shirley background subtraction algorithm was used for all samples.

2.2.4. Oxygen Permeability Techniques

2.2.4.1. Liquid Dissolved Oxygen-Carrier

Liquid oxygen-carrier (LOC) tests were performed to determine the mass transfer properties of DO through uncoated, coated, and environmentally fouled membranes. Two polymethyl methacrylate (PMMA) tanks were manufactured and conjoined so that each half contained a total possible volume of 2L. The oxygen-rich (OR) tank was filled with 1.8 L of water, while the

oxygen-poor (OP) tank was filled with 400 mL. A membrane support lies at the junction of the two tanks and can fit a 6.0 cm membrane. Two DO sensors were fitted adjacent to the membrane on both the OR and OP sides, both acquired from Atlas Scientific (Kit-103DX). An oxygen cylinder with a flashback arrestor was connected to the OR tank, and each of the OR and OP tanks were re outfitted with a 15-psig pressure release valve. The outputs from each DO sensor were recorded using an Arduino Uno. Using a LOC system enables the calculation of oxygen diffusion parameters utilizing an inexpensive, relatively simple device to assemble. While oxygen diffusion through a PTFE film is the same whether the film is exposed to water, it is hypothesized that additional electrostatic interactions due to the presence of zwitterions on the surface of the PTFE may reduce the effectiveness of the membrane's oxygen solubility. Additionally, as zwitterionic moieties are less compressed against the membrane surface when in an aqueous environment, this may also alter the membrane's permeability. An overview of the LOC setup is found in Figure 6.

Experiments were performed as follows. A day prior to sampling, tap water was poured into a 4 L beaker and allowed to equilibrate to room temperature. Following a temperature recording, each DO probe was removed, treated with dilute HCl solution, rinsed in DI water, and recalibrated. A sample was affixed to the membrane holder, which was then connected to each tank. Tap water was poured into each half, and the OP tank was sealed to reduce the volume to 400 mL in order to reduce testing times. Data recording was started, then O₂ was allowed to bubble into the OR tank, which occurred for about 10 minutes until DO levels had stabilized at around 35 mg/L. After stabilization, the O₂ was turned off, followed by a 5-second waiting period to allow the water to degas. The lids of each tank were sealed. Upon completion of a test, tanks were unsealed and cleaned. Each point in the data presented is an average of readings for 10-minute

intervals. 10 samples were tested in triplicate: PTFE, Foul-14, Foul-60, +PDA, +PDA/PEI, +Z5-24hr, +Z10-12hr, +Z10-24hr, +Z10-48hr, and +Z20-24hr.



Figure 6. LOC test prior to first use of the device, showing OP tank (no dye) and OR tank (pink dye). The dye test was performed to confirm no passage of micromolecules through the membrane.

Given that the LOC system behaves similarly to a traditional gas pressure differential testing, permeability coefficients, Q , could then be calculated by Equation (8) as observing a first order reaction [18, 19]:

$$Q = \frac{V_{OP} * d}{R * T * A * (pp_{OR,i} - pp_{OP,i})} \frac{dp}{dt} \quad (8)$$

where V_{OP} is the volume of the oxygen poor tank, d is the membrane thickness, R is the gas constant, T is the temperature in Kelvin, A is the membrane area, $pp_{OR,i} - pp_{OP,i}$ is the difference in partial pressure of DO on the OP side from the OR side at the beginning of the test, and dp/dt is the change of pp_{O_2} in the OP tank. The concentration of dissolved gases in the liquid outside the membrane can be determined with Henry's Law, using Henry's solubility constant H_s^{cp} , calculated from [20]. Given the known first order relationship, the calculated dp/dt at $t = 0$ is achieved by

dividing $ppOP,f-ppOP,i$ by the time constant, τ , the time at which $[C] = 1-e^{-1}$ % of steady state. Averaging the concentration of each of the three experiments per test condition could be fitted to Equation (9), which models the OR and OP concentration over time to find the remaining mass transfer coefficients:

$$[C] = -\alpha e^{-\beta t - \gamma} + \delta \quad (9)$$

Each of α , β , γ , and δ are constants determined by minimizing the square of residuals to fit the data best. The diffusion coefficients of each sample, D , are assumed to remain constant. The complete set of constants can be further examined in Table A.10 and Table A.11. Solubility coefficients were calculated from Equation (2). The permeabilities of individual layers were calculated using Equation (6).

2.2.4.2. *Gas Permeation Tests*

Traditional gas permeation tests were conducted to confirm the reliability of LOC results. Only PTFE and +PDA samples were tested due to expense. Each sample utilized a 0.762 mm thick PTFE base, and discs were cut to a width of 48 mm. Experiments were conducted at Element Labs' Cypress, TX facility using ISO-2782-1:2022 [21].

2.2.4.3. *Simulating Oxygen Transfer*

To visualize the effects of diffusion coefficients, a model was developed to realize the one-dimensional concentration profile through PTFE membranes and their associated coatings. The model produces two outputs: a two-dimensional image of the concentration profile over the length of the coated membrane at a single specified time, and a three-dimensional image of the concentration profile from $t = 0$ until the specified time.

The OR and OP tanks are assumed to be well-stirred, such that any DO transfer out of the OR volume immediately results in its replenishment from the bulk, and any transfer of DO to the

OP volume results in its scattering into the bulk. The OR and OP tank boundary conditions change according to Equation (9). Each bulk volume is assumed to be well mixed and has a uniform composition with consistent diffusivity properties. The only resistance to diffusion is assumed to be via the PTFE membrane, whether coated, fouled, or neither. Despite the fibrous, spindly, or porous nature of both the ZLs and FLs, the solution-diffusion model can be used to effectively model these differing volumes [22].

2.3. Results and Discussion

2.3.1. Surface Preparation

The GL solution was initially prepared by pouring it into 50 mL falcon tubes which were completely filled with PDA or PDA/PEI solution. A pH of 8.5 has been traditionally used as it is the typical pH of saltwater environments [23]. The brimming of this container was important as it allowed for a double-sided coating on each PTFE membrane. Additionally, it allowed for the inclusion of multiple PTFE membranes in one falcon tube. The literature completed the grafting stage in a 2mL Eppendorf tube for smaller inflexible membranes [15]. This tube sizing, however, would not work for wider and thinner membranes, which would stick to the Eppendorf tubes' interior wall due to the PTFE's hydrophobicity, yielding a single well-coated obverse and a poorly-coated reverse. Nonetheless, the addition of several membranes in each falcon tube was problematic as while many sank in the GL solution, others bound together and floated, creating patches with little coating. However, a double-sided membrane would be more important for AF tests rather than DO tests, as a fouled space adjacent to an antifoulant-coated region will allow for the latter to be more easily colonized [24]. Thus, due to water's high surface tension, the PTFE's hydrophobicity, and the samples' low mass, the 10 μm films cannot be submerged for even coatings

on both sides. Each membrane was instead floated in sealed Petri dishes filled with GL or ZL solutions, allowing for faster DO testing and more uniform coatings.

Increasing the reaction time of PDA and PDA/PEI results in a darker substrate colour, while PDA/PEI samples formed with an additional thin film on the substrate mixture's surface. What were presumed to be large clusters of high MW zwitterions were difficult to dissolve and were, therefore, not used in the coatings. The literature suggested temperatures well above 60°C, the optimized reaction temperature, would permit dissolution, but it also suggested that this could cause degradation of the polymer chains [25]. Fowler et al. found that lower molecular weights of PEI improved the deposition of PDA/PEI conjugates to the PTFE surface, thus increasing the possible sites where zwitterions could attach [15]. Although zwitterion purification was performed, this was not strictly necessary to maintain AF properties [26]. In preparation for lyophilization, the solution was frozen at -4°C, then moved to a -80°C freezer adjacent to the lyophilizer, but in a different building. This two-stage freezing process was necessary to prevent melting of the prepolymer before lyophilization, given equipment constraints, and possibly influenced later XPS characterization of the PGS powder. In addition, the coatings were able to be produced on the order of CAD \$1 per membrane, indicating that these coatings could be a relatively inexpensive addition to future sensor applications.

2.3.2. Surface Hydrophilicity

Figure 7 shows selected WCA measurements for bare PTFE, two GL, and two ZL samples. After waiting for approximately one minute, the WCA for all samples except PTFE, +PDA, and +PDA/PEI were reduced to around 0-1° and were unable to be resolved by the software. PTFE WCA remained consistently stable at 106.6°, +PDA stabilized at 37°, and +PDA/PEI stabilized at 6°.

The base PTFE membrane is hydrophobic. Literature records PTFE with a CA of 105° and above, but this depends on the method of preparation and, thus, the surface morphology [15, 27-29]. It is observed that the addition of an extra parameter to each coating increases hydrophilicity and decreases WCA of surface, thus lowers the surface energy between water and any potential foulant. However, a greater amount of zwitterion marginally increases hydrophilicity, and there is not a noticeable difference between changes in hydrophilicity at the examined zwitterion grafting times. Indeed, it has been shown that the benefits of increased grafting time begin to slow after 12 hours and become negligible after 48 hours.

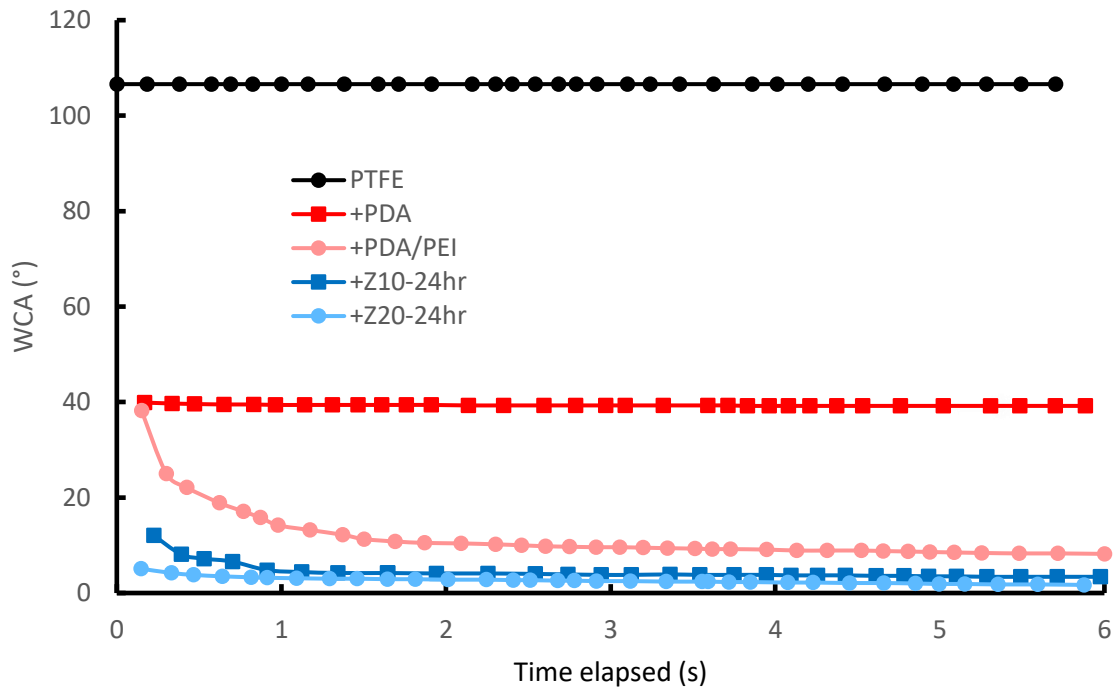


Figure 7. Selected coating WCA measurements. A single typical measurement is shown here.

2.3.3. Scanning Electron Microscopy

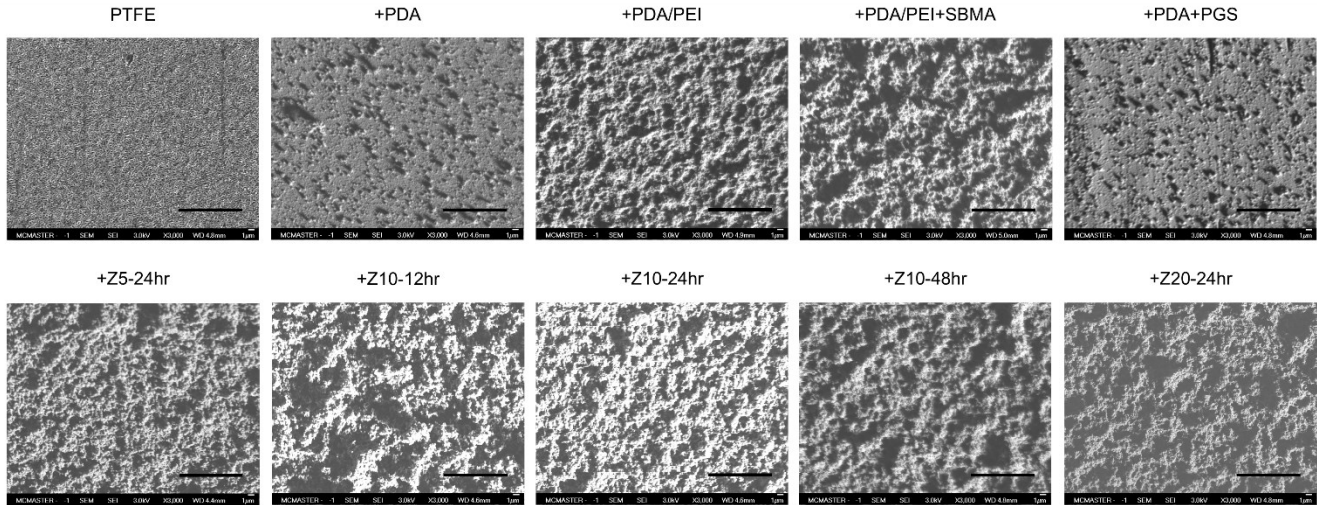


Figure 8. FESEM micrographs of the bare PTFE membrane and each of the nine coated samples. Images were taken at 3000x magnification. Scale bar represents 10 μm .

Figure 8 presents clear morphological differences between uncoated and coated samples. Imaging bare PTFE reveals small ellipsoid granules measuring around 100 nm x 500 nm, likely from the sputtering process performed in the original film fabrication process. A similar difference was observed between PDA GL samples and PDA/PEI samples. PDA GL samples present a mostly flat topography, smoother than that of PTFE, punctuated with larger grains of PDA up to 1 μm in size, while PDA/PEI samples are much rougher. No obvious differences are noted between coated samples. Literature has indicated the ability to achieve smooth ZLs, and as no difference is noted between +PDA/PEI and any sample using PDA/PEI as a GL, suggests that the ZL does not smooth out the surface, but portrays the underlying morphology [30]. FESEM is limited in its ability to characterize coatings of different thicknesses or type. Cross-sectional images could reveal an approximate magnitude of thickness. However, the thin uncoated and coated substrates were sensitive to higher magnifications, especially electron beam strengths above 3 kV, degrading the surface. Additionally, attempts to take cross-sectional images were unsuccessful due to material

necking when undergoing liquid nitrogen membrane cracking procedures. As such, AFM was deemed more helpful in determining coating thicknesses.

2.3.4. Atomic Force Microscopy

The chosen 1:3 sample aspect ratio allows confirmation that the scanned site is indeed at the coating boundary, as it can be difficult to detect given the extreme topography of each coating. It also allows sufficient surface detail to be processed on either side of the coating drop-off for further analysis. The chosen aspect ratio also ensures good consistency of the sample site and enables taking multiple cross-sections of the sample site without sacrificing the time required to get a typical 1:1 aspect ratio image. Additionally, as these surfaces are rough, which may cause large artifacts to appear on the image, a smaller image size increases the likelihood of achieving an artifact-free image. No consideration was given to the 'baseline' topography on PDA GL samples, given that the peaks that appear will theoretically contribute to raising the diffusion coefficient proportionally to layer thickness.

Although it is possible to take scans larger than 20 μm , larger images were not analyzed for several reasons. Firstly, the topography biases upward for larger scan sizes. Scanning a wider area while maintaining scan rate ensures that, due to the mountainous topography of the samples, many crevasses or cliffs that may allow for quicker mass transfer are instead smoothed over, resulting in a perceived higher average thickness. Second, larger scans require an increase in gain for effective surface tracking, but this comes at the cost of smoothing out the surface, resulting in a less detailed image. Finally, larger scan sizes wear out the AFM tip much quicker. AFM Images were not taken for environmentally fouled samples as they were too thick and rough for the tips, instead determining thickness using OCT.

In preparing samples, tape removal did not result in any deformation to the substrate and the coatings below were easily displaced. Most surfaces were difficult to image, as whenever they dried, they began to curl upwards, even after fixing with GA. This movement risks damaging the probe, as improper selection of a surface can result in damage to the probe, as well as producing incoherent images.

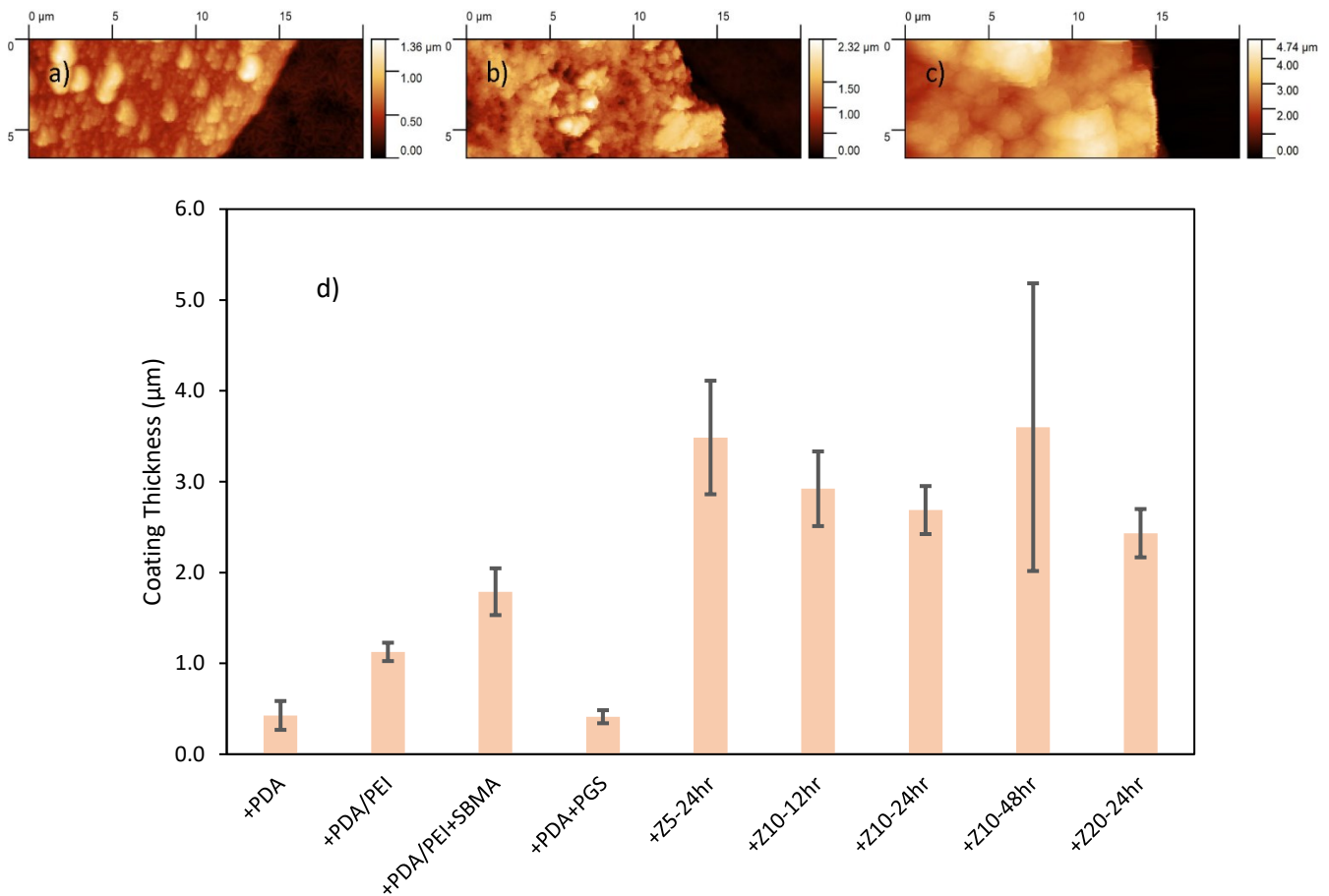


Figure 9. AFM scans on select coating surfaces: a) +PDA b) +PDA/PEI c) +Z10-Mid. d) Average coating thicknesses of all nine polymer coatings. Error bars are the standard deviation of height differences across three cross sections, averaged across three membrane samples (nine total cross sections per data point).

Figure 9 a) through c) shows the distinct edges present between coated and uncoated sample regions, simplifying thickness analysis. Surface morphologies correspond closely with those found in the literature [31]. Large, uniformly round particles exhibited from GL images likely form in solution before being slowly deposited over time, increasing the surface roughness,

as also seen in the FESEM micrographs [31]. Figure 9 d) indicates that the addition of most GL coatings increases the thickness of the coatings. +PDA coatings alone range around a few hundred microns. This thickness is drastically increased with the addition of PEI as a crosslinker. Adding SBMA to the PDA/PEI GL resulted in a half-micron increase in thickness. As this SBMA is monomeric, it should adhere in a monolayer to the PDA/PEI surface and, thus, should not noticeably increase thickness. This observation may suggest clumping of SBMA to the GL, or this may be caused by considerable variation in the measured sample. The latter seems more likely, given that the morphology does not significantly change between the two samples. Similarly, adding PGS zwitterion to a PDA GL oddly resulted in no significant change in thickness.

The combination of PDA/PEI GL with a copolymer ZL results in a significant increase in coating thickness of at least 1 μm , resulting in thicknesses around 3 μm . However, there is no significant difference between any of these coatings, though it appears a slight reduction in thickness occurs for increasing zwitterion concentration. As stated earlier, the significant increase in coating thickness does not correspond with what is observed in less modified GLs and ZLs. It appears as if the density of PDA/PEI complexes decreases, increasing GL void space due to the extreme branching of polymers, allowing zwitterionic chains to attach within the GL more easily.

OCT thicknesses for +Foul14 and +Foul60 samples were determined to be $59 \pm 11 \mu\text{m}$ and $160 \pm 23 \mu\text{m}$, respectively, with uncertainty representing standard deviation of triplicate samples. It was not possible to directly discern the fouling-substrate boundary for any sample, so thicknesses were determined by placing an unfouled substrate beside a fouled one, as shown in Figure A.2. Ellipsometry was attempted as a method to further quantify and verify coatings. However, no consistent results were obtainable due to the extreme surface roughness of any surface. Ellipsometry has been previously performed with thin polymer brush layers over silicon wafers,

indicating that zwitterionic coatings provide smoother surfaces than just the GLs [30]. The general roughnesses of these surfaces, at least in the manner prepared here, suggest much to be desired regarding AF abilities.

2.3.5. Elemental Analysis

Elemental analysis results generally reveal a significant prevalence of carbon for PTFE and +PDA samples and an increase in nitrogen, hydrogen, and sulfur for all other samples. The validity of these results can be assessed through analysis of the base PTFE sample. As each carbon in a PTFE polymer is attached to two fluorine atoms, 12 g/mol out of 50 g/mol of the sample, or 24%, is a carbon atom, which aligns with what is observed in Figure 10, and thus the remaining unknown atoms can be assumed to be fluorine.

Elemental ratios of PGS also reveal a correct proportioning of S:N at 2.28 compared to an expected 2:29, confirming the presence of SBMA. An assessment can also be made of the mass percent composition of each constituent monomer of PGS. SBMA is the only monomer with sulfur and nitrogen, containing one atom each, taking up 16.55% of the mass of SBMA. Given that the combined masses of sulfur and nitrogen in PGS is 13.63% according to elemental analysis, a total of 82.37% SBMA and 17.63% GMA is present in the sample, or a 1:4.67 mass ratio GMA/SBMA, corresponding to a molar ratio of 1:2.39. As such, the GMA is over-represented in the analysis compared to the expected molar ratio of 1:4. The ambiguity of the unregistered molecules may partially explain this. Calculated in another manner, a C:S ratio of 12.57 reveals a primarily SBMA composition, as the pure SBMA C:S ratio is 11, while a 1:1 monomer ratio yields a C:S of 18. As such, about 14.23% of the sample is GMA, or a GMA:SBMA ratio of 1:7.02. Analysis of relative percentages of the other molecules does not yield further convincing results. GMA and SBMA exhibit both around 7% hydrogen by mass and 34% and 29% respectively for oxygen, so they

cannot confidently be used for further analysis. However, elemental analysis reveals 44.62% carbon for PGS, lower than either of the mass percentages for either of its constituent monomers (47% for GMA and 59% for SBMA), certainly suggesting that adventitious carbon on the samples is not to blame for the monomer ratio disparity. However, a limitation of this characterization is that the samples are recommended to have high homogeneity, so exact quantifications of other membrane samples should be more difficult to discern; both the PTFE and PGS samples are relatively homogenous, so this should not be a cause for the discrepancy. In other samples, any change in composition is challenging to see, especially at low coating thicknesses. For example, in Figure 9, a +PDA coated sample only comprises approximately 1/20th of the sample's volume. In contrast, +Z5-Mid comprises a quarter of the volume, but given the porosity of these samples, the coating weights in these samples will account for less than the volume compositions.

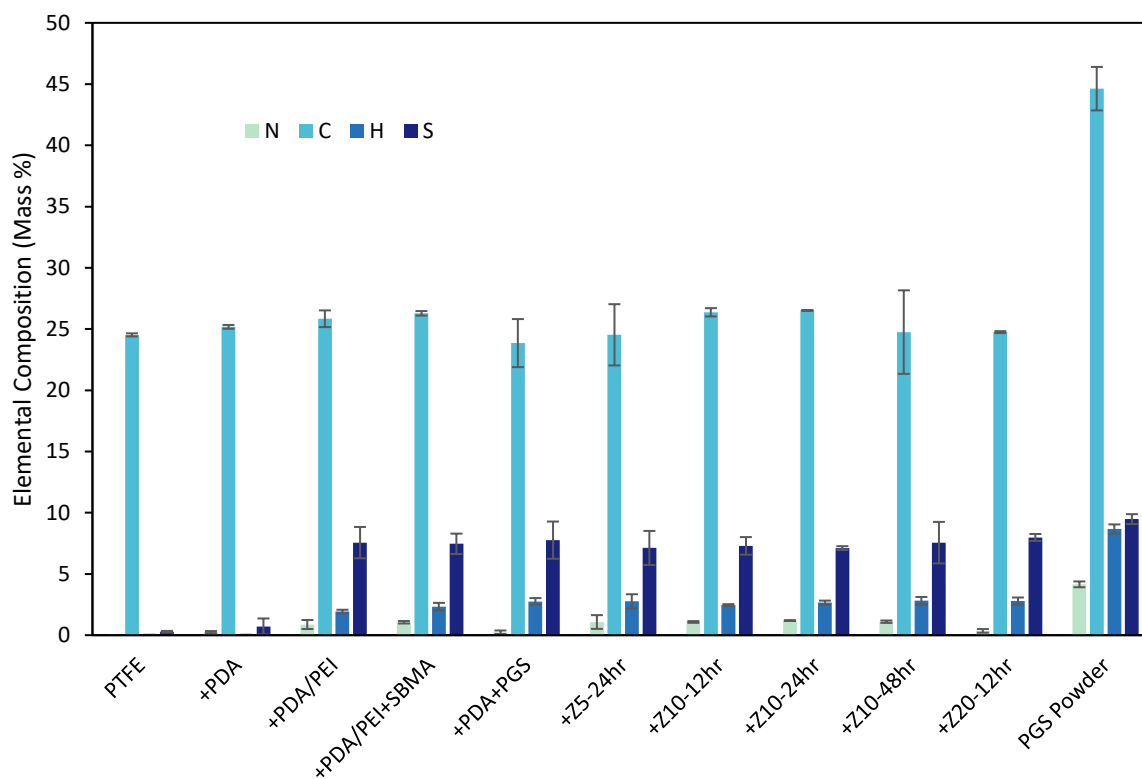


Figure 10. Elemental composition of samples by mass percent listed for nitrogen, carbon, hydrogen, and sulfur. Error bars represent standard deviation.

The carbon composition does not change significantly between samples, except for PGS, which lacks a PTFE backing layer. Non-carbon elements should lower the relative percentage of carbon, but this is not always the case; it suggests that the coating composition on each sample is too small to make a significant difference in carbon content, especially as carbon will already be present as the primary atom in all coatings.

Nitrogen in the samples is generally indicative of a strong presence of PEI, which is visible from the data. +PDA and +PDA+PGS exhibit around three to four times less nitrogen content than PEI-containing samples, which have about 1% nitrogen. Interestingly, +PDA records some nitrogen content despite the element not being present in any capacity. Similarly, +Z20-12hr possesses low nitrogen content. It is likely that although this decrease corresponds with an increased density of zwitterion in the sample, this is a coincidence as the nitrogen content should increase along with the sulfur increase observed, which is not observed. PGS samples show a marked increase, however, at 4.2% nitrogen. This nonetheless corresponds with a composition lower than either constituent monomer but is closest to that of SBMA, with 5.0% by mass.

However, observing sulfur patterns contradicts some previously held hypotheses and observations. There is a marginal difference between the zwitterionized sample with the lowest sulfur content (+Z10-24hr, 7.11%) and highest of all samples (PGS powder, 9.48%). While the latter value is obtained from a sample without PTFE, the first (and the rest of the zwitterionized samples) seems to suggest that PTFE has a marginal impact on the sample's composition (some 20%), which does not make sense, given previous AFM data indicating that PTFE will account for a majority of sample composition regardless of sample thickness. A second, more surprising disparity, is the clarity with which it appears for +PDA/PEI, given there should be no sulfur here at all. This is even more surprising given that +PDA/PEI samples were tested from five samples

in three different sample batches over three experimental days. It is therefore improbable to be human error, as other samples show results within the realm of possibility. Similarly unlikely is cross-contamination between samples, as this was usually sampled before any other sulfur-containing compounds.

Elemental analysis is occasionally used to confirm the zwitterionic functionalizing of a polymer, but characterizing a surface itself is not recommended [32, 33]. Therefore, although elemental analysis can provide a somewhat effective composition analysis of simpler samples and confirm the grafting of zwitterions to the PTFE surface, it cannot reliably differentiate between zwitterionic samples themselves.

2.3.6. X-Ray Photoelectron Spectroscopy

XPS was used to quantify the sample surface chemistry of the first eleven samples in Table 2 and is ideal for quantifying approximately the top 10 nm of a sample [26]. However, while elemental detection is most effective at the uppermost layers of the sample, signal strength exponentially decreases as a function of depth. EAL correction assumes the analysis of a bulk material with no overlayer, which is not appropriate for all samples. As the escape depth correction factor scales exponentially in a sample and the zwitterionic “overlayer” is the sample layer of interest, the effect of the bulk material on signal strength is mitigated [34]. Thus, due to sample coatings varying greatly in thickness across the scanned area or defects forming in the film likely due to shipping and handling, the PTFE underlayer appears in some characterizations. As the presence of fluorine in the samples is only derived from PTFE, and fluorine’s presence in the polymer is double that of carbon’s, PTFE can be removed from the XPS spectra. These “background-corrected” atomic concentrations derived from the deconvolutions of the primary XPS signal are shown in Table 2,

while the original concentrations are found in Table A.1. As the provenance of Si is ultimately unknown, its concentrations remain unaltered.

The PTFE, +PDA, and PGS powder samples all constitute relatively homogenous coatings, so their atomic percentages should be easily verifiable. The PTFE sample aligns well with the expected atomic percentages of a 2:1 F:C ratio, with only a 0.57% discrepancy. Similarly, a simple dopamine molecule contains 8 carbon atoms, 1 nitrogen atom, and 2 oxygen atoms, corresponding to expected percentages of around 73%, 9%, and 18%, respectively, which fits the data closely. Finally, counting the constituent atoms of SBMA and GMA from Figure 5, assuming a 1:1 ratio, gives expected compositions of 64% for carbon, 29% for oxygen, and 4% for both nitrogen and sulfur, which aligns well with the PGS powder sample. It is interesting to note that SBMA and GMA seem to indeed exist in a 1:1 ratio on this sample, despite being added in a 4:1 molar ratio, and despite elemental analysis confirming that ratio. The new ratio suggests a lack of uniformity in the powder used for analysis. Since the scanning area was very small (about 0.25 mm²), it is likely that several PGS crystals with higher GMA content happened to appear in only this scan area, even though the powders had been mixed for uniformity. Given that following polymerization the samples were frozen first in a -4°C freezer, then in a -80°C freezer in preparation for lyophilization, the slow freeze of the first cycle would allow for denser polymer chains to sink to the bottom before lyophilization occurred. As such, low- and high-density chains would have separated and led to an inaccurate SBMA and GMA ratio in the XPS results. Elemental analysis was likely to be more accurate in determining monomer composition as, in that case, zwitterions were grafted from dissolved polymer. Thus, the monomer compositions were averaged throughout the dozens of prepared sample slices. However, elemental analysis nonetheless over-represents GMA in the earlier analysis.

Table 2. Relative elemental percentage concentrations of bare PTFE, coated PTFE, and PGS powder samples as determined by XPS after removal of PTFE background from coated PTFE samples.

	C 1s	F 1s	N 1s	O 1s	S 2p	Si 2p
PTFE	32.76	67.24	-	-	-	-
+PDA	71.93	-	7.30	20.59	-	0.18
+PDA/PEI	69.12	-	15.23	15.65	-	-
+PDA/PEI+SBMA	67.52	-	11.29	20.16	1.03	-
+PDA+PGS	61.41	-	5.27	26.91	2.58	3.83
+Z5-24hr	65.60	-	7.84	23.57	3.00	-
+Z10-12hr	64.51	-	8.27	24.36	2.87	-
+Z10-24hr	64.99	-	8.09	23.86	2.74	0.32
+Z10-48hr	65.27	-	8.32	23.58	2.84	-
+Z20-24hr	64.93	-	6.79	24.51	3.78	-
PGS Powder	64.26	-	4.19	25.84	4.95	0.75

As PEI is added to the PDA sample, nitrogen content doubles at the expense of oxygen and carbon. A pure PEI sample would register one-third of nitrogen content. Thus, the nitrogen content of +PDA/PEI suggests around 30% of the registered nitrogen is derived from PEI and the rest from PDA. In fact, PDA and PEI were added in a 2:1 ratio, thus the characterization is reasonable. The nitrogen content is greatest in +PDA/PEI as PEI is the most nitrogen-dense polymer. Similarly, as oxygen is only present in PDA, the reduction of oxygen content is directly proportional to the amount of PEI added, but this suggests that the PDA:PEI ratio is close to 3:1 instead.

The smallest amount of sulfur is observed on +PDA/PEI+SBMA compared to other zwitterionized samples. While the ZL itself presents greater sulfur content due to the absence of GMA, the layer is very thin as no polymerization occurred, therefore the overall sample sulfur content is low. There is also a distinctly above-average nitrogen content for +PDA/PEI+SBMA due to two factors. Firstly, the ZL normally contains PGS, which does not contain nitrogen, increasing the relative percentage of nitrogen of the remaining SBMA-only coating. Secondly, the thin SBMA coating allows a greater signal from the PEI-rich GL, which is why elevated nitrogen does not appear in any subsequent samples. The opposite factors are exhibited for +PDA+PGS's

low nitrogen content. +PDA+PGS presents oxygen content slightly higher than the rest of the PGS-coated membranes also due to the lack of nitrogen signal from the GL.

No change in sulfur concentration is noted as a function of zwitterion grafting time. Similarly, little change is seen as zwitterion concentration increases, except for in high-concentration coatings. Comparing the sulfur concentration in +Z20-24hr with the PGS powder suggests that about 76% of the signal is derived from the PGS layer and the rest is acquired from the GL. Given that the individual thicknesses of GLs and ZLs are usually on the order of a micron, XPS's relatively limited surface penetration suggests a high level of ZL porosity for XPS penetration to occur. This is also evident as the increasing sulfur concentration seems to partially arise at the expense of nitrogen, which suggests a shielding of the GL.

Analysis of C 1s, F 1s, N 1s, O 1s, S 2p spectra reveal approximate expected concentrations of all major bonds. Locations of all BE data is found in Table A.2 to Table A.5, while relative bond ratios are found in Table A.6 to Table A.9. Note that while larger peaks can be reasonably confirmed to be accurate, the accuracy of smaller peaks are less secure and are but rough estimates based on extensive literature analysis. Each C 1s analysis features primary peaks centred around lower BEs corresponding to C-C, C-N, and C-O, together comprising at least 77% of bonds. C=C and C-H bonds are not parsed further in this data for a few reasons. Firstly, these bonds are generally difficult to separate from C-C signals, all centered at 284.6 or 284.7, which is made even more difficult by the complexity of the analyzed product [35-39]. Secondly, identifying these peaks does not reveal new information about the successful attachment of either GLs or ZLs, as it is other bonds that are altered as chemical changes take place. Figure 11 shows how adding successive layers alters the signal shape and the relative prominence of major deconvolution peaks. Around two-thirds of bonds in a DA molecule are comprised of C-C, C=C, or C-H bonds, the

percentage lowering slightly upon polymerization. Similarly, upon polymerization, C=N and C=O bonds arise due to indole formation, as well as the oxidation reactions, respectively. About half of all bonds in PEI are C-N bonds, and a leftward peak shift is accordingly seen in the +PDA/PEI sample. π - π interactions are seen around 291 eV due to PDA-PDA stacking [31]. While BEs are mostly affected by α bonds, β bonds also can affect BEs, especially when several highly electronegative elements occupy these positions [40]. For example, carbonyl β -carbons contribute to the intensity of amine signal strength [41]. As such, an unusual peak at 288 eV is thought to derive from a complex created due to binding with Tris buffer, resulting in one α -nitrogen and three β -oxygen interactions [42]. These interactions remain present in thinner-coated samples and are obscured as ZL layers thicken.

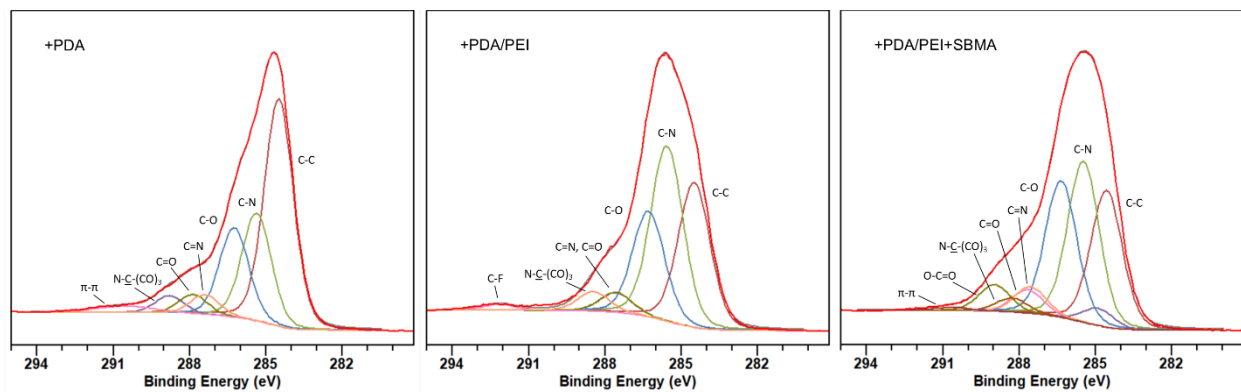


Figure 11. Carbon 1s spectra of +PDA, +PDA/PEI, and +PDA/PEI+SBMA samples.

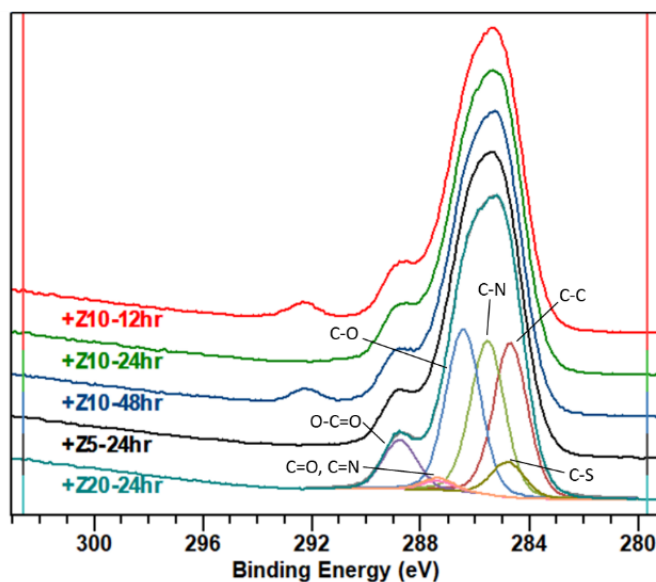


Figure 12. Normalized carbon 1s spectra of ZL coatings. A representative deconvolution is shown for the +Z20-24hr sample. Inconsistent peaks around 292 eV represent C-F bonds from underlying PTFE.

Samples of varying ZL grafting time and composition did not vary in XPS analysis, indicating that these did not have any chemical effect on the coatings. The addition of ZLs is confirmed by a consistent ester peak around 289 eV, replacing the Tris complex at the same BE. This corresponds with an ester on both SBMA and GMA monomers. In addition, the Tris complex signal appears to decrease as the magnitude of the drop in signal at the 288-eV depression may correspond to the increased density of ZL coating given the signal drop at +Z20-24hr and further dropping of the signal on the PGS powder sample, which lacks the Tris complex. Approximately equal amounts of C-C/C-H, C-N, and C-O are implied, where the increase in oxygen content is clearly attributed to the oxygen-rich nature of PGS. A small C-S peak strongly overlaps with that of C-C, with literature suggesting that the two peaks are separated by up to 1 eV [43]. C-S bonds comprise 5-6% of the deconvoluted peak area, near to the expected stoichiometric value of 5.7%. Traces of AIBN, while present due to zwitterionic synthesis, cannot be adequately detected due to its low concentration. Additionally, it is expected that most was washed off during the purification process.

The C 1s and F 1s peaks of 292.3 eV and 689.5 eV, respectively, obtained from the virgin PTFE sample correspond well with those found in the literature, namely a C 1s peak at 292.5 eV and an F 1s peak at 689.6 eV [44]. As previously mentioned, coating defects in other samples produced unexpected additional peaks in both C 1s and F 1s analysis, skewing the expected compositional results. However, this was shown to be advantageous in confirming the successful attachment of GLs. As with the Tris complex, extra electronegative atoms within close proximity of the CF₂ interaction increase the signal BE, as shown in Figure 13 [45]. Depending on the sample, as many as 25% of fluorine interactions are affected by these additional interactions, suggesting an extremely tight bond between the substrate and GL.

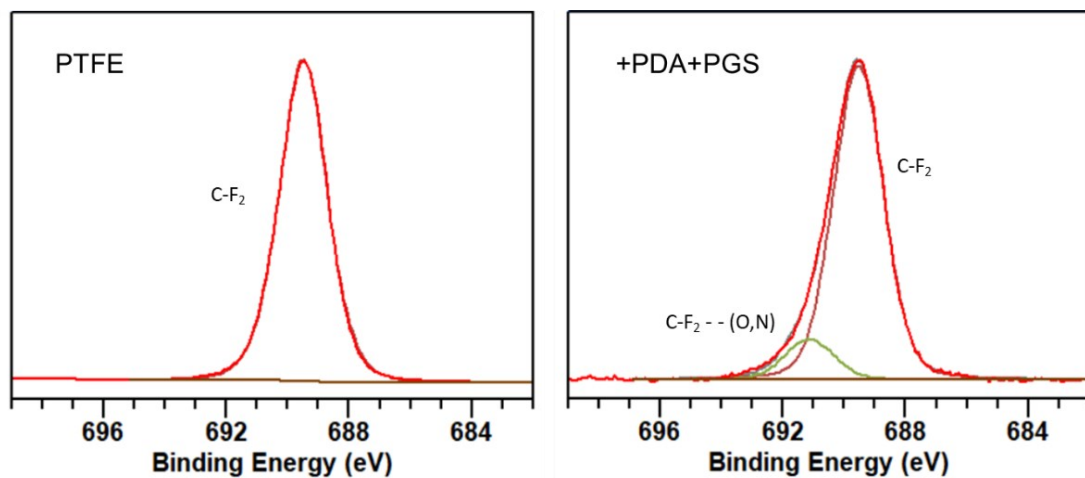


Figure 13. Fluorine F 1s from bare PTFE showing a single C-F₂ peak, and +PDA+PGS showing a C-F₂ peak and a C-F₂ peak with non-bonding interactions with other highly electronegative atoms.

All coated samples show a variety of N 1s peaks. Analysis of GL samples as seen in Figure A 6 primarily shows secondary amine peaks, with small primary amine peaks for uncyclized PDA and terminal PEI branches, and small imine peaks due to indole formation and the creation of PDA/PEI complexes. A small π - π satellite peak is characteristic of some aromatic polymers and appears around 406 eV [46]. ZL samples show an elimination of the primary amine peak, a reduction of the secondary amine peak and the addition of a prominent quaternary amine peak, as

shown in Figure 14. It is worth noting that the quaternary ammonium (QA) cation appears at the same peak as that of primary amines [26, 47]. Each appears in significant amounts in samples where the other should be absent. As such, it therefore makes sense that PGS powder exhibits a large QA peak, but with a small imine peak which does not appear present in any literature, suggesting a breakdown in the QA. The change of bond types is also visible as ZL concentration changes. The relative size of QA peak is indicative of the relative concentration of zwitterion. All membranes coated in 10 mg/mL zwitterion solution present identically, with a higher relative QA peak in +Z5-24hr. However, +Z20-24hr exhibits a doubling in QA peak area indicative of a higher amount of zwitterion. Similarly, a thicker zwitterion coat reduces the secondary amine and imine peaks as the underlying GLs are covered.

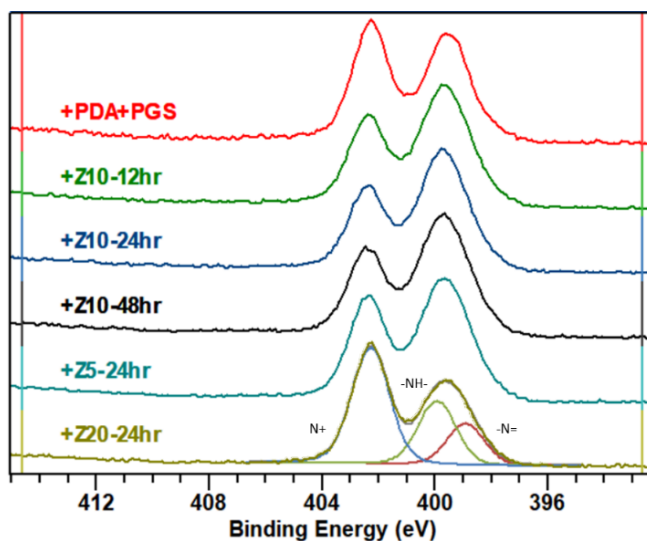


Figure 14. Normalized nitrogen 1s spectra showing a characteristic SBMA signal for ZL coatings. A representative deconvolution is shown for the +Z20-24hr sample.

Figure A.7 and Figure 15 show the deconvolutions of O 1s signals. +PDA coatings show the presence of both carbonyl and hydroxyl groups, indicating the undergoing of oxidation reactions for some one-third of PDA monomers [48, 49]. An increase in the relative amount of carbonyl groups is seen in the +PDA/PEI sample due to amine attachment via condensation

reactions [15]. Samples with ZLs all suggest the presence of carbonyl and hydroxyl groups, as well as ester and sulfonate groups. The former two appear almost entirely from PDA/PEI interactions, as suggested by similar carbonyl/hydroxyl peak ratios in Figure 15 to those in the +PDA/PEI sample. The similarities also suggest a very porous ZL. Similarly, the carbonyl/hydroxyl peak ratio in +PDA+PGS is like that of the +PDA sample. The low relative prominence of both ester and sulfonate peaks also suggests that most signal is derived from the GLs. The ester/sulfonate peak ratio ranges from around 2-4 per sample, indicating a higher concentration of GMA to SBMA. Other side reactions are likely partially responsible for the areas of these peaks, given ester and sulfonate peaks fit within literature ranges [50, 51].

S 2p analysis as shown in Figure A.8 confirms the presence of a sulfonate group for each sample where SBMA is present. The peaks consist of a SO_3^- 3/2 peak around 167.4 eV and a SO_3^- 1/2 peak at 168.7 eV with an area ratio of 1:2, some 4 eV higher than elemental sulfur [51-53]. Silicon was noted in a few samples despite not appearing anywhere in the constituent GL or ZL monomers. It is possibly a vestige of the SBMA manufacturing process as it appears clearly in the PGS powder sample, while also being most prominent in +PDA+PGS. Figure A.8 suggests that as the convoluted silicon peak centers around 102 eV, the signal most likely represents a Si-C structure [54]. A corresponding broadening of the C 1s peak on this sample at 283.8 eV also suggests this to be the case. In general, XPS analysis confirms the successful grafting of ZLs and GLs to the substrate.

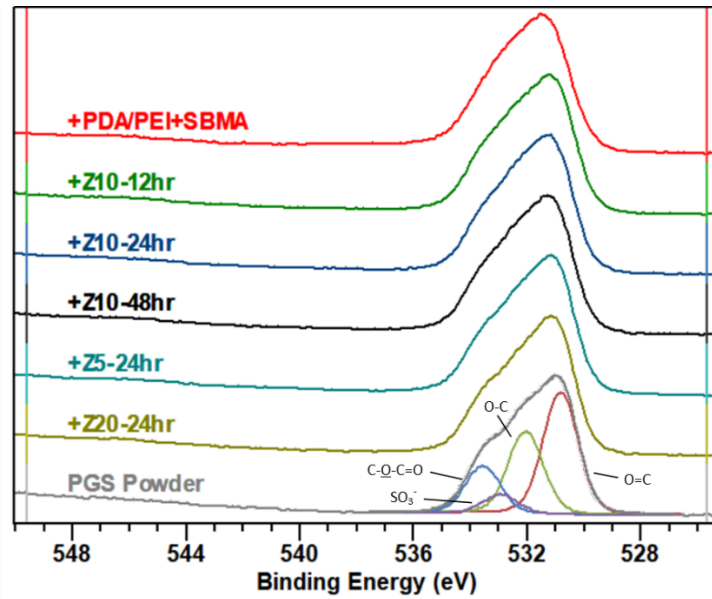


Figure 15. Normalized oxygen 1s spectra showing a characteristic SBMA signal for ZL coatings. A representative deconvolution is shown for the PGS powder sample.

2.3.7. Oxygen Permeability Tests

Figure 16 shows typical timeseries data for a bare PTFE experiment. The differences in magnitude between OR and OP curves are due to differences in the water volumes of the two containers. Mass balance calculations consistently suggest that there is a consistent discrepancy between DO transfer out of the OR tank and the incoming DO to the OP tank. In the case above, the ratio of OR mass transfer to OP mass transfer is 1.47, but other experiments reveal ratios up to 10. This large discrepancy suggests a few critical issues with the device's functionality. Firstly, the gaskets that prevent gas transfer between the containers and lids have a limited lifespan. As they undergo transverse compression and relaxation, the material loosens, allowing greater gas permeability. Additionally, as the OR tank's partial pressure is higher than the OP tank pressure and that of the system's surroundings, oxygen consistently permeates through the relatively thin studied membrane and the thick PMMA walls. While the literature indicates a higher oxygen Q through PTFE compared to PMMA, the surface area of the container is over an order of magnitude higher than that of the membrane. Additionally, the tendency for OR-tank oxygen to flow away from the

membrane increases as the concentration in the OP tank increases, thereby reducing the partial pressure difference across the membrane. This behaviour is especially prevalent during tests with longer running times. Samples with more dense coatings also further minutely redirect flow away from the OP tank. Another issue arises from the concentrations at which steady states are reached. While Figure 16 shows an extreme example of the difference in OR-OP steady state concentrations of some 20 mg/L, most tests encountered a steady state difference of around 10 mg/L. Theoretically, no significant difference should emerge. This discrepancy is more challenging to explain. Perhaps oxygen is preferentially adsorbing to the PTFE surface or remains absorbed within the PTFE itself, though literature does not suspect this to be the case [55, 56]. However, regardless of the unideal LOC performance, the consistency of the experimental procedure and clear differences between mass transfer parameters of different coatings, as described below, indicate that conclusions can be drawn from this procedure.

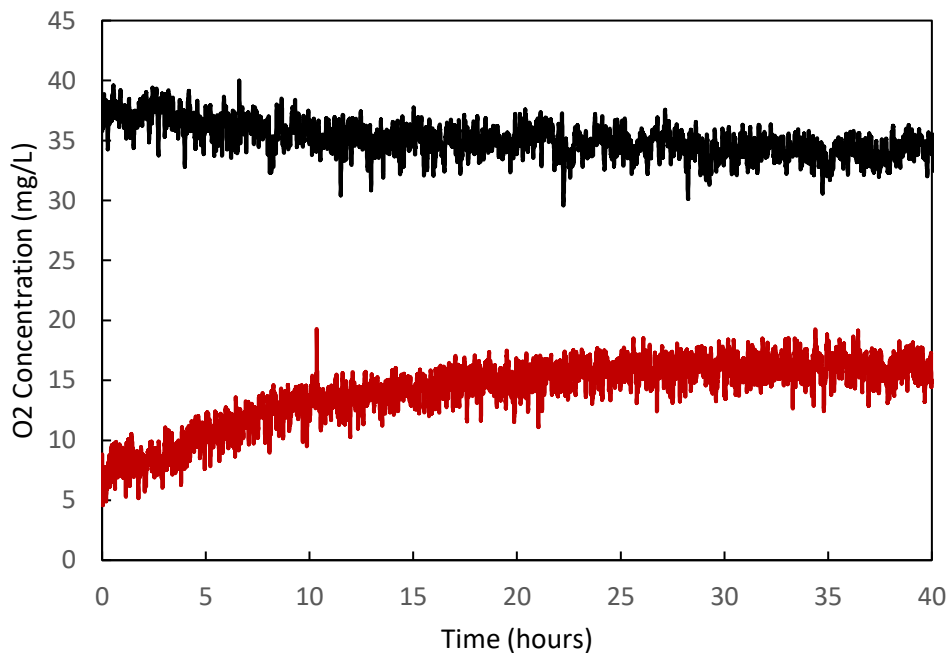


Figure 16. Profile of a typical LOC test for bare PTFE, showing the initially OR tank (black) and OP tank (red).

Construction of the LOC system was chosen as it was technically simple to fabricate while still being similar in concept to traditional gas differential pressure testing. However, refining the functionality of the LOC system posed several challenges. As the difference in partial pressure across a gas membrane proportionally affects its flux, increasing the pressure in the OR tank would speed up the experiment time as it was known that the duration of experiments would be orders of magnitude more time when compared to traditional gas permeability experiments due to both the low concentration of DO involved and the lower atmospheric partial pressure gradient. An obvious solution to expedite this process was to bubble oxygen gas into the OR container, which increased ppO_2 by nearly a factor of five and eliminated the need to displace oxygen from the OP side. Decreasing the volume of the OP half to 400 mL also proved helpful. Another solution involved thinning the membrane from the mm scale to the μm scale. However, a thick membrane offers mechanical stability against high pressure differences. This became apparent after bubbling ceased and the OR tank was sealed. Sealing the tank too quickly led to insufficient degassing, increasing the pressure in the OR tank. While this increased the partial pressure gradient across the membrane by increasing oxygen solubility in the OR tank, the membrane suffered severe plastic deformation, then broke within 30 minutes of the start of the increased pressure tests. The 5-second degassing interval was determined as this was the lowest time where plastic deformation of the membrane was not observed during testing. Waiting longer than 5 seconds resulted in a decrease in OR tank DO concentration. To prevent deformation, a steel mesh was installed on the OP side of the membrane, but this led to no concentration increase on the OP side as the mesh likely created a small gap for gas to escape the LOC system. In any case, the final pressure within the OR tank before membrane rupture is unknown when degassing was not performed (though the 15-psig

pressure release valve never activated) and would thus widely vary mass transfer parameters obtained during these experiments, in addition to accelerating OR tank leakage.

The concentration profile over time is clearly shown to vary depending on coating type, as shown in Figure 17. Testing of bare PTFE membranes consistently resulted in the quickest stabilization of DO concentration, followed closely by the +Foul14. The remaining samples appeared to take at least twice as long to stabilize. Supplementary profiles can be found in Figure A.9. PTFE curves exhibited the smoothest data and fit most cleanly to the expected first-order relationship, attributed to the relative uniformity of the material between experiments. Compare this to +PDA, where averaged DO values appear to increase linearly with a small standard deviation until levelling off after 40 hrs, and both +Z20-24hr and +Foul60, which are subject to sudden and prolonged mean deviations. These deviations are not due to sudden changes in DO but appear to be intrinsic to the functioning of each sensor. Similarly, a sinusoidal pattern was often observed in DO measurements, usually oscillating over minutes as much as 1 mg/L, clearly not indicative of a true fluctuating of DO. Tests were concluded upon visual inspection to determine entry into a steady state regime, or in some cases, upon the imposition of automatic operating system updates. As such, some internal variation existed in determining the steady state for each coating type. The implementation of Equation (9) is an attempt to determine steady state more accurately.

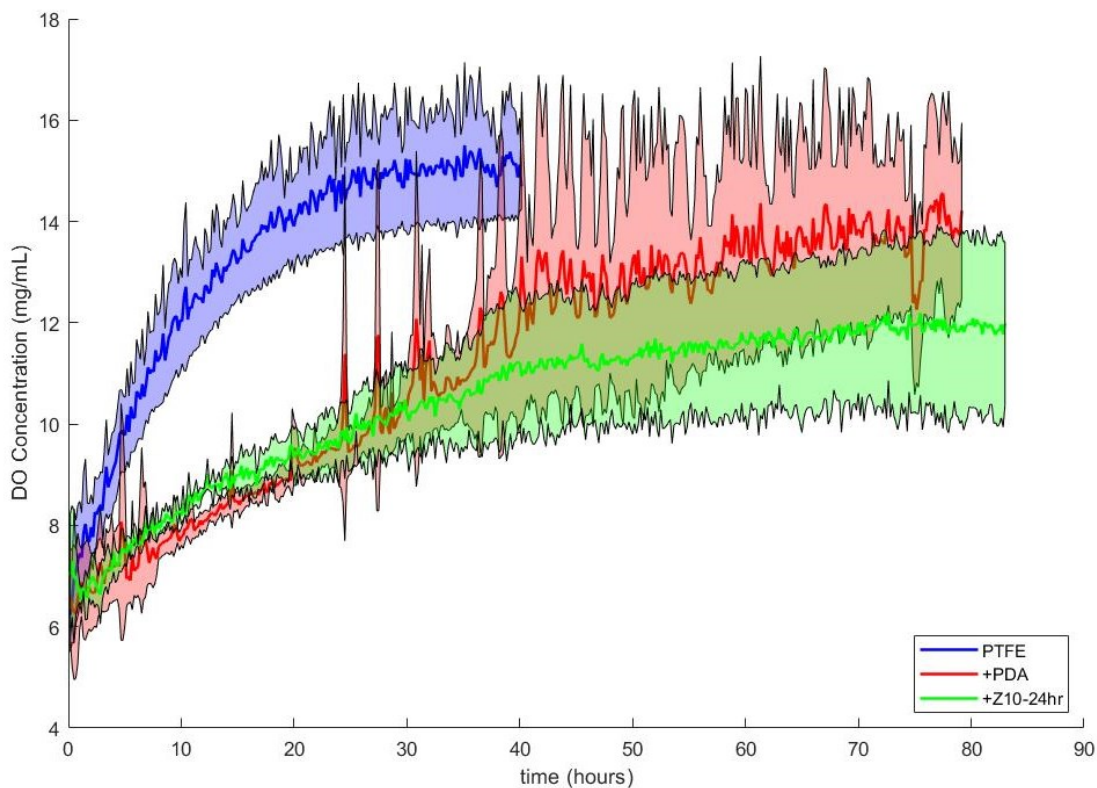


Figure 17. LOC tests for three coating samples, namely PTFE (blue), +PDA (red), and +Z10-24hr (green), taken at averaged 10-minute intervals. Shaded regions represent the standard deviation of three trials.

For comparison of mass transfer parameters, traditional gas permeation experiments were performed on PTFE and +PDA samples. Table 3 shows the results of these experiments. Adding a PDA GL halves a sample's permeability, despite the PDA layer being thinner than the PTFE substrate by a factor of nearly 2000. Similarly, the lack of variation in diffusivities between samples is reasonable as diffusion is a measure of a solute's tendency to move through the bulk material, here overwhelmingly comprised of PTFE. As such, the decreases in permeability are primarily caused due to difficulties in oxygen adsorption into the PDA layer. The diffusivities of O_2 through PTFE match those found in the literature to within an order of magnitude, and are within an order of magnitude of similar gases such as N_2 , H_2 , Ar, CO_2 , and NH_3 [9, 18, 55, 57, 58]. The diffusion through the GL cannot be determined here due to its relative thinness, so it cannot

be determined from this data if the low solubility of O₂ into the GL is genuinely the factor limiting permeability or if it is the diffusivity itself through PDA.

Table 3. Permeability (Q), diffusivity (D), and solubility coefficients (S) of oxygen through PTFE adjusted to the experimental run temperature [19]. Adjustments were made using Equation (5) and parameters from [18]. Uncertainty measurements are for the standard deviations of two measurements.

Sample ID	Q, mol/m/s/Pa	D, m ² /s	S, mol/m ³ /Pa	Samp. thickness, mm
PTFE	$5.63 \times 10^{-16} \pm 9.05 \times 10^{-18}$	$2.37 \times 10^{-11} \pm 1.50 \times 10^{-11}$	$2.23 \times 10^{-5} \pm 1.39 \times 10^{-5}$	0.80
+PDA	$2.87 \times 10^{-16} \pm 3.84 \times 10^{-17}$	$2.37 \times 10^{-11} \pm 1.57 \times 10^{-11}$	$1.21 \times 10^{-5} \pm 9.27 \times 10^{-6}$	0.79

Permeability values derived from the calculation of LOC-test time constants (τ) are shown in Figure 18. Permeabilities extend to nearly an order of magnitude beyond those measured by gas permeability tests, and there is no significant difference between any of them except for the unmodified membrane, which has the highest permeability. The tenfold discrepancies in values will be discussed later. Interesting to note is the 76% decrease in permeability from bare PTFE with the addition of a PDA GL as the relative thickness of PDA increases across the membrane (compared to 49% decrease in Table 3). Deriving Q from τ requires knowledge of the steady state value to within 2% accuracy as the steady state condition is assumed to occur after 4τ . However, premature assumption of steady state over the long duration of experimentation may result in misidentified steady state concentrations.

Only oxygen permeability can be calculated using the empirical data method, for two primary reasons. High amounts of signal noise, even after significant curve smoothing, result in Equation (7) being unusable as taking logarithms of negative partial pressure changes over short periods prevents the usual calculating of mass transfer parameters by data linearization. Another method, following gas permeability methods, depends on observing the dead time (Θ) according to Equation (4). While PTFE and +PDA gas permeability tests resulted in an easily observable dead time of 56 minutes due to the thickness of the tested samples, using a 10 μ m film yields dead times in the order of seconds. Indeed, a long dead time would make this film unsuitable for DO

probes. As such, diffusivity and solubility coefficients can only be derived from concentration gradient models.

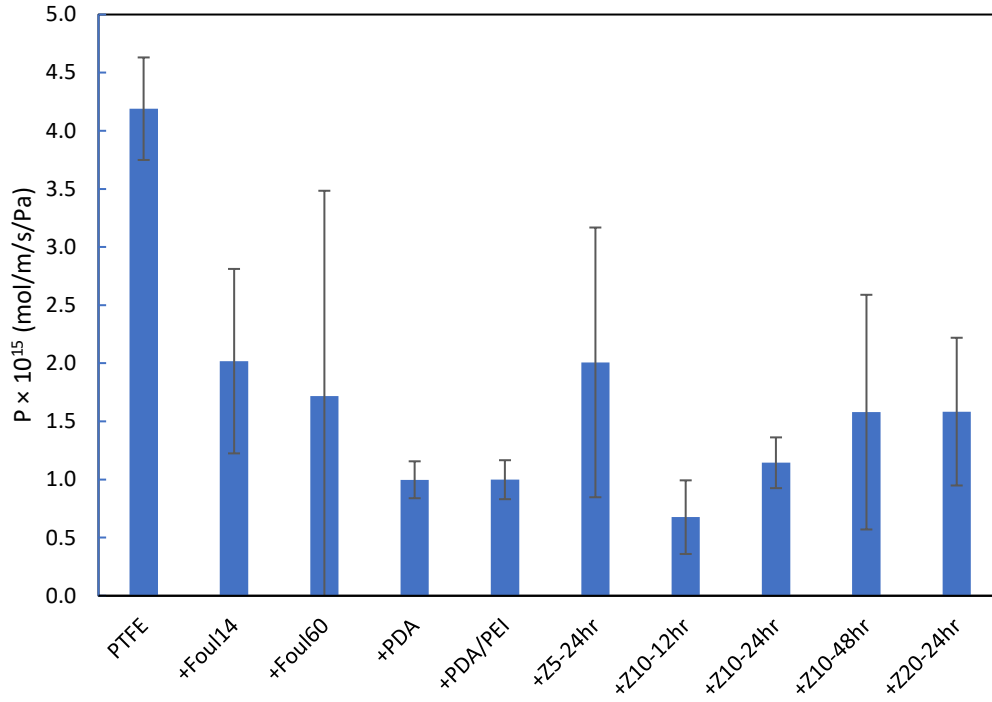


Figure 18. Permeability coefficients as calculated via Equation (8). Uncertainty measurements represent standard deviations of triplicate experiments.

A best-fit concentration profile model was created for each coating, allowing for the calculation of all three mass transfer coefficients as shown in Table 4. It additionally allowed verification of steady state conditions. The calculation of the diffusion coefficient resulted from a rearrangement of Equation (7). However, for D to remain constant, dc and J must change proportionally, which does not occur given that leaked oxygen is accounted for in dc but not in J . Therefore, D appears to decrease over time. Presented diffusion coefficients were calculated at $t = 0$ to minimize errors derived from gas leakage. All model-derived permeabilities fit well with the empirically derived permeabilities despite some evident discrepancies in steady state concentrations. For example, Figure 17 shows +PDA appearing to level off around 14 mg/L, but

the model predicts that steady state conditions occur at 16.3 mg/L. The diffusion coefficient of PTFE is again higher than that of other coated samples, which range within a factor of two of one another. Additionally, the exceptionally high +Foul14 and +Foul60 diffusivities are due to the porous FL being much thicker than the substrate. The low diffusion variance amongst coated samples indicates that there are no differences in oxygen diffusivity despite the variety of GL and ZL configurations, suggesting that the primary resistor of oxygen transfer is the GL. As such, the time to develop these GLs can likely be greatly reduced while not affecting ZL attachment, improving DO transfer [23, 30]. As ZL resistance to DO diffusion is minimal, future use of the LOC setup is moot. However, like FLs, the addition of a ZL itself does introduce signal bias, as shown in Figure A.10. Therefore, the use of zwitterions for long-term AF applications may show biased data upon first use but will slowly outperform an uncoated sensor used for an equivalent amount of time. This bias introduces additional error to the mass transfer parameters found in this work but does not affect the general trends observed.

Table 4. Permeability, diffusion, and solubility coefficients of measured samples, as calculated via concentration models obtained from Equation (9).

Sample	Q ($\times 10^{15}$ mol/m/s/Pa)	D ($\times 10^{11}$ m ² /s)	S ($\times 10^4$ mol/m ³ /Pa)
PTFE	3.865	1.404	2.752
+Foul14	1.716	3.569	0.481
+Foul60	0.920	5.381	0.171
+PDA	0.954	0.342	2.791
+PDA/PEI	0.909	0.314	2.898
+Z5-24hr	1.217	0.443	2.747
+Z10-12hr	0.648	0.223	2.909
+Z10-24hr	1.162	0.378	3.070
+Z10-48hr	1.064	0.368	2.887
+Z20-24hr	1.564	0.497	3.145

While there is not a significant difference between the permeability model and empirical LOC values, a difference of an order of magnitude exists between the gas permeation and LOC tests. It is most likely that a difference in manufacturing techniques is the cause, owing to the

versatility of PTFE's industrial and commercial use. Polymers created via dissimilar manufacturing processes will differ in grain size and thus void fraction, which is the primary manner by which gas passes through PTFE [18]. However, as LOC tests require a thin membrane to lower test time, while gas permeation requires a thicker membrane for mechanical stability, these PTFE products are produced by different methods. The manufacturer was unwilling to disclose details of the thin film fabrication, but the thick membrane is skived from its polymer block [59]. This method of fabrication is used due to PTFE's decomposition temperature being lower than its melting point [60]. Therefore, the extent to which PTFE transfers oxygen directly correlates with a reduction in void space, resulting in the 762 μm having less void space per unit volume than the 10 μm membrane. Similarly, increased OR-tank pressure likely causes these void spaces to grow via tearing, either increasing diffusivity or, as noted earlier, resulting in membrane failure. It has been noted elsewhere that polymer strain can substantially increase mass transfer [61, 62]. The true difference in diffusivities between the 762 μm and 10 μm membranes is also likely to be larger than the displayed values, given much of the pressure gradient from the OR tank was lost, which would result in higher diffusivities. Given that finding the porosity of these films is essential in predicting diffusion coefficients, it will be crucial for future studies to implement and adapt the Kozeny-Carman equation, which is directly applicable to pore-flow flux models, rather than the usual solution-diffusion model [22, 63].

As noted in Equation (5), diffusion is strongly dependent on temperature. While gas diffusion experiments take place over hours within well-controlled temperature conditions, starting ambient lab conditions varied by up to 4°C and were not recorded throughout the duration of experimentation. Raising the temperature from 22°C to 23°C increases permeability by 3.7%. A temperature effect is also exhibited with O₂ solubility in water, where it increases at lower

temperatures. As such, a container filled with cold water saturated with O₂ will gradually expel O₂ as the water warms to room temperature, which explains some supersaturated oxygen levels at t = 0 despite waiting for the water to warm.

The permeabilities of each membrane layer are calculated, as shown in Table 5, using model-derived total permeability values. The permeability of PTFE is four orders of magnitude greater than that of the FLs, which is itself two orders of magnitude greater than the GLs and ZLs. Comparing gas diffusion and samples suggests that reduction in solubilities become more prominent as more layers are added. However, it is impossible to calculate interlayer solubilities with the current data, though it is known that adsorption into the preceding layer will be the rate-limiting process rather than desorption from the preceding layer [64]. Similarly, layer diffusion coefficients cannot be calculated. Despite low GL and ZL permeabilities, GL+ZL coatings show little delay in allowing oxygen to pass compared to real-time oxygen monitoring conditions. Due to time constraints, the AF coatings were unable to be tested in the field. While only two quick tests were performed, one of which is shown in Figure A.10, it is clear that despite the emergence of a 0.5 mg/L bias, there is not a noticeable difference in the shape and of the concentration profiles and that ZLs should not affect DO readings in the environmental monitoring settings. However, future work may seek to reduce GMA concentration in the coatings. The opening of the epoxide when binding to PDA and PEI results in hydroxide and carboxyl groups, which can lead to the accumulation of foulants.

Table 5. Individual layer permeabilities.

Sample	Layer Type			
	PTFE	Grafting	Zwitterionic	Fouling
PTFE	3.865E-15	-	-	-
+Foul14	3.865E-15	-	-	1.012E-19
+Foul60	3.865E-15	-	-	1.472E-19
+PDA	3.865E-15	4.074E-22	-	-
+PDA/PEI	3.865E-15	1.024E-21	-	-
+Z5-24hr	3.865E-15	1.024E-21	2.872E-21	-
+Z10-12hr	3.865E-15	1.024E-21	1.164E-21	-
+Z10-24hr	3.865E-15	1.024E-21	1.814E-21	-
+Z10-48hr	3.865E-15	1.024E-21	2.632E-21	-
+Z20-24hr	3.865E-15	1.024E-21	2.044E-21	-

2.3.8. Simulating Oxygen Transfer

Concentration profile data was visualized as shown in Figure 19. As individual layer diffusion coefficients other than PTFE were unable to be determined, placeholder diffusivities are instead used and are seen in Table A.13. For simplicity, the high solubility effects are negated, assuming no interlayer resistivities and assuming equal rates of interlayer adsorption and desorption. Upon acquiring more interlayer experimental data, further work may incorporate these parameters into the model. Concentration changes of OR and OP tanks were incorporated into the model but did not affect the short-term steady profile of the membranes.

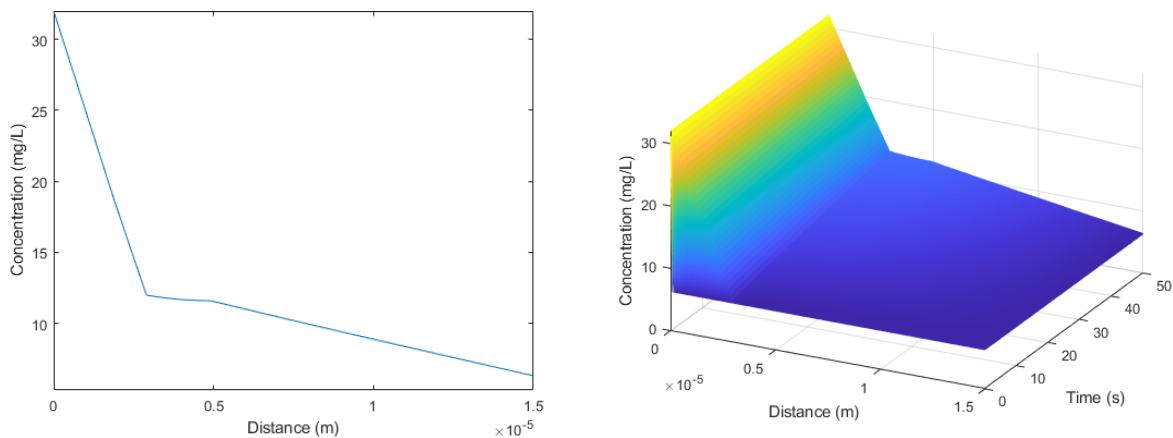


Figure 19. 2D and 3D models of diffusion profiles across a theoretical coating profile consisting of a 10 μm -thick PTFE substrate, a 2 μm -thick GL, a 1 μm -thick ZL, and a 2 μm -thick FL.

2.4. Conclusions

This chapter summarized the successful development and characterization of cost-effective zwitterionic polymer coatings, demonstrating successful oxygen transfer and suggesting their potential utility in future DO sensing applications. The development of a LOC device did not prove to be an optimal solution for DO testing, though it does produce reasonable results and is a cheap instrument with which to compare membrane parameter trends. However, the device works very slowly and is ineffective as a closed system due to leakage issues, leading to difficulty in producing accurate and repeatable mass transfer parameter predictions. Furthermore, the results obtained from LOC suggest that there is no benefit to submerging zwitterionized membranes in order to increase mass transfer for use in DO applications, which further renders the widespread implementation and use of this device unwarranted.

Gas permeability and LOC tests revealed PTFE mass transfer parameters that corresponded well with literature values. A model was successfully created to determine mass transfer parameters for coated membranes and the permeabilities of individual layers, but diffusivity and solubility measurements could not be determined. Future work should examine the interlayer interactions and quantify how mass transfer parameters can be predicted using PTFE porosity measurements. Furthermore, it is crucial to conduct a MW distribution characterization for these coating materials, given that the characterization was absent from this study. Similarly, while it has been shown here that zwitterionic materials do not pose a significant barrier to DO monitoring, verification should be repeated for other AF materials in future studies. It was found to be unnecessary to polymerize PDA or PDA/PEI GLs for up to 24 hours, as these are equally functional at a fraction of the thickness while allowing faster rates of gas transfer. While 5 mg/mL and 10 mg/mL coatings appeared similar, 20 mg/mL exhibited apparent physical and chemical

differences. In any case, neither the zwitterion grafting time nor the concentration of the zwitterion grafting solution had a noticeable effect on oxygen transfer.

2.5. References

- [1] V. C. Malshe and N. S. Sangaj, "Fluorinated acrylic copolymers," *Progress in Organic Coatings*, vol. 53, no. 3, pp. 207-211, 2005, doi: 10.1016/j.porgcoat.2005.03.003.
- [2] M. N. Zainol Abidin, M. M. Nasef, and T. Matsuura, "Fouling Prevention in Polymeric Membranes by Radiation Induced Graft Copolymerization," *Polymers (Basel)*, vol. 14, no. 1, Jan 4 2022, doi: 10.3390/polym14010197.
- [3] H. Keum *et al.*, "Impeding the Medical Protective Clothing Contamination by a Spray Coating of Trifunctional Polymers," *ACS Omega*, vol. 7, no. 12, pp. 10526-10538, Mar 29 2022, doi: 10.1021/acsomega.1c04919.
- [4] L. C. Clark, Jr., R. Wolf, D. Granger, and Z. Taylor, "Continuous Recording of Blood Oxygen Tensions by Polarography," *Journal of Applied Physiology*, pp. 189-193, 1953, doi: 10.1152/jappl.1953.6.3.189.
- [5] P. M. A. Fraher and D. W. Clarke, "Fouling Detection and Compensation in Clark-Type DOx Sensors," *IEEE Transactions on Instrumentation and Measurement*, vol. 47, no. 3, pp. 686-691, 1998, doi: 10.1109/19.744325.
- [6] S. Bhatia *et al.*, "Biofouling of an All-Optical Sensor for Seafloor Monitoring of Marine Carbon Capture and Storage Sites," *Energy Procedia*, vol. 63, pp. 3848-3852, 2014, doi: 10.1016/j.egypro.2014.11.414.
- [7] Y. Zhu *et al.*, "Cellulose paper sensors modified with zwitterionic poly(carboxybetaine) for sensing and detection in complex media," *Anal Chem*, vol. 86, no. 6, pp. 2871-5, Mar 18 2014, doi: 10.1021/ac500467c.
- [8] O. Samuelsson, A. Bjork, J. Zambrano, and B. Carlsson, "Fault signatures and bias progression in dissolved oxygen sensors," *Water Sci Technol*, vol. 78, no. 5-6, pp. 1034-1044, Oct 2018, doi: 10.2166/wst.2018.350.
- [9] M. J. Smith, A. Kerr, and M. J. Cowling, "Effects of marine biofouling on gas sensor membrane materials," *J Environ Monit*, vol. 9, no. 12, pp. 1378-86, Dec 2007, doi: 10.1039/b714187b.
- [10] L. Wang *et al.*, "In-vitro antibacterial and anti-encrustation performance of silver-polytetrafluoroethylene nanocomposite coated urinary catheters," *J Hosp Infect*, vol. 103, no. 1, pp. 55-63, Sep 2019, doi: 10.1016/j.jhin.2019.02.012.
- [11] F. Bayat, D. Maddiboina, T. F. Didar, and Z. Hosseinidoust, "Regenerating heavily biofouled dissolved oxygen sensors using bacterial viruses," *RSC Adv*, vol. 11, no. 14, pp. 8346-8355, Feb 17 2021, doi: 10.1039/d0ra10156g.
- [12] H.-H. Hsu and P. R. Selvaganapathy, "Development of a Low Cost Hemin based Dissolved Oxygen Sensor with Anti-Biofouling Coating for Water Monitoring," *SENSORS, 2013 IEEE*, pp. 1-4, 2013, doi: 10.1109/ICSENS.2013.6688588.
- [13] M. Osborne, A. Aryasomayajula, A. Shakeri, P. R. Selvaganapathy, and T. F. Didar, "Suppression of Biofouling on a Permeable Membrane for Dissolved Oxygen Sensing Using a Lubricant-Infused Coating," *ACS Sens*, vol. 4, no. 3, pp. 687-693, Mar 22 2019, doi: 10.1021/acssensors.8b01541.
- [14] Y. N. Chou, T. C. Wen, and Y. Chang, "Zwitterionic surface grafting of epoxylated sulfobetaine copolymers for the development of stealth biomaterial interfaces," *Acta Biomater*, vol. 40, pp. 78-91, Aug 2016, doi: 10.1016/j.actbio.2016.03.046.

- [15] P. M. P. T. Fowler *et al.*, "Surface Zwitterionization of Expanded Poly(tetrafluoroethylene) via Dopamine-Assisted Consecutive Immersion Coating," *ACS Appl Mater Interfaces*, vol. 12, no. 37, pp. 41000-41010, Sep 16 2020, doi: 10.1021/acscami.0c09073.
- [16] Y. Lv, S. J. Yang, Y. Du, H. C. Yang, and Z. K. Xu, "Co-deposition Kinetics of Polydopamine/Polyethyleneimine Coatings: Effects of Solution Composition and Substrate Surface," *Langmuir*, vol. 34, no. 44, pp. 13123-13131, Nov 6 2018, doi: 10.1021/acs.langmuir.8b02454.
- [17] "UNICUBE® Organic elemental analyzer." Elementar.
<https://www.elementar.com/en/products/organic-elemental-analyzers/unicube> (accessed March 15, 2023).
- [18] R. A. Pasternak, M. V. Christensen, and J. Heller, "Diffusion and Permeation of Oxygen, Nitrogen, Carbon Dioxide, and Nitrogen Dioxide through Polytetrafluoroethylene," *Macromolecules*, vol. 3, no. 3, pp. 366-371, 1970, doi: 10.1021/ma60015a020.
- [19] X. Hu, "Oxygen Gas Permeation Test of Films," Element, Cypress, TX, 2022.
- [20] P. Warneck and J. Williams, "The Atmospheric Chemist's Companion: Numerical Data for Use in the Atmospheric Sciences," Springer, 2012, ch. Chapter 8: Aqueous Phase Chemistry, p. 290.
- [21] *Rubber, vulcanized or thermoplastic — Determination of permeability to gases Part 1: Differential-pressure methods*, 2022.
- [22] J. G. Wijmans and R. W. Baker, "The solution-diffusion model: a review," *Journal of Membrane Science*, vol. 107, pp. 1-21, 1995, doi: 10.1016/0376-7388(95)00102-1.
- [23] H. Lee, S. M. Dellatore, W. M. Miller, and P. B. Messersmith, "Mussel-Inspired Surface Chemistry for Multifunctional Coatings," *Science*, vol. 318, no. 5849, pp. 426-430, 2007, doi: 10.1126/science.1147241.
- [24] A. Delgado, C. Briciu-Burghina, and F. Regan, "Antifouling Strategies for Sensors Used in Water Monitoring: Review and Future Perspectives," *Sensors (Basel)*, vol. 21, no. 2, Jan 8 2021, doi: 10.3390/s21020389.
- [25] P. Liu, E. Domingue, D. C. Ayers, and J. Song, "Modification of Ti6Al4V substrates with well-defined zwitterionic polysulfobetaine brushes for improved surface mineralization," *ACS Appl Mater Interfaces*, vol. 6, no. 10, pp. 7141-52, May 28 2014, doi: 10.1021/am501967y.
- [26] S. P. Nikam, P. Chen, K. Nettleton, Y. H. Hsu, and M. L. Becker, "Zwitterion Surface-Functionalized Thermoplastic Polyurethane for Antifouling Catheter Applications," *Biomacromolecules*, vol. 21, no. 7, pp. 2714-2725, Jul 13 2020, doi: 10.1021/acs.biomac.0c00456.
- [27] Y. Jiang, D. Choudhury, M. Brownell, A. Nair, J. A. Goss, and M. Zou, "The effects of annealing conditions on the wear of PDA/PTFE coatings," *Applied Surface Science*, vol. 481, pp. 723-735, 2019, doi: 10.1016/j.apsusc.2019.03.076.
- [28] S. Wang, J. Li, J. Suo, and T. Luo, "Surface modification of porous poly(tetrafluoroethylene) film by a simple chemical oxidation treatment," *Applied Surface Science*, vol. 256, no. 7, pp. 2293-2298, 2010, doi: 10.1016/j.apsusc.2009.10.055.
- [29] R. Henda, G. Wilson, J. Gray-Munro, O. Alshekhli, and A. M. McDonald, "Preparation of polytetrafluoroethylene by pulsed electron ablation: Deposition and wettability aspects," *Thin Solid Films*, vol. 520, no. 6, pp. 1885-1889, 2012, doi: 10.1016/j.tsf.2011.09.035.
- [30] S. Edmondson, N. T. Nguyen, A. L. Lewis, and S. P. Armes, "Co-nonsolvency effects for surface-initiated poly(2-(methacryloyloxy)ethyl phosphorylcholine) brushes in alcohol/water mixtures," *Langmuir*, vol. 26, no. 10, pp. 7216-26, May 18 2010, doi: 10.1021/la904346j.
- [31] R. A. Zangmeister, T. A. Morris, and M. J. Tarlov, "Characterization of polydopamine thin films deposited at short times by autoxidation of dopamine," *Langmuir*, vol. 29, no. 27, pp. 8619-28, Jul 9 2013, doi: 10.1021/la400587j.

- [32] C. M. Laureano-Anzaldo, J. R. Robledo-Ortíz, and R. Manríquez-González, "Zwitterionic cellulose as a promising sorbent for anionic and cationic dyes," *Materials Letters*, vol. 300, 2021, doi: 10.1016/j.matlet.2021.130236.
- [33] N. B. Haro-Mares, J. C. Meza-Contreras, F. A. Lopez-Dellamary Toral, R. Gonzalez-Cruz, J. A. Silva-Guzman, and R. Manriquez-Gonzalez, "A Simplified Method of Synthesis to Obtain Zwitterionic Cellulose under Mild Conditions with Active Ionic Moieties," *Molecules*, vol. 25, no. 13, Jul 5 2020, doi: 10.3390/molecules25133065.
- [34] C. Palacio and M. Martínez-Duart, "Correction of the escape depth effect in sputter depth profiles," *Thin Solid Films*, vol. 129, pp. L49-L51, 1985, doi: 10.1016/0040-6090(85)90106-3.
- [35] X. Luo *et al.*, "High efficient corrosion inhibition of steel by nano-micro aggregates of *Sapindus mukorossi* Gaertn peel extracts," *Chemical Industry and Engineering Society of China Journal*, vol. 71, no. 10, pp. 4760-4772, 2020, doi: 10.11949/0438-1157.20200065.
- [36] B. Pang *et al.*, "One-Step Synthesis of Quadrilateral-Shaped Silver Nanoplates with Lamellar Structures Tuned by Amylopectin Derivatives," *ACS Omega*, vol. 3, no. 6, pp. 6841-6848, Jun 30 2018, doi: 10.1021/acsomega.8b00833.
- [37] T. Xiang, L. S. Zhang, R. Wang, Y. Xia, B. H. Su, and C. S. Zhao, "Blood compatibility comparison for polysulfone membranes modified by grafting block and random zwitterionic copolymers via surface-initiated ATRP," *J Colloid Interface Sci*, vol. 432, pp. 47-56, Oct 15 2014, doi: 10.1016/j.jcis.2014.06.044.
- [38] T. Kato, Y. Yamada, Y. Nishikawa, T. Otomo, H. Sato, and S. Sato, "Origins of peaks of graphitic and pyrrolic nitrogen in N1s X-ray photoelectron spectra of carbon materials: quaternary nitrogen, tertiary amine, or secondary amine?," *Journal of Materials Science*, vol. 56, no. 28, pp. 15798-15811, 2021, doi: 10.1007/s10853-021-06283-5.
- [39] G. Zhou *et al.*, "Fibrous Hybrid of Graphene and Sulfur Nanocrystals for High-Performance Lithium-Sulfur Batteries," *ACS Nano*, vol. 7, no. 6, pp. 5367-5375, 2013, doi: 10.1021/nn401228t.
- [40] T. Duguet, A. Gavrielides, J. Esvan, T. Mineva, and C. Lacaze-Dufaure, "DFT Simulation of XPS Reveals Cu/Epoxy Polymer Interfacial Bonding," *The Journal of Physical Chemistry C*, vol. 123, no. 51, pp. 30917-30925, 2019, doi: 10.1021/acs.jpcc.9b07772.
- [41] S. R. Kelemen, M. Afeworki, M. L. Gorbaty, and A. D. Cohen, "Characterization of Organically Bound Oxygen Forms in Lignites, Peats, and Pyrolyzed Peats by X-ray Photoelectron Spectroscopy (XPS) and Solid-State ¹³C NMR Methods," *Energy Fuels*, vol. 16, no. 6, pp. 1450-1462, 2002, doi: 10.1021/ef020050k.
- [42] N. F. Della Vecchia *et al.*, "Tris buffer modulates polydopamine growth, aggregation, and paramagnetic properties," *Langmuir*, vol. 30, no. 32, pp. 9811-8, Aug 19 2014, doi: 10.1021/la501560z.
- [43] H. Marsh, P. M. A. Sherwood, and D. Augustyn, "An XPS study of binding energies of sulphur in carbon," *Fuel*, vol. 55, no. 2, pp. 97-98, 1976, doi: 10.1016/0016-2361(76)90002-8.
- [44] C. Girardeaux and J.-J. Pireaux, "Analysis of Poly(tetrafluoroethylene) (PTFE) by XPS," *Surface Science Spectra*, vol. 4, no. 2, pp. 138-141, 1996, doi: 10.1116/1.1247814.
- [45] J. Piwowarczyk, R. Jedrzejewski, D. Moszynski, K. Kwiatkowski, A. Niemczyk, and J. Baranowska, "XPS and FTIR Studies of Polytetrafluoroethylene Thin Films Obtained by Physical Methods," *Polymers (Basel)*, vol. 11, no. 10, Oct 9 2019, doi: 10.3390/polym11101629.
- [46] "Nitrogen." ThermoFisher Scientific. <https://www.thermofisher.com/ca/en/home/materials-science/learning-center/periodic-table/non-metal/nitrogen.html> (accessed November 22, 2022).
- [47] W. Hu *et al.*, "Poly(dopamine)-inspired surface functionalization of polypropylene tissue mesh for prevention of intra-peritoneal adhesion formation," *J Mater Chem B*, vol. 5, no. 3, pp. 575-585, Jan 21 2017, doi: 10.1039/c6tb02667b.

- [48] H. Luo, C. Gu, W. Zheng, F. Dai, X. Wang, and Z. Zheng, "Facile synthesis of novel size-controlled antibacterial hybrid spheres using silver nanoparticles loaded with poly-dopamine spheres," *RSC Advances*, vol. 5, no. 18, pp. 13470-13477, 2015, doi: 10.1039/c4ra16469e.
- [49] H. Shan *et al.*, "Sulfur/Nitrogen Dual-doped Porous Graphene Aerogels Enhancing Anode Performance of Lithium Ion Batteries," *Electrochimica Acta*, vol. 205, pp. 188-197, 2016, doi: 10.1016/j.electacta.2016.04.105.
- [50] Q. Liu, J. Liu, J. Wang, and Y. Chong, "Corrosion inhibition effect of betaine type quaternary ammonium salt on AA2024-T3 in 0.01 mol·L⁻¹ NaOH: Experimental and theoretical research," *Journal of Molecular Structure*, vol. 1274, 2023, doi: 10.1016/j.molstruc.2022.134395.
- [51] A. K. Friedman, W. Shi, Y. Losovyj, A. R. Siedle, and L. A. Baker, "Mapping Microscale Chemical Heterogeneity in Nafion Membranes with X-ray Photoelectron Spectroscopy," *Journal of The Electrochemical Society*, vol. 165, no. 11, pp. H733-H741, 2018, doi: 10.1149/2.0771811jes.
- [52] A. d. C. Fraga, C. P. B. Quitete, V. L. Ximenes, E. F. Sousa-Aguiar, I. M. Fonseca, and A. M. B. Rego, "Biomass derived solid acids as effective hydrolysis catalysts," *Journal of Molecular Catalysis A: Chemical*, vol. 422, pp. 248-257, 2016, doi: 10.1016/j.molcata.2015.12.005.
- [53] S. Y. Lee, Y. Lee, P. Le Thi, D. H. Oh, and K. D. Park, "Sulfobetaine methacrylate hydrogel-coated anti-fouling surfaces for implantable biomedical devices," *Biomaterials Research*, vol. 22, no. 1, 2018, doi: 10.1186/s40824-017-0113-7.
- [54] J. Guo, K. Song, B. Wu, X. Zhu, B. Zhang, and Y. Shi, "Atomically thin SiC nanoparticles obtained via ultrasonic treatment to realize enhanced catalytic activity for the oxygen reduction reaction in both alkaline and acidic media," *RSC Advances*, vol. 7, no. 37, pp. 22875-22881, 2017, doi: 10.1039/c7ra01701d.
- [55] W. J. Koros, J. Wang, and R. M. Felder, "Oxygen permeation through FEP Teflon and Kapton polyimide," *Journal of Applied Polymer Science*, vol. 26, no. 8, pp. 2805-2809, 1981, doi: 10.1002/app.1981.070260832.
- [56] S. J. Gill and I. Wadsö, "Flow-microcalorimetric techniques for solution of slightly soluble gases. Enthalpy of solution of oxygen in water at 298.15 K," *J. Chem. Thermodynamics*, vol. 14, pp. 905-919, 1982, doi: 10.1016/0021-9614(82)90001-5.
- [57] B. Sebők, M. Schülke, F. Réti, and G. Kiss, "Diffusivity, permeability and solubility of H₂, Ar, N₂, and CO₂ in poly(tetrafluoroethylene) between room temperature and 180 °C," *Polymer Testing*, vol. 49, pp. 66-72, 2016, doi: 10.1016/j.polymertesting.2015.10.016.
- [58] L. W. McKeen, "Chapter 11: Fluoropolymers," in *Permeability Properties of Plastics and Elastomers*, Fourth ed.: Elsevier William Andrew, 2017, pp. 249-287.
- [59] C. H. Company. *15-__ F Series, 0.030" through 0.125" Film made with Teflon® Fluoropolymers*, CS Hyde Company, Lake Villa, IL.
- [60] "PTFE Film (.002 to .025 thick)." Professional Plastics: The Leader in Plastic Sheets, Rods, Tubing, Profiles, & Components. https://www.professionalplastics.com/PTFE_FilmTeflon (accessed March 8, 2023).
- [61] H. Sha and I. R. Harrison, "CO₂ permeability and amorphous fractional free-volume in uniaxially drawn HDPE," *Journal of Polymer Science Part B: Polymer Physics*, vol. 30, no. 8, pp. 915-922, 1992, doi: 10.1002/polb.1992.090300814.
- [62] H. Yasuda and A. Peterlin, "Gas permeability of deformed polyethylene films," *Journal of Applied Polymer Science*, vol. 18, no. 2, pp. 531-546, 1974, doi: 10.1002/app.1974.070180218.
- [63] J. Dvorkin, "Kozeny-Carman Equation Revisited." [Online]. Available: https://pangea.stanford.edu/~jack/KC_2009_JD.pdf
- [64] G. Firpo *et al.*, "The Role of Surfaces in Gas Transport Through Polymer Membranes," *Polymers (Basel)*, vol. 11, no. 5, May 20 2019, doi: 10.3390/polym11050910.

3. Real-time Water Quality Monitoring Stations (WQMSs)

3.1. Introduction

In light of natural and anthropogenic factors, real-time water quality monitoring stations have emerged as a critical tool for ensuring the responsible management of this vital resource. Traditional ‘spot sampling’ methods involve intermittent sampling and laboratory analysis and are time-consuming, costly, and inherently limited in their ability to capture the dynamic nature of water systems. Real-time monitoring offers the continuous collection of data for immediate response to deviations from established water quality standards for benefits to the health, recreation, and overall well-being of the communities who rely on these waters. Implementing these systems also allows for sensing with little human intervention [1-3].

Real-time water quality monitoring is usually performed by large research buoys, measuring a diverse array of physical, chemical, and biological parameters, particularly in open-water environments. However, while robustly constructed to withstand harsh wind, waves, and currents of marine environments, these buoys are not suitable for all aquatic environments. Buoys may sustain damage or pose installation challenges in rivers characterized by low or fluctuating flow rates, primarily due to their substantial weight. Additionally, live monitoring buoys may cost tens of thousands of dollars and are difficult to justify for impoverished or remote communities, especially in providing long-term maintenance [1].

The Six Nations of the Grand River (SNGR) community is an Indigenous community which has long suffered from water quality stressors. There has been community concern regarding the water quality of the Grand River watershed and the McKenzie-Boston subwatershed on which the community lies, as this area is vital for health, cultural, and spiritual reasons for the Haudenosaunee people. Elevated nutrient and fecal coliform concentrations have been observed

within the subwatershed, prompting concerns regarding both illegal dumping and the effectiveness of local water treatment infrastructure. [4]. While the majority of the surface water in the Grand River basin is actively characterized by the Grand River Conservation Authority (GRCA), as well as by local municipalities, the SNGR waterways themselves have seen only intermittent spot monitoring by the Provincial Water Quality Monitoring Network (PWQMN) [5]. As such, implementation and installation of a series of field-installed WQMSs was seen as a priority for characterizing the waterways of SNGR to reliably detect point anomalies in water quality data stemming from anthropogenic sources.

In this chapter, a small network of three cost-effective water quality monitoring station (WQMS) buoys were designed, built, and deployed for hourly monitoring along the McKenzie Creek. These WQMSs measured water temperature, DO, pH, conductivity, and turbidity over a period of two autumn months while providing real-time updates on a publicly accessible website via 3G and LoRa connectivity. Acquired hourly data was compared with spot sample data and historical data to assess the validity of the WQMSs' readings. Temperature data was consistently and accurately transmitted to the server, yielding expected and coherent outputs. DO, pH, and conductivity results were less consistent, with turbidity data being the least reliable. Further investigation is required into the causes behind data transmission unreliability, with preliminary indications pointing towards a potential interplay of factors, including elevated power consumption, operation at hardware constraints, fouling, and various electrical anomalies.

3.2. Materials & Methods

3.2.1. Live Monitoring WQMSs

The WQMSs enclosures are constructed from a hinged polycarbonate waterproof washdown enclosure with dimensions 37 x 32 x 19 cm, purchased from McMaster Carr. These enclosures

were bolted to two sheets of PVC, which were then tightened to a ring buoy purchased from a local hardware store. This buoy provided 10.8 kg of buoyancy. A 4.5 kg anchor was attached with nylon rope to the buoy with enough extra rope to accommodate a 2 m fluctuation in water levels. The length of rope was not increased further as it was suspected that varying wind directions could cause the WQMS to swing against the shoreline, grounding the system or damaging the sensors. The final dimensions of each WQMS were 60 x 60 x 40 cm. An electrical shock warning sticker was adhered to the box to deter passersby from interacting with the box.

The interiors of one of the WQMSs can be seen in Figure 20a). A PVC sheet lined the bottom of the enclosure so as not to degrade the box's waterproofing when components were screwed in. This also acted to keep sensitive electrical components off the enclosure floor in case of rainwater leakage. The enclosure has a capacity of four 12V, 7.2 AH batteries, though due to weight and balance issues, only two can be used at once. These are connected to an Arduino Uno, a 3G module (used for data transmission to the university), a LoRa (Long Range) module (used for inter-WQMS data transmission), an antenna, and five water quality parameters sensors (temperature, DO, pH, conductivity, and turbidity). These parameters were chosen due to their ubiquity in assessing water health and are easily verifiable against the Grand River Conservation Authority's database. A GPS module, humidity sensor, and 9V solar panel were initially installed but were removed due to design changes. Five sensors were included in each system to measure water temperature, DO, pH, conductivity, and turbidity. Atlas Scientific was the source of the pH, DO, and conductivity sensors. The consumer (#ENV-30-pH) and industrial (#ENV-50-pH) pH probes were used, while only the lab-grade DO probe (#ENV-40-DOX) and K1.0 conductivity probes (#ENV-40-EC-K1.0) were used. Temperature and turbidity sensors were purchased from DFRobot (SKU:KIT0021 and SKU:SEN0189, respectively). The turbidity sensor is the only

sensor which was not built to be directly submerged in water, so a waterproof enclosure was created using additive manufacturing techniques. The waterproof shell was screwed together, and silicone was added to leak-prone areas to prevent water seepage. A rain-resistant ledge was added over probe connection ports. Each probe was hung from the WQMS so that it reached a depth of 30 cm below the surface. The data from these sensors were recorded on a near-hourly basis, controlled by an Adafruit TPL5110 Power Timer, which was then transmitted via 3G signal to the server at McMaster University, where the data was stored and uploaded to the website. A secondary copy of the data was stored on an SD card within the enclosure. Sample output from the website (macwater.cas.mcmaster.ca) is found in Figure A.12.

WQMSs were deployed by wading into the creek with chest waders and setting the anchor at a depth of about 1 m. This depth allowed for a reduction in water level without damaging the sensors while allowing for the WQMSs to be retrievable with chest waders in the event of a slight rise in water level. WQMSs were usually positioned halfway along the river's width. WQMS that were too deep to be recovered by wading were recovered instead by a dinghy. Each system was checked every week or two weeks, depending on troubleshooting success and availability of site access. Null data was removed, and then remaining data was then compared to spot samples obtained from the Provincial Water Quality Monitoring Network's (PWQMN) McKenzie Creek site obtained from 2010 to 2021, the last year available [5].

3.2.2. Spot Sampling

Spot sampling was performed to validate the readings obtained by WQMSs. Onsite sampling was performed using a YSI ProQuatro multiparameter meter, which measured water temperature, DO, pH, and atmospheric pressure. Readings were taken by lowering the multiprobe into the stream so that the probe's base was around 30 cm below the surface. Readings were recorded after signal

stabilization was achieved. This was repeated twice after wading perpendicular to the stream's flow direction to get an average parameter assessment across the stream while moving slightly upstream each time to minimize the effect of stirred-up silt on the data. The mean and standard deviation of each sample were calculated. 500 mL sample HDPE bottles were used to collect samples for later lab characterization, which consisted of conductivity, turbidity, chemical oxygen demand (COD) and total organic carbon (TOC) measurements. Water collection was performed at the surface without total immersion of each bottle. Lab tests were performed within 24hrs of collection after storage in a 4°C refrigerator. Turbidity data was acquired using a 2100Q portable turbidimeter, taking the mean and standard deviation of five readings. Conductivity measurements were acquired using a Thermo Fisher A212 benchtop meter, taking the mean and standard deviation of three readings. COD readings were obtained using the procedure outlined in [6] using Hach COD test kits (3-150 mg/L), Hach DRB200 reactors, and a Hach DR3900 lab spectrophotometer. TOC measurements were obtained using a Shimadzu TOC-LCPH Analyzer. All the above samples were collected on a weekly or biweekly basis, depending on the installation or removal of the WQMSs.

Samples were sent for *E. coli*, Total Coliform (TCF), and anion testing to provide an additional layer of context for the WQMSs and were tested at AGAT Laboratories in Mississauga, Ontario. Characterizations of *E. coli* and Total Coliform (TCF) were accomplished using USEPA Method 1604 [7]. Microbiological samples were collected in 100 mL bottles with sodium thiosulfate preservative. As *E. coli*, TCF, and anion values were found not to vary considerably throughout the sampling period, these tests were only performed four times at the most downstream location.

3.2.3. Sample Site Selection and Monitoring

Sampling sites were chosen based on input from community partners, ease of sampling access, alignment with previously conducted biological studies, and signal strength. Community partner Rod Whitlow had previously published two reports on the health of the McKenzie-Boston subwatershed containing water temperature, DO, pH, conductivity, and turbidity data [8, 9]. Makhdoom's recent report utilizes mostly the same sampling sites as it sought to provide updates on water quality conditions since the time of Whitlow's writing thirty years prior [4].

Signal strength troubleshooting was accomplished by finding locations where bridges crossed the McKenzie Creek. After assessing whether the bank of the creek could be easily accessed from the bridge, the WQMS was pinged to assess 3G connectivity.

3.3. Results and Discussion

3.3.1. WQMS Troubleshooting

Although the polycarbonate washdown enclosures were equipped with a gasket to make the box contents impervious to water penetration, this was found not to be sufficient over extended periods of humid weather or under heavy rain. Water may also have penetrated the box through the sensor holes sealed in silicone. Water would condense in the WQMSs and remained until their retrieval. As such, desiccants were purchased to manage water ingress. Similarly, although sufficient nylon rope was installed to allow for fluctuation in river height, extreme flow rates cause the WQMS to tip and cause water to seep in, as shown in

Figure A.11. These extreme flow rates, sometimes varying as much as 2 m, also necessitated the use of a dinghy to retrieve the WQMSs, as shown in Figure 20d), increasing the complexity of the work.

Initial comprehensive tests were set to be conducted in Cootes Paradise. Like the McKenzie Creek and Grand River basin, this was also a body of water which had been extensively characterized but was far easier to access and lay in an area of good cell reception. Subsequent site examination showed a gently sloping lake bottom at the shoreline, necessitating the perpetual use of a boat for accessing sampling locations due to the substantial draft requirement for the WQMSs. Following in-lab connectivity tests, it was determined that deploying the WQMSs directly at SNGR would be more advantageous, but where signal acquisition would prove more challenging.

The enclosure interiors varied throughout WQMS development. Initially, the system was expected to collect power using a solar panel to charge a 5V battery, but the battery's charge depleted very quickly. Most tests ran for two or three hours, with the longest uninterrupted data being acquired over 40 hours. For unknown reasons, the solar panel was unable to extend the battery's discharge time. A GPS module was initially included due to concerns over environmental factors causing movement of the WQMS, but each system remained in place throughout testing, and eventually, the GPS module was removed due to high power consumption. The solar panels were eliminated in favour of 12V batteries, which provided a more stable power supply. This change allowed each WQMS to be installed below the sample site bridge, preventing rainwater seepage. Indeed, only early WQMS tests suffered from water penetration issues. The addition of four 12V batteries, expected to last on the WQMSs for up to one month, could not be supported on the station without it sinking. Two batteries were therefore used instead but could only supply power for up to two weeks. As such, sample sites were visited every two weeks unless data collection was found to have been interrupted within the first week, in which case the sites were visited weekly. The size and shape of each WQMS makes transportation, especially of several systems, inconvenient. Each system is difficult for a single person to carry, especially when

removing it from the sample site. As the required components of each WQMS have either shrunk or been removed entirely since the project's outset, the system can be redesigned to ensure a more straightforward installation.

Investigating potential WQMS installation sites began with an assessment of the locations found in [4], as seen in Figure 1. This was further reduced to sites just on the McKenzie Creek, for a few reasons. Residents professed concern over the state of the McKenzie Creek over the Boston due to wastewater lagoons adjacent to the creek. Therefore, eliminating Boston Creek sites allowed for a more comprehensive sampling of the McKenzie Creek instead, allowing the observation of a potential difference in parameters upstream and downstream of the wastewater lagoons. Similarly, more of the McKenzie's length was accessible from within SNGR, indicating a greater chance of seeing a change in parameters across its length, while the Boston Creek ran partially through another Indigenous community. Finally, as each WQMS was expected to deliver live results across a 3G network, it was crucial that the sites, or at least the end node site, maintained good signal strength. Therefore, choosing a site proximal to cell towers, as shown in Figure 21, was the easiest way to ensure a good connection. The first sites were chosen as they were more likely to pick up any potential contaminants given their downstream location, as well as because one was easily accessible from the property of a community partner. However, the WQMSs were soon moved from these sites as despite the proximity to a cell tower, signal strength was poor, and tree cover affected solar panel efficiency. Therefore, new sampling locations were required.

Timing errors were a small but persistent problem. Hourly data acquisition was originally scheduled, but due to the power timer's reliance on manually adjusting a small screw to determine the time duration, precision was compromised. This variability necessitated subsequent manual timing adjustments. Variations in weather conditions also appeared to influence the timing.

Weather may have affected accuracy of DO, pH, and conductivity probes, which have a low working cutoff of 1°C. Combined with potential damage done to sensors due to ice, this cutoff renders these sensors incapable of year-round operation without necessitating sensor upgrades. Yearlong monitoring is possibly less of a concern for the detection of anthropogenic point source anomalies, but further consultation with the community will be needed to confirm.

In contrast to the technical challenges in implementing this floating WQMS design, the successful installation of three stations was greatly eased with the collaboration of our community guide and expert. His efforts highlighted the unique collaboration between FN environmental experts, chemical engineers, and electrical engineers that was central to this project.

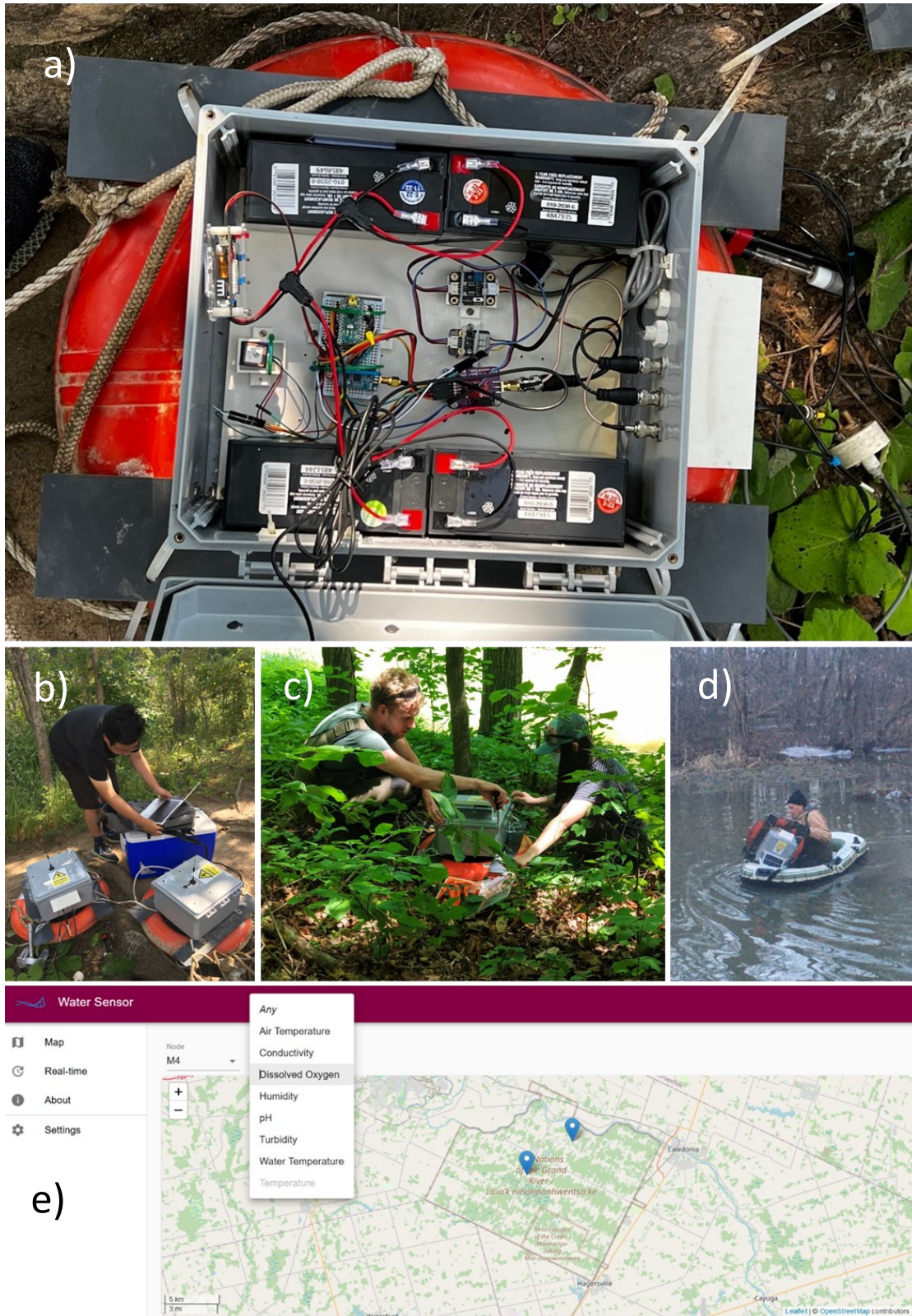


Figure 20. A finalized interior of one of the WQMSs (a), pinged the WQMSs to ensure proper functionality before deployment (b), deploying a WQMS (c), community partner retrieving a WQMS with a dinghy (d), website portal for accessing real-time water quality measurements (e).

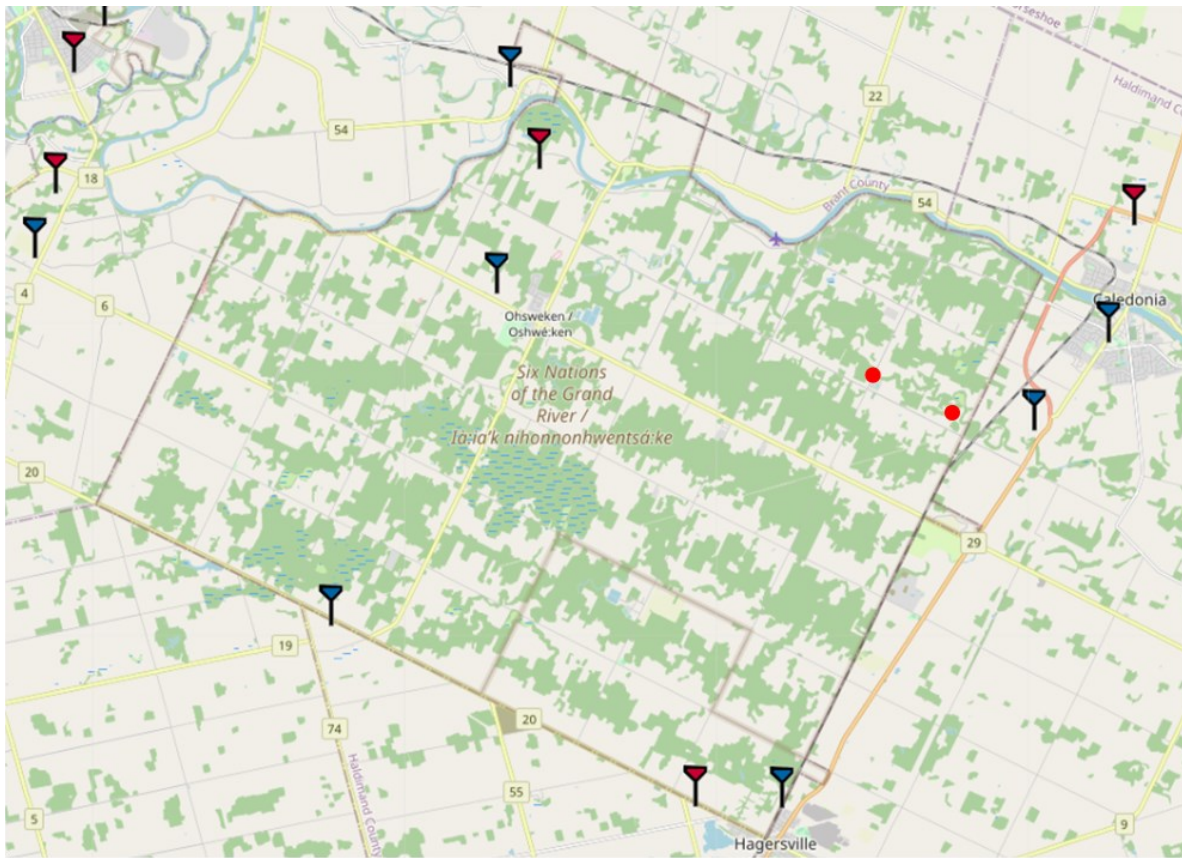


Figure 21. Cell tower locations in the vicinity of SNGR, July 2021. Blue markers represent Bell Canada towers, while towers marked in red are owned by Rogers Communications [10]. Red dots indicate the initial WQMS installation sites.

A survey of McKenzie Creek crossings revealed many sites with acceptable 3G connection, as shown in Figure 22. The area around the original two sites was deemed to have weak signal strength. Much of the areas in the centre of the community showed good signal strength, so WQMSs were moved to this area instead, with three stations being installed at locations M4, M4.5, and M5. The selection of these sites also allowed for a better pinpointing of the source of potential contaminants should they emerge from the nearby wastewater lagoons. The site sample numbering

system is inherited from [4], where locations M4 and M5 correspond precisely to the sites found in that work, while M4.5 is located halfway between M4 and M5.

Initial WQMS construction incorporated a distinct gateway node positioned at an elevated location, typically atop a tree, which was separate from the primary system. The use of a separate gateway was due to the poor signal strength at the initial downstream sites, and it was thought that increasing the visibility of the gateway node by elevating it would allow the gateway to have a better likelihood of contacting nearby cell towers. This elevation change did not help. The interior of the preliminary WQMS also needed more room to fit the gateway, so setting it up as a separate build was not a problem.

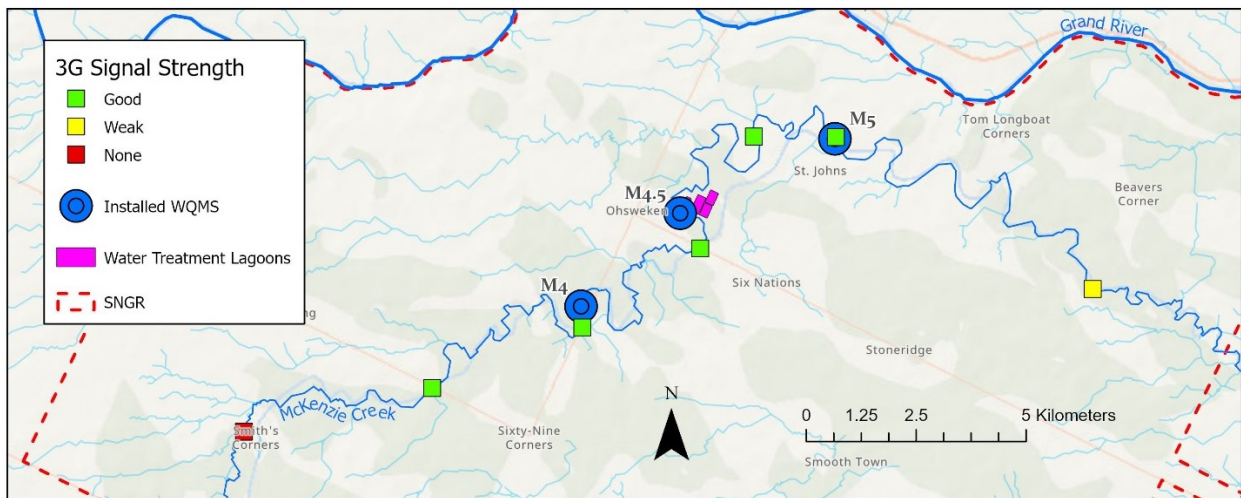


Figure 22. Locations of gateway 3G signal test sites (green, yellow, red squares) and locations at which WQMS were ultimately installed during this study (blue circles). Created in ArcGIS Pro 3.1.0.

3.3.2. Water Temperature

Temperature data acquired throughout the WQMS deployment period is the most consistent of all measured parameters, as shown in Figure 23. These results make sense, as the temperature sensor is the most robust, least complex sensor of the five examined and the only one which should not be affected by the presence of foulants on its surface should that be an issue. A gradual reduction in temperature throughout the sampled period is observed, consistent with the historical data.

Day/night cycles are easily discerned, and the matching of these cycles between M4 and M5 in the last week of data collection showcases the reliability of the data, their temperatures straying no more than 1°C from each other. A slight error is observed in the M4.5 data on November 12, where the temperature abruptly lowers by several degrees between 4:37 PM and 5:37 PM. This is unlikely to be a temporary shift due to external phenomena, as the proceeding data follows normal cycling until contact is lost with the sensor. The change must likely be due to an internal electronic issue. Spot sample data also confirms the reliability of WQMS data. Overall, there is no reason to believe that this data suffers from any major errors in reading that would affect the proper assessment of long-term water quality trends. Short-term changes in data can also likely be adequately assessed, but most likely in the context of other sensor data.

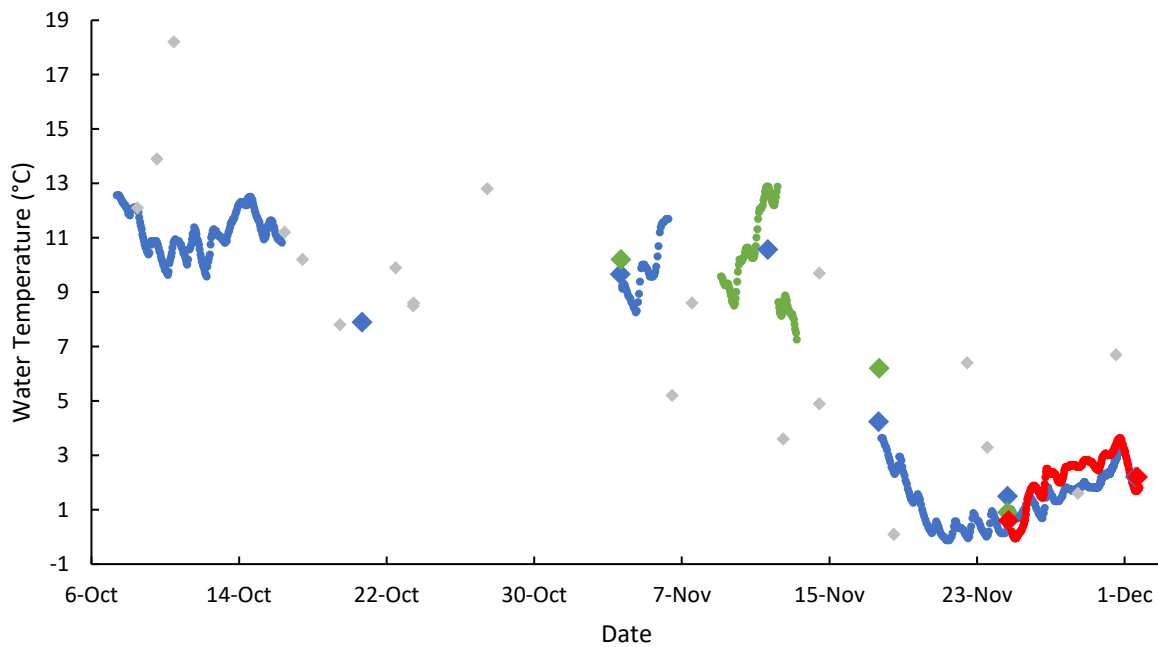


Figure 23. Water temperature data obtained from McKenzie Creek WQMS at points M4 (●), M4.5 (●), and M5 (●). Spot data obtained from the same locations M4 (◆), M4.5 (◆), and M5 (◆) are also shown, along with spot data from 2010-2021 (◆) taken from the PWQMN McKenzie Creek site. Uncertainties are standard deviations for triplicate measurements.

3.3.3. Dissolved Oxygen

As a decrease in temperature is correlated with an increase in DO concentration, an increase of the latter is expected as winter sets in, as is observed in Figure 24. Spot samples also consistently show DO near saturation concentrations, if not above them. However, unlike temperature data, WQMSs do not agree with historical or spot sample data. M4 and M5 agree well, within 1 mg/L, and the cyclical increase of DO at night and decrease during the day can be seen. M4 and M5 spot data may differ due to the presence of a small waterfall upstream of M4, increasing its DO levels. Given the delayed timing of experimentation in the calendar year, a reduced probability of organic matter proliferation, potentially obstructing high DO levels, is expected. The data from M4 and M5 is half what they would otherwise be expected to read. Meanwhile, M4.5 reads far more in line with the spot sample data, but with much more noise in the original data. Like the pH and conductivity sensors purchased from Atlas Scientific, this sensor is marketed as being fully and indefinitely waterproof, so it is unlikely that the value discrepancy is caused by the probe malfunctioning due to unintended full submersion. Differences in sampling analysis due to DO stratification in water are also doubtful, as all methods sample at the same depth. Instead, WQMS/spot differences may be partially explained by calibration error, as each probe is calibrated at room temperature. The rates of oxygen reduction within the electrolyte chamber are significantly reduced with lowered temperature, suggesting that a temperature correction factor should be thoroughly investigated and implemented [11]. The probe is working at the limits of its temperature range with an operating floor of 1°C, but the embedded circuit is functional down to -40°C [12, 13]. Given the intermittence of the data at large, such a temperature correction solution is currently impractical.

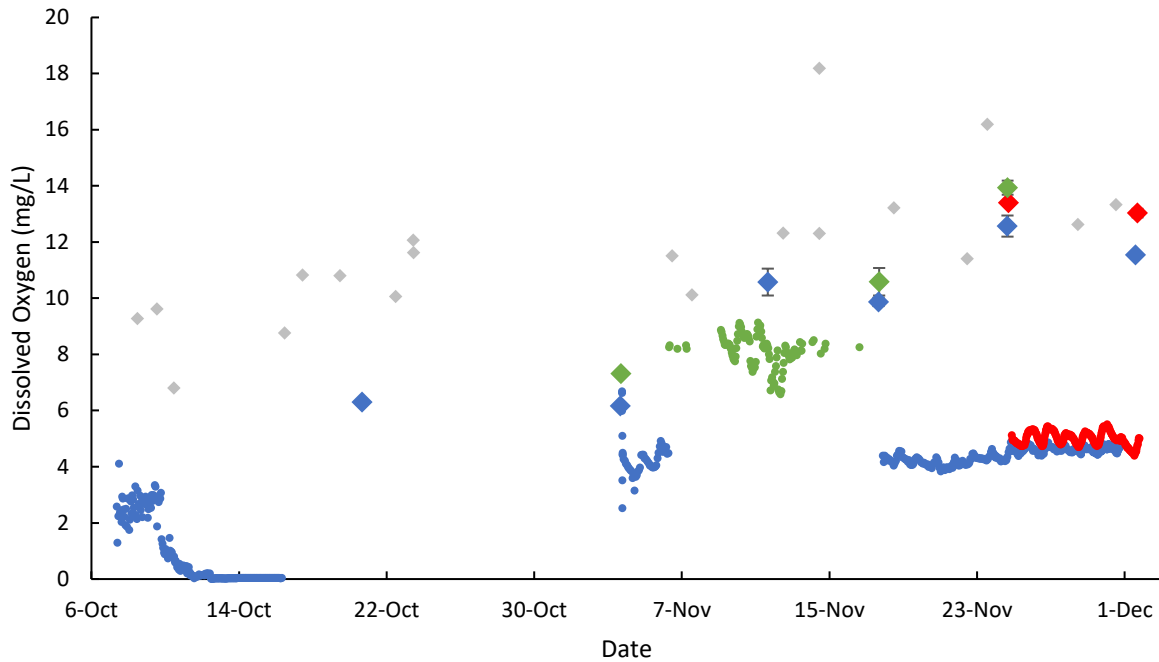


Figure 24. DO data obtained from McKenzie Creek WQMS at points M4 (●), M4.5 (●), and M5 (●). Spot data obtained from the same locations M4 (◆), M4.5 (◆), and M5 (◆) are also shown, along with spot data from 2010-2021 (◆) taken from the PWQMN McKenzie Creek site. Uncertainties are standard deviations for triplicate measurements.

While most incorrect data was easily discernable, a gradual decrease in DO was noted in mid-October. Examining the membrane after retrieval revealed a few sharp abrasions on the membrane, as indicated in Figure 25. The minimal fouling depicted in this image implies that macrofouling likely does not exert a substantial influence on the unusual DO values. The slow leaking of electrolyte from the sensor would have caused a drop in current. As such, the sensor was replaced. It is unknown whether these abrasions emerged due to careless installation or waterborne detritus. Decreases in water level were noted around that time, which may have caused the sensor to impact features on the creek bed.

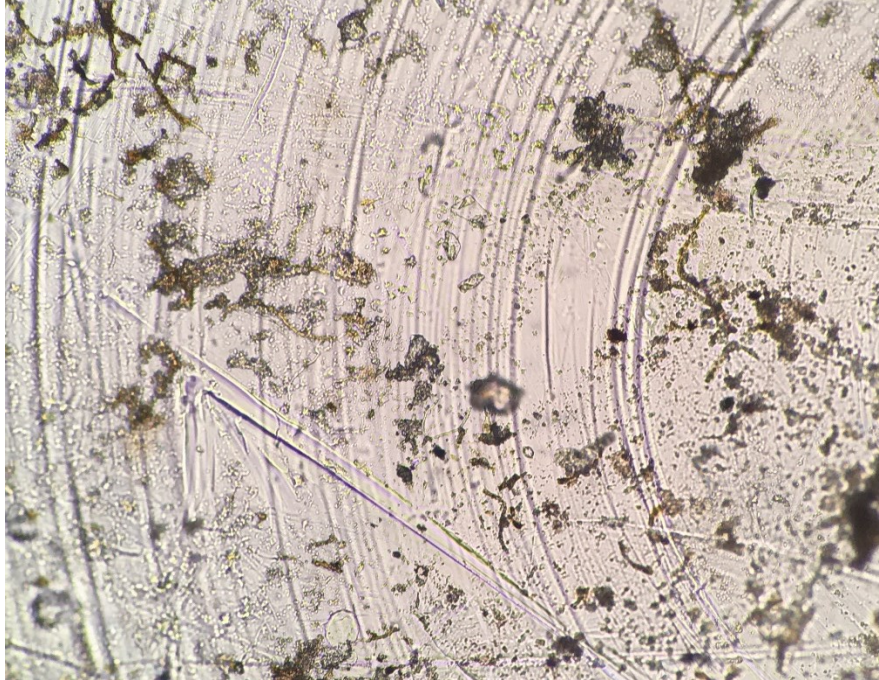


Figure 25. Abrasions on a DO membrane fouled for two weeks in the McKenzie Creek between October 6 and 20, 2022.

3.3.4. pH

Recorded pH values are normal for riverine systems, if slightly high, pointing to no signs of eutrophication [14]. These high pH values are likely due to elevated amounts of local limestone and clay [15, 16]. Numerous inconsistencies are observed between spot data and WQMS data. While spot and historical data agree well, M4 and M5 stations do not. Station M4.5 did not produce any viable data during this period. The pH is generally higher upstream in both grab samples and live data. However, more data is likely required to confirm that this comparison is accurate. A day/night cycle can be clearly observed in M4 but only very faintly in both M5 readings, possibly due to a temperature dependence of the solubility of CaCO_3 or other minerals. This solubility dependence is also likely to cause the increase in pH throughout the season as temperatures drop. An increase in photosynthesis, and thus DO, during daylight hours may also account for part of the daily periodicity [17]. However, this difference is not observed historically as pH levels remain consistent throughout the year in the Grand River and McKenzie Creek, as shown in Figure A.13

despite greater summer sunlight hours. The modest diurnal fluctuations in pH levels suggest limited occurrences of extensive photosynthetic activity [18]. The difference in amplitudes between two sensors monitoring simultaneously may be a product of biofouling. While the M5 sensor had been periodically used for months on the same station, the M4 sensor was new. The buildup of foulants would have caused a reduction in ion exchange, reducing the voltage measured from the reference electrode, thus sensibly producing lower pH readings. Additionally, the M5 station used the consumer probe, while the M4 station used the industrial pH probe, which is an order of magnitude more expensive than the former probe. Although the industrial probe is more costly, it is much more fouling-resistant. It can be cleaned easily compared to the consumer probe, whose glass membrane is very fragile.

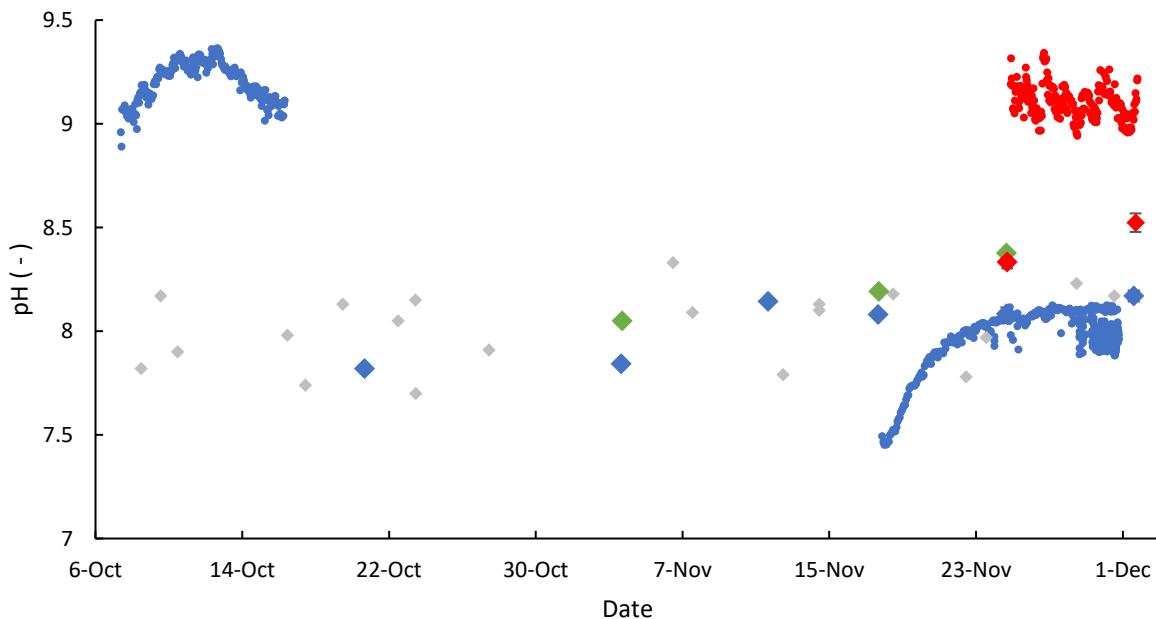


Figure 26. pH data obtained from McKenzie Creek WQMS at points M4 (●), M4.5 (●), and M5 (●). Spot data obtained from the same locations M4 (◆), M4.5 (◆), and M5 (◆) are also shown, along with spot data from 2010-2021 (◆) taken from the PWQMN McKenzie Creek site. Uncertainties are standard deviations for triplicate measurements.

3.3.5. Conductivity

WQMS conductivity data appear segregated into two regimes, as shown in Figure 27. The lower regime, centred around 500-700 $\mu\text{S-cm}$, appears within the magnitude of historical data values but does not exhibit any noise. All M4.5 data and some M5 data fall into this category. The high regime exhibits noise characteristic of realistic data acquisition yet exists several magnitudes higher than the historical value data. As such, the first regime acquires nonsense data, while the second produces improperly calibrated data and is more indicative of general trends, though magnitudes of conductivities, as found in the high data regime, are not found in freshwater environments [19]. As with other parameters, a daily fluctuation of electrical conductivity is observed, as conductivity increases with increasing temperature [20]. The direct dependence on temperature is apparent as the M5 data beginning November 4th and 17th align with the corresponding temperature data in Figure 23. The same periodicity is observed in M4, and while temperature data overlap between M4 and M5, this is not the case in the conductivity data, which is again likely due to sensor calibration issues. Otherwise, grab samples align well with historical trends and remain constant throughout the monitoring period. The irregular WQMS conductivity data is peculiar as initial calibration against standard solutions yielded acceptable readings, thus it is unlikely that the fault lies with the sensors themselves. In addition, these same sensors were not rotated throughout the field tests, so the sudden improvement of functionality of each sensor may be due to a loose connection. In any case, further work is required to improve the reliability of conductivity readings.

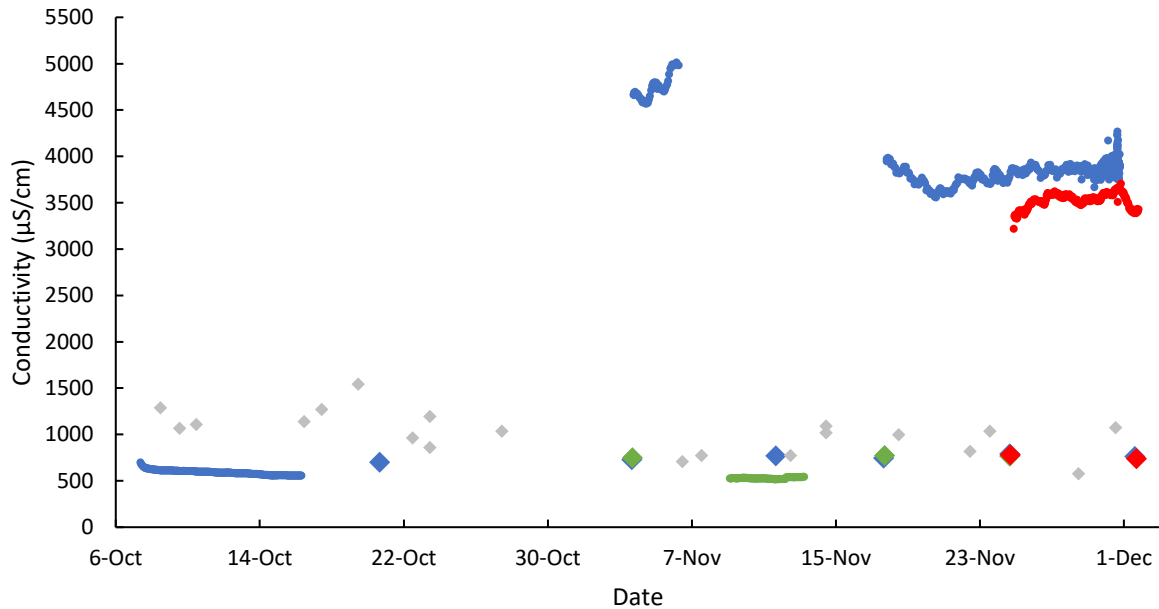


Figure 27. Conductivity data obtained from McKenzie Creek WQMS at points M4 (●), M4.5 (●), and M5 (●). Spot data obtained from the same locations M4 (◆), M4.5 (◆), and M5 (◆) are also shown, along with spot data from 2010-2021 (◆) taken from the PWQMN McKenzie Creek site. Uncertainties are standard deviations for triplicate measurements.

3.3.6. Turbidity

The turbidity data acquired from the WQMSs was the least useful of all parameters. There is a two-order-of-magnitude difference between WQMS data and grab sample data, as shown in Figure 28. As usual, PWQMN data correspond well with the grab data obtained in this work, and data spikes are more representative of abrupt high-flow events that may skew seasonal data [21]. PWQMN data does not show a seasonal change in turbidity. Spot samples show a decrease in turbidity as winter approaches, which makes sense as by the end of November, the bottom of the creek becomes clearly visible. Despite waterproofing efforts, water was found in each live-monitoring sensor post-retrieval which lowered the likelihood of achieving useful data. Unchanging data near zero and below 1000 NTU may be caused by a short circuit [22]. Final readings from M5 may show an accurate trend due to the buildup of foulants on or inside the sensor. M4 data appears less believable. The accuracy of this sensor is not high according to the

manufacturer, only being 10% of the full measurement range from 0-3000 NTU. While this is appropriate for turbidity measurement in dishwasher applications for which this sensor is made, it is less so for environmental applications. However, more accurate sensors cost thousands of dollars, defeating the project's low-cost goal.

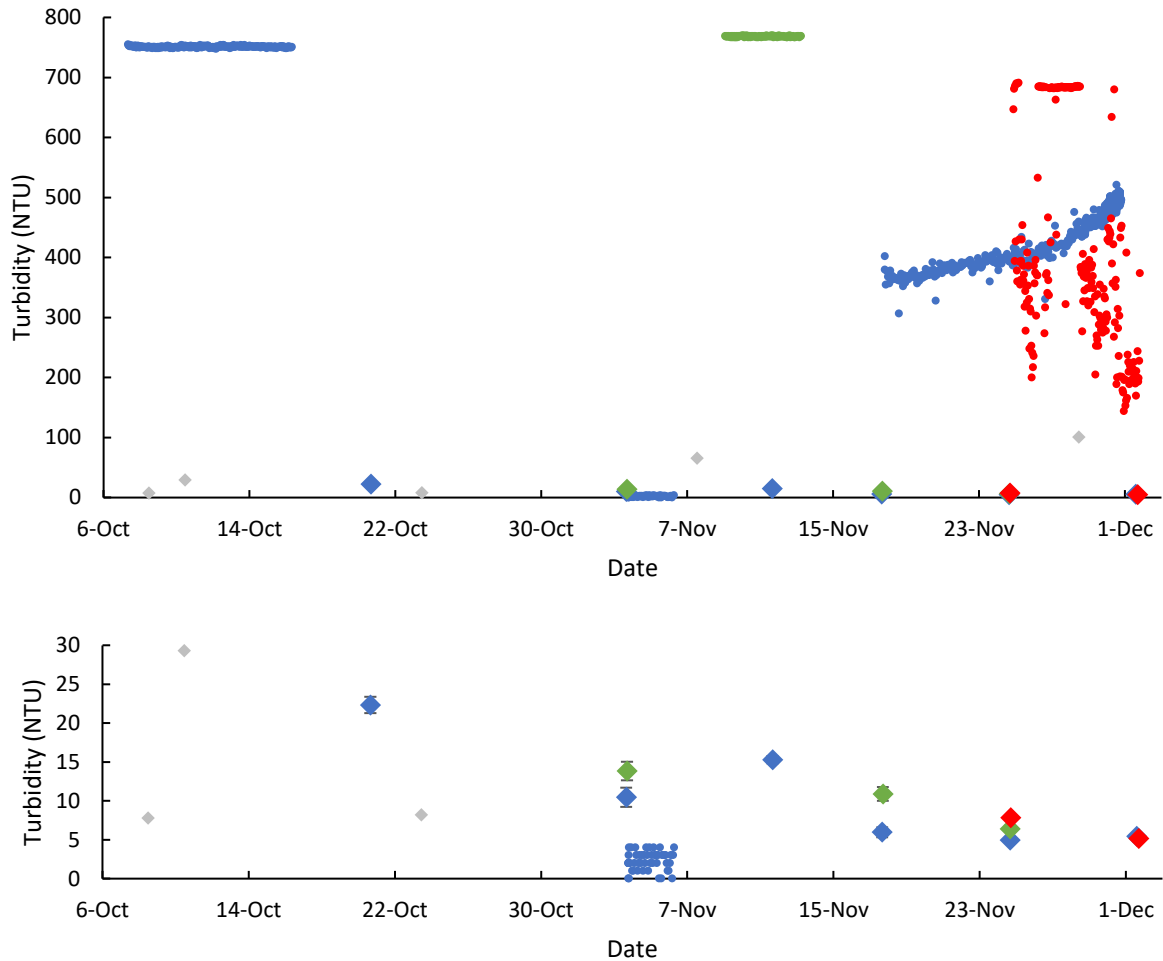


Figure 28. Turbidity data obtained from McKenzie Creek WQMS at points M4 (●), M4.5 (●), and M5 (●). Spot data obtained from the same locations M4 (◆), M4.5 (◆), and M5 (◆) are also shown, along with spot data from 2010-2021 (◆) taken from the PWQMN McKenzie Creek site. b) shows lower magnitude data at a different scale for clarity. Uncertainties are standard deviations for triplicate measurements.

3.3.7. Chemical Oxygen Demand & Total Organic Carbon

The collection of COD and TOC data helps to serve as further indicators of water quality and offers other directions for future WQMS sensor research. COD values remain stable throughout the sample period, except for a sudden drop on the last day of spot sampling, as shown in Figure 29. COD is theoretically inversely correlated with DO, as increasing oxygen demand results in less available oxygen. The fact that COD remains stable throughout the monitoring period suggests that DO changes are primarily caused by temperature and not by excess bacterial or algal growth. However, analyzing potential eutrophic conditions late in the calendar year may not yield optimal results due to the timing of the study period. These values, consistent with typical riverine conditions, do not indicate a significant presence of materials causing elevated COD levels.

Meanwhile, TOC values exhibit a slow decline from mid-October to the beginning of December and consistently exhibit higher than typical riverine values [23, 24]. This trend is not noticeable in M4.5 and cannot be meaningfully commented upon given the two samples obtained in M4. This general trend is expected, given the high correlation between TOC and turbidity [25, 26]. Therefore, it is likely that turbidity can be used as an appropriate surrogate for TOC in future, though correcting for total dissolved solids that are detected via TOC and are not detected by the turbidimeter.

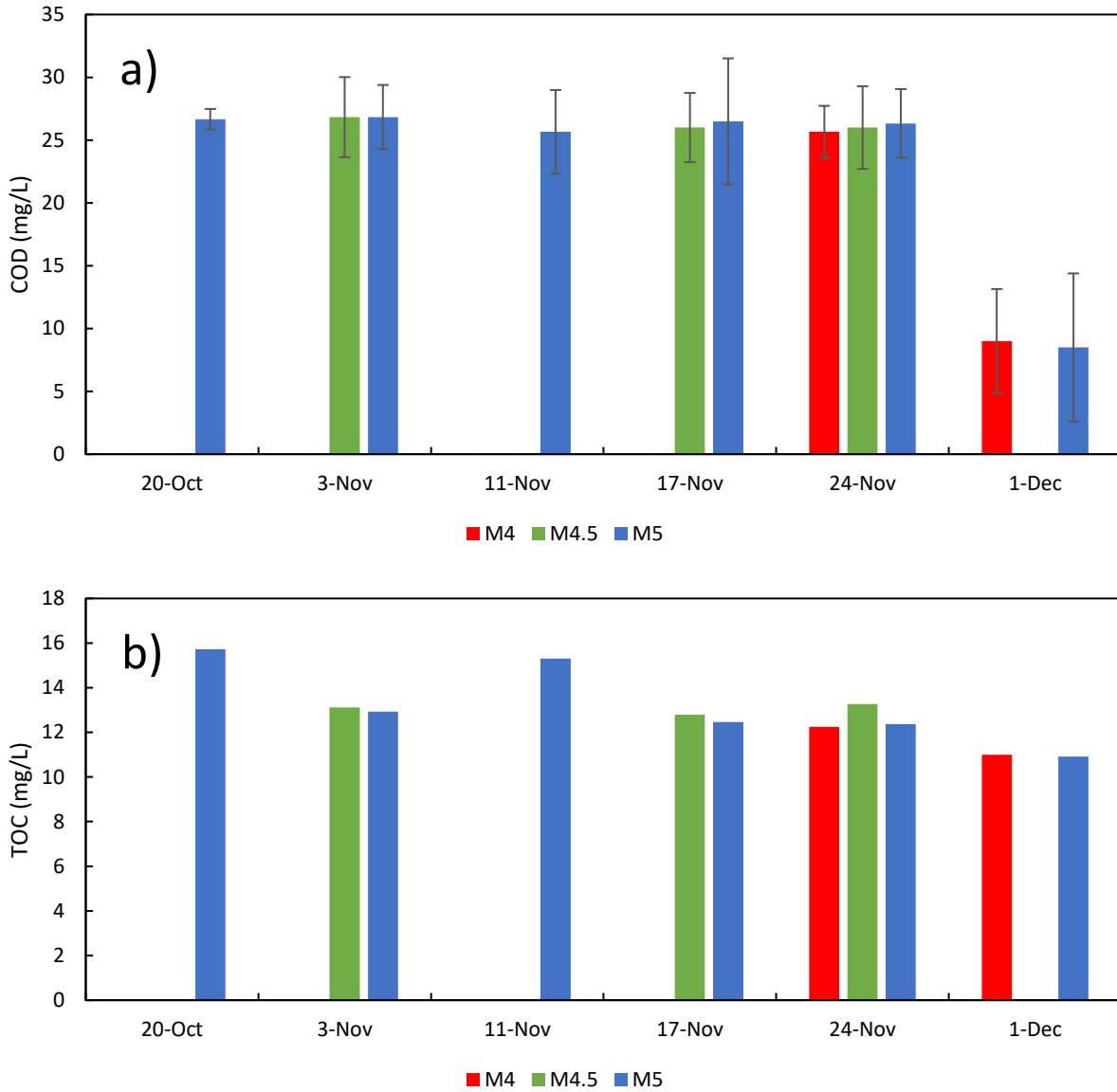


Figure 29. COD (a) and TOC (b) data obtained from sample sites M4, M4.5, and M5. Uncertainty is calculated as the standard deviation of two COD samples. No uncertainty is available for TOC.

3.3.8. Cost

The primary components for the construction of each WQMS are listed in Table 6, but the exact composition of each WQMS varied slightly. Extra components, such as cables, cable ties, mounts, nuts, bolts, screws, SMA-BNC adapters, silicone sealant, stickers, 3D printed pieces were able to be acquired relatively cheaply or were already on hand. Prices varied considerably throughout the course of the COVID-19 pandemic due to supply chain issues. Prices are shown before tax and

shipping. pH, DO, and conductivity kits were purchased and sold with extra wiring, calibration fluids, isolated carrier boards, and EZO circuits. Temperature and turbidity kits were sold with carrier boards attached. pH, DO, and conductivity sensors accounted for around half of the cost of the WQMS, depending on the sensor configuration used. Accounting for tax and shipping, the cost of building a WQMS may reach 2500 CAD. Further sensor upgrades or additions may extend this price to 3000 CAD or beyond, depending on research requirements. or comparison, this pricing is in the range of many commercially available handheld multiparameter meters, which are only available for spot sampling. Commercially available continuously monitoring buoys are an order of magnitude more expensive but can offer more sensing options than what has been implemented here. This sizeable price difference suggests that these WQMSs are a viable, inexpensive option for continuous surface water monitoring.

Table 6. Price list for constructing a single WQMS.

Component	Quantity per WQMS	Unit Cost (CAD)
Polycarbonate Enclosure	1	205
Anchor (4.5 kg)	1	40
Ring Buoy	1	90
Nylon Rope (100 ft, 3/8 in)	0.1	33
White PVC Floor (12"x12"x1/8")	1	9
PVC Enclosure Supports (24"x4"x0.25")	2	17
Arduino UNO	1	35
Arduino Nano	1	31
12 V, 7.2 AH Pb-Acid Battery	2-4	43
GPS Module	1	~30-40
SIM5320 3G Module	1	~50-100
LoRa Mesh Module	1	~50
MicroSD Card Module	1	~3-5
LoRa Antenna	1	~10
Consumer Grade pH Probe Kit	0-1	92
Industrial pH Probe Kit	0-1	428
Lab Grade DO Probe Kit	1	353
Conductivity K1.0 Kit	1	272
Temperature Sensor Kit	1	11
Turbidity Sensor Kit	1	14
Additional Materials	-	~100
Total Estimated Cost Before Tax	-	~1500-1975

3.4. Conclusions

Three low-cost WQMSs were successfully designed, built, and deployed on McKenzie Creek at SNGR. The reliable transmittance of accurate temperature data throughout nearly the entirety of the monitoring period shows that the same can be achieved for DO, pH, conductivity, and turbidity parameters if the robustness of other electrical components is improved. However, there are numerous issues of this design that remain impedimentary to wide-scale WQMSs distribution. The default manufacturer calibrations are not sufficient, and thus DO, pH, conductivity data require mild to significant corrections for it to be useful. These corrections will be primarily based on temperature, as DO, conductivity, and to a lesser degree, pH, are dependent on it, but the nature of the remaining correction factors is not fully known at present and will require more study. The turbidity monitoring unit will require a substantial redesign. Additionally, the possibility of severe fouling on several sensors continues to motivate further antifouling (AF) research. At this stage, these WQMSs are not sufficient to reliably detect point anomalies in water quality data stemming from anthropogenic sources.

The devices remain complicated for a lay user to set up and troubleshoot. Difficulties in setup are less problematic, as a technician would be engaged with community members to discuss effective monitoring locations. Troubleshooting difficulties pose a greater program risk as they undermine a primary goal of ensuring rapid WQMS transition to a community-led project. However, the development of these WQMSs suggests future success in their eventual deployment in more remote communities.

The current state of the WQMSs is suboptimal for long-term usage due to their limited data recording capability of two weeks and the necessity for constant technical support in cases of infrequent damage; nevertheless, a redesign is underway employing a more compact casing after

removing the bulky materials installed at the outset of the project. When prioritizing precision over cost in advancing the development of these containers, it is advisable to utilize industrial pH, DO, and turbidity meters due to their enhanced cleanability, thereby improving data accuracy; however, it is crucial to note that the incorporation of AF coatings, while beneficial in extending cleaning intervals during site visits, necessitates recalibration of these sensors. Power consumption permitting, the addition of nitrate, nitrite, and phosphate sensors will likely additionally provide better corroboratory data, given the agricultural land use in the McKenzie-Boston subwatershed, and will allow for better detection of point source anomalies. Establishing a live monitoring station at the confluence of McKenzie Creek or upstream of the confluence along the McKenzie Creek, similar to existing stations along the Grand River, would enhance the GRCA's comprehensive monitoring network, considering that the York station currently serves as the most downstream live station on the Grand River prior to the McKenzie's confluence.

3.5. References

- [1] M. Chu *et al.*, "SitkaNet: A low-cost, distributed sensor network for landslide monitoring and study," *HardwareX*, vol. 9, p. e00191, Apr 2021, doi: 10.1016/j.ohx.2021.e00191.
- [2] A. T. Demetillo, M. V. Japitana, and E. B. Taboada, "A system for monitoring water quality in a large aquatic area using wireless sensor network technology," *Sustainable Environment Research*, vol. 29, no. 1, 2019, doi: 10.1186/s42834-019-0009-4.
- [3] M. Pule, A. Yahya, and J. Chuma, "Wireless sensor networks: A survey on monitoring water quality," *Journal of Applied Research and Technology*, vol. 15, no. 6, pp. 562-570, 2017, doi: 10.1016/j.jart.2017.07.004.
- [4] S. Makhdoom, "Assessing potability of drinking-water sources and quality of surface water on the Reserve of the Six Nations of the Grand River, Ontario (Canada)," Master of Science, Department of Biology, McMaster University, Hamilton, Ontario, 2021. [Online]. Available: <http://hdl.handle.net/11375/27030>
- [5] *Provincial (Stream) Water Quality Monitoring Network*, Environmental Monitoring and Reporting Branch. [Online]. Available: <https://data.ontario.ca/dataset/provincial-stream-water-quality-monitoring-network>
- [6] *Oxygen Demand, Chemical - Method 8000*. (2021). [Online]. Available: <https://www.hach.com/asset-get.download.jsa?id=7639983816>
- [7] (2002). *Method 1604: Total Coliforms and Escherichia coli in Water by Membrane Filtration Using a Simultaneous Detection Technique (MI Medium)*. [Online] Available: https://www.epa.gov/sites/default/files/2015-08/documents/method_1604_2002.pdf

- [8] R. Whitlow, "Stream habitat assessment and aquatic resource inventory of the Six Nations of the Grand River watershed," Six Nations of the Grand Band Council, Unpublished, 1989.
- [9] R. Whitlow, "Six Nations of the Grand River Fisheries Project Discussion Paper," Six Nations of the Grand Band Council, Unpublished, 1990.
- [10] S. Nikkel. "Canadian Cellular Towers Map." https://www.ertyu.org/steven_nikkel/cancellsites.html (accessed Jan 15, 2023).
- [11] G. Shi, T. Tano, D. A. Tryk, A. Iiyama, M. Uchida, and K. Kakinuma, "Temperature Dependence of Oxygen Reduction Activity at Pt/Nb-Doped SnO₂ Catalysts with Varied Pt Loading," *ACS Catalysis*, vol. 11, no. 9, pp. 5222-5230, 2021, doi: 10.1021/acscatal.0c05157.
- [12] *Gen 2 Lab Grade D.O. Probe*. [Online]. Available: https://files.atlas-scientific.com/LG_DO_probe.pdf
- [13] J. Press and N. Press. *EZO-DO(TM) Embedded Dissolved Oxygen Circuit*. [Online]. Available: https://files.atlas-scientific.com/DO_EZO_Datasheet.pdf
- [14] G. Suter II, S. Cormier, K. Schofield, J. Gilliam, and C. Barbour. "pH." United States Environmental Protection Agency. <https://www.epa.gov/caddis-vol2/ph> (accessed December 12, 2022).
- [15] "Limestone Industries of Ontario," vol. Volume 1: Geology, Properties, and Economics, 1989. [Online]. Available: <http://www.geologyontario.mndm.gov.on.ca/mndmfiles/pub/data/imaging/NSP001//nsp001.pdf>
- [16] Soil Survey Complex [Online] Available: <https://geohub.lio.gov.on.ca/datasets/ontarioca11::soil-survey-complex/>
- [17] J. P. Michaud, "A Citizen's Guide to Understanding and Monitoring Lakes and Streams," 1991.
- [18] L. Radke. "pH of coastal waterways." OzCoasts: Australian Online Coastal Information. https://ozcoasts.org.au/indicators/biophysical-indicators/ph_coastal_waterways/ (accessed December 12, 2022).
- [19] A. F. Rusydi, "Correlation between conductivity and total dissolved solid in various type of water: A review," *IOP Conf. Ser.: Earth Environ. Sci.*, vol. 118, no. 012019, 2018, doi: 10.1088/1755-1315/118/1/012019.
- [20] M. Hayashi, "Temperature-Electrical Conductivity Relation of Water for Environmental Monitoring and Geophysical Data Inversion," *Environmental Monitoring and Assessment*, vol. 96, no. 8, pp. 119-128, 2004, doi: <https://doi.org/10.1023/B:EMAS.0000031719.83065.68>.
- [21] R. J. Davies-Colley and D. G. Smith, "Turbidity Suspended Sediment, and Water Clarity: A Review," *Journal of the American Water Resources Association*, vol. 37, no. 5, pp. 1085-1101, 2001, doi: 10.1111/j.1752-1688.2001.tb03624.x.
- [22] "WM1 & WIND Contacting Conductivity Sensor Troubleshooting Guide," Walchem. [Online]. Available: https://www.walchem.com/TechSupport/WebM/WM_WIND_ContactCond_Sensor%20Troubleshooting.pdf
- [23] P. J. Mulholland and J. A. Watts, "Transport of organic carbon to the oceans by rivers of North America: a synthesis of existing data," *Tellus A: Dynamic Meteorology and Oceanography*, vol. 34, no. 2, 1982, doi: 10.3402/tellusa.v34i2.10800.
- [24] M. Meybeck, "Carbon, Nitrogen, and Phosphorus Transport by World Rivers," *American Journal of Science*, vol. 282, no. 4, pp. 401-450, 1982, doi: 10.2475/ajs.282.4.401.
- [25] H. S. Lee, J. Hur, Y. H. Hwang, and H. S. Shin, "A Novel Procedure of Total Organic Carbon Analysis for Water Samples Containing Suspended Solids with Alkaline Extraction and Homogeneity Evaluation by Turbidity," *Int J Environ Res Public Health*, vol. 17, no. 11, May 31 2020, doi: 10.3390/ijerph17113901.

- [26] J. Gong, Y. Ran, D. Chen, Y. Yang, and E. Y. Zeng, "Association of endocrine-disrupting chemicals with total organic carbon in riverine water and suspended particulate matter from the Pearl River, China," *Environmental Toxicology and Chemistry*, vol. 31, no. 11, pp. 2456-2464, 2012, doi: 10.1002/etc.1961.

4. Co-Creative Practices in Reconciling Traditional Indigenous Knowledge and Western Science

The co-creative framework in this section was developed in collaboration with Hannah Grewal.

4.1. Introduction

The academic community's engagement with Indigenous communities has historically been characterized by an unequal partnership, marked by extractive research tactics, resource theft, and the mistreatment of Indigenous peoples [1, 2]. While the legacy of colonialism across Canada remains entrenched, the promotion of Indigenous Knowledge (IK) and Traditional Ecological Knowledge (TEK) has taken on renewed significance in the face of water insecurity caused by climate change and unsustainable resource production and extraction [3]. The contemporary landscape offers a chance to address historical injustices and facilitate cooperative research endeavours aimed at safeguarding Indigenous culture, language, nationhood, and sovereignty, ultimately serving as a vital asset for environmental conservation efforts and the sustenance of Indigenous livelihoods. Exclusively adhering to the WS framework confines IK within a paradigm that empowers researchers to exert authority over Indigenous communities and their identities [4]. Efforts to enhance collaboration between researchers and Indigenous communities in ecological research have been ongoing, yet substantial progress is required to attain equitable incorporation of IK within the scientific community [2, 5, 6].

To address this imperative, it is crucial that the promotion of Indigenous-led climate and environmental studies be continued. Such endeavours ensure that research involving Indigenous peoples, cultures, and lands is guided and directed by individuals within these communities, thereby maximizing the effectiveness and relevance of project outcomes for each individual

community. This approach is crucial for respecting Indigenous sovereignty and fostering research partnerships built on trust and mutual benefit. The achievement of this equitable collaboration is dependent on the scientific community's continued willingness to engage with Indigenous peoples.

Through the personal experience of working with the Six Nations of the Grand River (SNGR) via water quality monitoring of the McKenzie Creek, as well as via performing household tap water collection and analysis work as found in [7], a general co-created framework for scientists and engineers was developed for working with Indigenous communities with the goal of harmonizing IK and Western Science (WS) practices, while maintaining adherence to OCAP principles. These experiences will provide a foundational framework for scientists and engineers seeking to engage with Indigenous communities. The framework's purpose is to facilitate meaningful collaboration that bridges the gap between IK and WS using principles of community-based participatory research (CBPR), nurturing an equitable partnership that benefits both parties and ultimately contributes to the well-being of Indigenous communities, their environments, and the broader scientific community.

4.2. Methods: Co-Creative Framework

The framework for conducting research in collaboration with Indigenous communities is found in Figure 30. It was developed by two students of WS methodology with continual feedback from community partners. It acknowledges the pre-eminence of Indigenous ways of knowing in conducting research in Indigenous communities. The central wheel describes the four core principles which led the development of the outer rungs. The middle wheel describes the cyclical process of carrying out community research, while the outer wheel describes the sub-steps that were found most relevant for the development of research with SNGR in the context of this work.

The framework is not comprehensive, nor does it serve as a ‘checklist’ of steps to accomplish during the research process, though ignoring sub-steps is not recommended. Some sub-steps are direct actions, while others are more abstract. It is important to note that while the framework’s wheel shape designates a set pattern of action, the circular shape of the framework speaks to the importance of iteration in the project process and the emphasis on the holistic inter-relational nature of each sub-step. Each step in this wheel should be performed iteratively and continuously. The divisions of the wheel, namely the four steps in the core principles, the four steps in the iterative framework, and the sixteen steps in the framework sub-steps, appear somewhat arbitrary, primarily chosen for organizational convenience and to present a manageable set of points for consideration. In addition, many sub-steps are not exclusive to one of the four main framework steps. For example, *Cultural Differences in Time Perception* can affect both effective Community Engagement and efficient Data Collection & Analysis. However, the sub-steps were placed under the heading that was felt best suited to this project. Finally, given the recent rapid pace at which Indigenous-settler relations have been changing, the framework is expected to act as a ‘living document’.

This framework is also rooted in the principles of OCAP (Ownership, Control, Access, and Possession). Fundamental to Indigenous data governance, it affirms the rights of communities to determine how data collected on their lands is used and shared. This control is crucial for maintaining Indigenous self-determination and nationhood in order for communities to be a part of the interpretation of their own data [1]. This also affirms the validity and allows for the flourishing of IK and TEK as separate epistemological systems to WS which need not compete against one another.

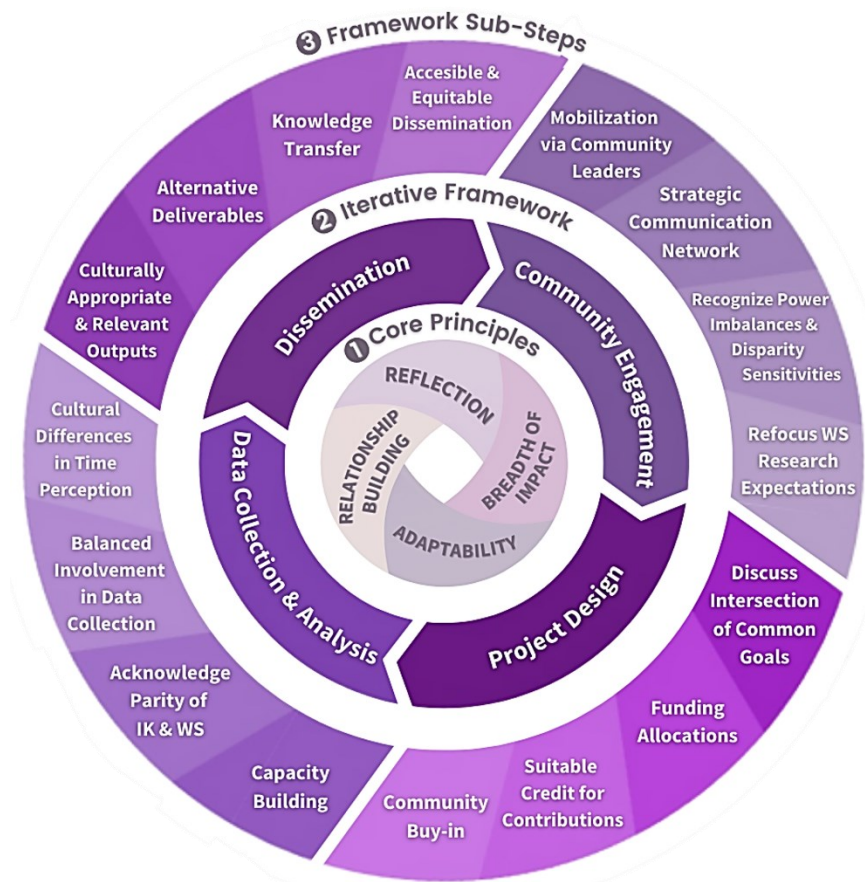


Figure 30. The developed co-creative framework.

4.2.1. Wheel 1: Core Principles

The core principles, briefly introduced here, are important to consider throughout the entire community engagement process and will receive further elaboration in subsequent subsections.

4.2.1.1. *Breadth of Impact*

The project’s breadth of impact should focus on the needs of one or many Indigenous communities, rather than those of the researchers. It is equally important to consider how the knock-on effects of a project’s or researcher’s actions can help contribute to the well-being of a community. These considerations are crucial because they facilitate meaningful alignment of perspectives to enhance co-development and foster community trust. In assessing next steps, the breadth of impact should be continuously assessed, as it can be easy to stray from the relevant breadth onto a path that

provides disproportional incentives for the researcher or institution. Breadth of impact is also to be considered on a personal level, emphasizing the use of one's own abilities and expertise as a WS researcher while not interfering in the implementation and translation of Indigenous ways of knowing [8].

4.2.1.2. Adaptability

While Indigenous and Western societies have long proximally coexisted, the survival and failure of Indigenous societies to be assimilated into Western colonial culture speaks to their continued existence as a series of independent and unique societies throughout the otherwise colonial landscape of Turtle Island. It is thus vital to be adaptable to differing cultural and epistemological baselines within an Indigenous nation throughout one's work as one would when abroad. As settler-Canadians are entwined in the architecture of colonialism, effective adaptability will require the dismantling of assumptions previously thought to be universal or fundamental and will be an ongoing point to monitor [9]. Do not be surprised if an entire project method is deemed inappropriate for use with the community. Be open and receptive to criticism from the community.

4.2.1.3. Relationship Building

The essence of Indigenous relationship-building hinges on dismantling the imperialist and colonialist mindset [10]. This necessitates not only recognizing Turtle Island as Indigenous territory but also actively comporting in accordance with its Indigenous status [11]. In the context of Indigenous identity, it is imperative to note that while many individuals prefer to be addressed by their specific constituent nation, there lacks a universally preferred terminology for self-identification among Indigenous populations. As is the case with any relationship, maintaining a working relationship requires constant attention and nurturing, especially in closely-knit indigenous societies where relational accountability is paramount [12, 13]. Nurturing this

relationship may require more navigating the social and political landscapes than might otherwise be necessary in WS-oriented research.

4.2.1.4. Reflection

Finally, reflection and open-mindedness are essential in maintaining critical and introspective mental pathways and show respect and a commitment to behaving ethically. Reflection is crucial in preserving accountability on the part of the research team. Lack of accountability is characteristic of parachute research [14]. Reflection additionally shows effective listening and willingness to maintain the role of an ally rather than attempting to dominate the intellectual space [8]. Active listening also encourages asking questions. Examining how one's personal biases can be managed and acknowledging the confluence of worldviews during the research process will lead to healthier, more genuine dialogue with project partners. On the other hand, blindly following a research method, even if it yielded positive results with another community, can lead to a loss of trust from the community. Following a strict method may oversimplify complex issues, missing key details which end up causing a misapplication of the project. Even in the most seamless research endeavours, working with Indigenous communities as an outsider necessitates preparedness for receiving constructive criticism.

4.3. Results: Implementing the Co-Creative Framework

4.3.1. Community Engagement

Engaging directly with the community is to be done first, well before any of the other framework steps. Ideally, the community should be engaged years before the first data collection takes place. Community engagement also involves keeping the community involved and informed regarding ongoing project activities. Publishing a paper requires formal consent of Indigenous legal bodies, especially when acting as a knowledge translator of IK. When engaging, be mindful of nonverbal

communication. Indigenous communities are high-context societies, which will not be as direct if a request is inappropriate, even if made in a manner which may be otherwise ‘normal’ in a Western context [15]. Jokes or stories may be used as indirect answers to questions [13, 16]. Avoid participation in events not explicitly intended for outsiders, such as ceremonial gatherings, particularly when uninvited [16]. But being invited to and participating in community events, even those initially perceived as unrelated, builds community trust, and indicates that the researcher is invested in the community’s long-term well-being.

4.3.1.1. Mobilization via Community Leaders

Mobilization via community leaders is one of the most important steps for approaching a community with co-creation in mind. Facilitating active engagement of community leaders as project stakeholders increases the likelihood of project information effectively permeating their networks. Ideally, such as in the case with Dawn Martin-Hill, community leaders may also be leaders in the academic community, allowing for community trust that research will be conducted in an unobtrusive and respectful manner. Her long history of community engagement enabled making connections with local community experts and educators who were keen to offer their help. This demonstrates the importance of maintaining connections with a wide variety of leaders, not just political ones [8]. Some community members will not be comfortable regardless of whether the project is led by an Indigenous or non-Indigenous member of academia due to their overt ties to colonial institutions.

4.3.1.2. Strategic Communication Network

Choosing a strategic communication network carefully will help dictate the success of the project. Discerning members who are respected and well-trusted by the community may take time, but it is important in ensuring the credibility of one’s intentions [8]. It is also important to connect with

community members with similar interests. Rod Whitlow, a trained biologist, has extensive experience bringing public attention to water quality issues on SNGR and provided studies of water quality parameters along the McKenzie and Boston Creeks some three decades prior. Meanwhile, Christopher Martin is intimately involved with providing hands-on environmental instruction to high school students at the Six Nations Polytechnic Science, Technology, Engineering, Arts, & Math (STEAM) Academy. Both partners were key community relays. Allowing community members to voice their concerns is needed. Field experiments were rescheduled to alternative dates with improved attendance rates due to insufficient initial student participation. Maintaining this communication network was done by texting or calling community members directly rather than using e-mail. However, community access to technology may differ.

4.3.1.3. Recognizing Power Imbalances & Disparity Sensitivity

Engaging with Indigenous communities requires acknowledging the history and continued effects of colonialism [17]. Without acknowledging this, there is no basis to acknowledge how and why one's co-creative work plays a part in underscoring Indigenous self-determination [9]. Recognizing treaty obligations underscores Canada's historical context beyond that of a nation composed solely of peaceful immigrants [18, 19]. Much has also been written about the non-white or non-Indigenous researchers who, while also up against white privilege, still benefit from its current implementation [9]. The decolonization process, while Indigenous-led, must be also carried on by settlers [9, 18]. Enrolling in an online indigenous history course, even if one has previously completed such a course, will serve as a valuable means of refreshing one's understanding of the subject [2]. While it is acceptable to acknowledge the grief of the past, this does not encourage metaphorical self-flagellating, as there is no advantage in disadvantaging a group of individuals for the benefit of another [10].

4.3.1.4. Refocus WS Research Expectations

Refocusing research expectations here refers to reframing research expectations to community members, emphasizing openness and transparency. Regardless of the small number of knowledge holders that the researcher may interact with, the work often requires the community at large to be indirectly involved with the research. The installation of water quality monitoring systems (WQMSs) required parking access on the property of community members and access to the McKenzie Creek via their waterfront. Community members were contacted via community partners for permission. A pamphlet describing the planned activities was distributed to local community members (Figure 31). It is important to use accessible, non-technical language, especially given the Western educational disparities observed between FN members living on reserves and the general Ontario population [20, 21]. Throughout the installation process, community members exhibited a keen interest and enthusiasm for participation, with the majority actively observing the fieldwork.

Featured here is one of two water quality monitoring stations intended for use in the McKenzie Creek.

It consists of a floating pool ring, anchored in place with a polymer rope and anchor (not pictured). The ring supports a waterproof plastic box. The box components are powered by an internal battery, which, in turn, is charged by the solar panel on top of the box. The battery is used to power a series of sensors and data relay systems for use of live, continuous monitoring of the McKenzie Creek water.

The monitoring station supports monitoring of five parameters: pH, conductivity, dissolved oxygen, water temperature, and turbidity. These sensors dangle off the monitoring station via ~20 in cables. The presence of these sensors in the water has no effect on the water quality itself. The first two sensor stations are slated to be deployed at the Cayuga Rd bridge and at a location a few hundred meters upstream from there.

On each box is a bright yellow sticker advertising the danger of an electric shock risk should one tamper with the box. While this is not actually the case and this sign primarily acts as a deterrent, it is important that residents stay clear of the area of the box, as these boxes are custom-built for deployment on the creek, with many sensitive pieces of electronic equipment inside and custom 3D-printed parts that are not easily fixed.

Feel free to contact Erik Fr chet te (frecheeee@mcmaster.ca) or Charles de Lannoy (delannoc@mcmaster.ca) for any questions.



Figure 31. Pamphlet sent out to alert community members of the upcoming activities on the McKenzie Creek in the first year of WQMS operation.

4.3.2. Project Design

Project design should highlight Indigenous identity through their relationships to the land and fellow community members. Research projects seeking to involve Indigenous communities should reevaluate their focus if they do not address these dimensions. Acquiring institutional ethics approval is not sufficient grounds to run experimentation. Here, the project directly involved monitoring the McKenzie Creek with a series of real-time WQMS due to community concerns over water quality. When the WQMSs are working more reliably, the community intends to continue the development of these systems and use their data for future community projects, emphasizing the community's long-term well-being and self-determination.

4.3.2.1. Discuss Intersection of Common Goals

Discussing common goals ensured WQMSs were used in a manner more appropriate to the community. The optimal placement for WQMSs on the reserve was initially considered to be the most downstream point of McKenzie Creek, within the reserve boundaries, to enhance its ability to detect community-wide contamination originating from point source disposal and wastewater lagoons. Subsequent discussions with residents led to the examination of only the wastewater lagoons, entailing the placement of WQMSs in locations situated directly upstream, directly downstream, and adjacent to the lagoons along the creek. Community events also offer some of the best opportunities to discuss common goals. One such event attended provided an opportunity for knowledge exchange between the Grand Traverse Band in Michigan, who were seeking cost-effective monitoring solutions for the Boardman River, and SNGR, aiming to gain insights from the band's experience in removing aging dams along the Boardman River to enhance aquatic health, a parallel initiative of interest for SNGR along the Grand River [22].

4.3.2.2. Funding Allocations

Fairly compensating holders of IK and TEK for their time, particularly during fieldwork, is crucial due to their daily commitments to their families and communities, making the provision of community aid to WS researchers a dedicated and time-consuming endeavour. This includes providing honoraria for student helpers. The acceptability of land transfer as a component of the decolonization process is also possible, contingent upon the specific research context [10]. Funding bodies must also ensure that local talent is directly incorporated into the funding model as not to encourage an unbalanced power dynamic [2, 23].

4.3.2.3. Suitable Credit for Contributions

Indigenous knowledge holders often face marginalization within academic spheres due to the absence of formal doctoral qualifications. The inclusion of Indigenous authorship on research papers draws attention to their essential contributions. The creation of secondary or post-secondary certificates to acknowledge Indigenous involvement in the project not only highlights their contributions but also fosters capacity building within the community [7].

4.3.2.4. Community Buy-In

Obtaining community buy-in for the SNGR surface water investigation project was facilitated by the preexisting demand for such research within the community. Community buy-in still necessitates ongoing renewal and a steadfast commitment to the foundational framework principles rather than being a one-time authorization for perpetual research. The distribution of the community pamphlet was not a barrier to continued community interaction via online or in-person community events.

4.3.3. Data Collection & Analysis

Data collection must be done with respect to local conventions, and formal data-sharing agreements should be crafted to determine the conditions of its use [6]. Data analysis and interpretation must occur in a manner that is balanced between Indigenous and non-Indigenous researchers, while acknowledging the validity of IK and WS, and considering how collection of the data can further highlight Indigenous self-determination.

4.3.3.1. Capacity Building

Capacity building is defined as the building up of skills and abilities of communities for their survival. CBPR, in allowing community members direct access to the participation of research, allows community members to gain new skills, provides filling in knowledge gaps with the help

of IK and TEK, and contributes to a shared sense of purpose, among other benefits [24]. Many Indigenous communities are located far from large population centres, and Indigenous maintenance of devices in their backyard can reduce overhead costs for researchers. However, efforts are still underway to reduce the maintenance requirements of WQMSs to a monthly or less frequent interval. Youth capacity building is especially important in this context [2]. Through community partner Chris Martin, students from the STEAM Academy expressed interest in learning about water monitoring and testing. Students gained an understanding of these concepts through the collection of preliminary samples along the McKenzie Creek and the installation of WQMSs. This was followed up by researchers conducting a two-day workshop at the academy to enhance students' practical exposure to water monitoring and testing concepts. This relationship continued throughout the development of the WQMSs. Capacity building efforts can be seen in Figure 32.

4.3.3.2. Acknowledge Parity of IK & WS

Recognizing power imbalances is key to acknowledging the parity of these two epistemological systems. It must be emphasized that harmonizing IK and WS means treating each as its own equally valid knowledge system, as many previous attempts to combine these two epistemologies resulted in the selective incorporation of IK into Western societies to the detriment of maintaining Indigenous identity [7]. It will become apparent with greater interaction with Indigenous communities that many IK concepts cannot be directly related to those in WS. Maintaining this separation is essential to minimize the risk of misinterpreting Indigenous knowledge.

4.3.3.3. Balanced Involvement in Data Collection

Data collection should always involve the onsite expertise of a community partner. One of the community partners was always onsite for sampling or WQMS installation which involved

coordinating around their schedule. Students from the STEAM Academy were often present as well, though natural scheduling changes and COVID-19 protocols frequently required rescheduling or resulted in student absences. Fears of COVID-19 were most noticed at this stage, as community vigilance against the virus persisted after complacency emerged from the non-Indigenous public.



Figure 32. Students and staff members from STEAM, as well as SNGR community partners, in various stages of setting up a WQMS (a-c), STEAM staff (community partner Chris Martin) and students learning about the workings of a WQMS (d), selfie with community partner Rod Whitlow following successful installation of a WQMS (e).

4.3.3.4. *Cultural Differences in Time Perception*

Time perception plays a key role in broadcasting in emphasizing what societies value. Many Western societies tend to place value on performing one task at a time, called monochronism,

while most others, including Indigenous societies, do not regulate a linear task order as strictly [15, 25]. Polychronism is associated with a lowered importance of deadlines and punctuality, but a higher importance is placed on interpersonal relationships [26]. These differences have manifested in the last-minute rescheduling of meetings, sudden community event invitations, or cancellations. This phenomenon was also observed when individuals from one's personal network, seemingly unrelated to the project, participated in project meetings. Addressing broad societal organizational needs within a project scope may lead to project delays [2]. As such, being aware of these differences in time perception can allow academics to plan accordingly without tying the community to a Western academic schedule.

4.3.4. Dissemination

Dissemination here encompasses *how* the data obtained from the community can be reintegrated into the community for its utilization by the community. Dissemination needs to occur in a manner which disincentivizes WS notions of ownership, as this otherwise implies that knowledge can be reserved for a knowledgeable 'elite' and that the knowledge does not have universal relevance [27]. Traditionally, academic ecological knowledge is transmitted by paywalled scientific journals, which use technical language not suited for community use [2]. Dissemination also means engaging with the community to determine the data's acceptability for publication, given Indigenous ownership of data produced in their communities, as well as to correct errors in knowledge translation [6]. Proper dissemination ensures that information is used in a culturally relevant context so that it appeals to the Indigenous audience. Many of the steps in dissemination are currently in the process of being realized.

4.3.4.1. Culturally Appropriate & Relevant Outputs

Outputs will vary across Indigenous communities. This variation necessitates the allocation of time during community events for the acquisition of knowledge regarding the most suitable approach to appeal to an Indigenous audience. Researchers provided research updates and capacity-building opportunities through the community podcasts. The dissemination of these podcasts through community members' social media channels and their hosting by community members fostered a sense of relevance and facilitated productive dialogue in harmonizing WS and IK [28]. Another community-focused output included the framework design. While intended for a WS audience, the framework design emphasizes visual representation over tabular or written formats, incorporating Indigenous emphasis on visual knowledge transfer.

4.3.4.2. Alternative Deliverables

While the water quality data is useful in itself for WS empirical research, its integration with Indigenous epistemologies is limited, necessitating alternative project outcomes to maximize community benefit. As mentioned, WQMSs were used in youth community capacity building. In maintaining knowledge transfer relationships with youth, engaging youth in their community with water research technology enhances the likelihood of their continued interest in STEM/environmental monitoring education due to the positive experiences gained. This capacity building is extended to the community at large when the WQMSs become fully operational, as well as other communities that wish to benefit from this technology. Additionally, a community project using the open-access online multimedia platform Terrastories (terrastories.app) will include this sensor setup to not only share environmental knowledge, but connect the community more deeply with stories associated with water and local environment [7].

4.3.4.3. Knowledge Transfer

Conceptualizing knowledge transfer into WS disciplines does not map with Indigenous thinking, which allows for a more holistic approach [29]. Meeting with elders at community events provided the opportunity for storytelling and exchange of cultural practices. While knowledge transfer of project goals and deliverables is important to accomplish within Indigenous communities, it is arguably more important as WS practitioners to be able to use one's experiences working with communities to act as examples for settler populations [9]. Bringing those results to the community and engaging in dialogue sets an example of a productive relationship for the wider scientific community on interacting respectfully with Indigenous ways of knowing [8]. This work has noted the importance of Indigenous community members for their time and expertise in providing community knowledge that sped up the WQMS installation process and their direct involvement in the installation process itself while referencing elements of my personal decolonization process. For some working directly with Indigenous knowledge this will involve positioning oneself as a translator of traditional knowledge, rather than as someone who has entered the community with their own goals and agenda [27]. Ultimately, the onus of accurately representing Indigenous knowledge rests solely with the researchers.

4.3.4.4. Accessible & Equitable Dissemination

The dissemination of data must be done in accordance with data-sharing protocols put in place early in the project's development. Data should be made accessible to the community, such as in allowing research papers to be published without a paywall. Keeping data segregated allows for the proliferation of socioeconomic divides [23]. Results obtained will be shared with the community, but they do not yet present new insight into the state of internal SNGR waterways.

Some data is clearly unrealistic, given data collected in previous monitoring work, while the remaining perceived accurate data reveals little about community concerns on their internal waters.

4.4. Discussion: Reflecting on Implementing the Framework

The framework seeks to guide academics for research protocols within Indigenous communities, given the history of helicopter research. However, as helicopter research has historically involved mishandling or misrepresentation of IK, TEK, or Indigenous peoples themselves, much of the literature noted previously emphasizes project design with this history in mind. WQMS deployment would have been possible on bodies of water not on Indigenous communities, but lacking a precise reason for monitoring would have rendered this only a case study in building WQMSs and thus implementing minimal useful constraints on their engineered parameters. Designing WQMS with Indigenous communities in mind, many of which are located in remote areas with limited cell service, prompted exploration of LoRa technology for remote data transfer as well as a monitoring system that could easily be transported by one or at most two people. It also allows for the community to gain insight into their waters using quantitative measurements. Of course, the WQMS development and installation benefited the community through gainful social activities. While the community and researchers both gained from this co-creative experience, and considering the current literature, the framework appears to have greatest relevance when researchers are acting as direct knowledge translators of IK or TEK rather than when implementing WS tools on Indigenous communities.

Despite earlier commentary regarding cultural differences in time perception, delays in WQMS deployment were exclusively caused by difficulties in troubleshooting. Troubleshooting progressed on a slow enough timescale to allow for the coordination of field days several days in advance. Even so, implementing a shared online calendar may have been useful in coordinating

quicker turnaround on scheduling field days. However, this would require both researchers and community partners to provide frequent and comprehensive calendar updates, but this is not realistic. While the support of community members was positive, there was still room for more student engagement. Lowered engagement may be attributed in part to the incomplete state of the WQMSs network and the ongoing considerations regarding the community's data utilization, with the prospect of increased student engagement contingent upon the output of stable and consistent data.

4.5. Conclusions

This work has outlined a co-creative framework for scientists and engineers when conducting research in collaboration with Indigenous communities. The framework was developed through experiences working with the SNGR community, seeking to harmonize IK and WS epistemologies while respecting the sovereignty and self-determination of Indigenous communities on which research is taking place. While the framework is presented with reference to water quality monitoring, it can be expanded and adapted to fit the research need. However, it is incumbent upon the scientific community to maintain a commitment to engaging with Indigenous peoples in a way that upholds the foundational principles of this framework and, in doing so, contributes to a more just and collaborative future for research endeavours. It is important to acknowledge that the journey toward equitable and respectful research collaboration with Indigenous communities is ongoing. The more Indigenous research is done with care and attention to those living on community, the more likely others are to follow in that example, prompting social pressure for those who do not conform to reconsider their approach to Indigenous research.

4.6. References

- [1] B. Schnarch, "Ownership, Control, Access, and Possession (OCAP) or Self-Determination Applied to Research: A Critical Analysis of Contemporary First Nations Research and Some Options for First Nations Communities," *Journal of Aboriginal Health*, vol. 1, no. 1, pp. 80-95, 2004. [Online]. Available: <https://jps.library.utoronto.ca/index.php/ijih/article/view/28934/24060>.
- [2] C. Wong, K. Ballegooyen, L. Ignace, M. J. Johnson, H. Swanson, and I. Boran, "Towards reconciliation: 10 Calls to Action to natural scientists working in Canada," *Facets*, vol. 5, no. 1, pp. 769-783, 2020, doi: 10.1139/facets-2020-0005.
- [3] D. Groenfeldt, "Learning from Indigenous water ethics," in *The Cultural Dynamics in Water Management from Ancient History to the Present Age*, X. Y. Zheng Ed., 2021.
- [4] J. Kolopenuk, "Provoking Bad Biocitizenship," *Hastings Cent Rep*, vol. 50 Suppl 1, pp. S23-S29, May 2020, doi: 10.1002/hast.1152.
- [5] L. Day *et al.*, "'The Legacy Will Be the Change': Reconciling How We Live with and Relate to Water," *International Indigenous Policy Journal*, vol. 11, no. 3, pp. 1-23, 2020, doi: 10.18584/iipj.2020.11.3.10937.
- [6] M. S. Adams *et al.*, "Toward increased engagement between academic and indigenous community partners in ecological research," *Ecology and Society*, vol. 19, no. 3, 2014, doi: 10.5751/es-06569-190305.
- [7] D. Martin-Hill *et al.*, "Striving toward reconciliation through the co-creation of water research," in *Indigenous Water and Drought Management in a Changing World*, (Current Directions in Water Scarcity Research, 2022, pp. 13-40.
- [8] E. Carlson-Manathara, "What Indigenous Peoples Have Asked Of Us," in *Living In Indigenous Sovereignty*, E. Carlson-Manathara and G. Rowe Eds.: Fernwood Publishing, 2021.
- [9] E. Carlson-Manathara, "Settler Colonialism and Resistance," in *Living In Indigenous Sovereignty*, E. Carlson-Manathara and G. Rowe Eds.: Fernwood Publishing, 2021.
- [10] G. T. Alfred, "Restitution is the Real Pathway to Justice for Indigenous Peoples," *Response, Responsibility, and Renewal: Canada's Truth and Reconciliation Journey*, pp. 179-187, 2009.
- [11] N. Klein, "An Evening with Naomi Klein: This Changes Everything," 25:35-25:45 ed, 2016, p. <https://www.youtube.com/watch?v=TyVymale9EI>.
- [12] A. J. Mills, "Miinigowiziwin: All That Has Been Given for Living Well Together: One Vision of Anishinaabe Constitutionalism," Doctor of Philosophy, Faculty of Law, University of Victoria, 2019. [Online]. Available: <http://hdl.handle.net/1828/10985>
- [13] E. Carlson-Manathara and Anonymous, "Introducing the Narratives," in *Living In Indigenous Sovereignty*, E. Carlson-Manathara, A. Craft, D. Kennedy, L. Star, and C. Richard Eds.: Fernwood Publishing, 2021.
- [14] P. A. Cochran *et al.*, "Indigenous ways of knowing: implications for participatory research and community," *Am J Public Health*, vol. 98, no. 1, pp. 22-7, Jan 2008, doi: 10.2105/AJPH.2006.093641.
- [15] E. Würtz, "Intercultural Communication on Web sites: A Cross-Cultural Analysis of Web sites from High-Context Cultures and Low-Context Cultures," *Journal of Computer-Mediated Communication*, vol. 11, no. 1, pp. 274-299, 2005, doi: 10.1111/j.1083-6101.2006.00013.x.
- [16] E. Carlson-Manathara and Anonymous, "Franklin Jones," in *Living In Indigenous Sovereignty*, E. Carlson-Manathara and G. Rowe Eds.: Fernwood Publishing, 2021.
- [17] S. M. Hill, "Introduction," in *The Clay We Are Made Of: Haudenosaunee Land Tenure on the Grand River*, J. Brownlie Ed. Winnipeg, Manitoba: University of Manitoba Press, 2017, pp. 1-11.

- [18] C. Hiller, "'No, do you know what your treaty rights are?'" Treaty consciousness in a decolonizing frame," *The Review of Education, Pedagogy, and Cultural Studies*, vol. 38, no. 4, pp. 381-408, 2016, doi: 10.1080/10714413.2016.1203684.
- [19] P. Regan, *Unsettling the Settler Within*. UBC Press, 2010, pp. 83-4.
- [20] *First Nations, Inuit and Métis Education in Ontario*. (2017). [Online]. Available: <https://www.cfsontario.ca/wp-content/uploads/2018/10/2017.01-Indigenous-Education-fact-sheet.pdf>
- [21] *Education as a Social Determinant of First Nations, Inuit and Métis Health*. (2017). [Online]. Available: <https://www.ccnsa-nccah.ca/docs/determinants/FS-Education-SDOH-2017-EN.pdf>
- [22] N. Rao, "Tribal elder raises river restoration awareness," in *Great Lakes Echo*, ed: Capital News Service, 2018.
- [23] B. Minasny, D. Fiantis, B. Mulyanto, Y. Sulaeman, and W. Widyatmanti, "Global soil science research collaboration in the 21st century: Time to end helicopter research," *Geoderma*, vol. 373, 2020, doi: 10.1016/j.geoderma.2020.114299.
- [24] A. A. Mamun and D. C. Natcher, "The promise and pitfalls of community-based monitoring with a focus on Canadian examples," *Environ Monit Assess*, vol. 195, no. 4, p. 445, Mar 6 2023, doi: 10.1007/s10661-022-10841-y.
- [25] C. F. Kaufman, P. M. Lane, and J. T. Lindquist, "Exploring More than 24 Hours a Day: A Preliminary Investigation of Polychronic Time Use," *Journal of Consumer Research*, vol. 18, no. 3, pp. 392-401, 1991, doi: <https://www.jstor.org/stable/2489348>.
- [26] S. J. M. Adams and W. van Eerde, "Time use in Spain: is polychronicity a cultural phenomenon?," *Journal of Managerial Psychology*, vol. 25, no. 7, pp. 764-776, 2010, doi: 10.1108/02683941011075292.
- [27] C. Bennett, K. Fitzpatrick-Harnish, and B. Talbot, "Collaborative untangling of positionality, ownership, and answerability as white researchers in indigenous spaces," *International Journal of Music Education*, vol. 40, no. 4, pp. 628-641, 2022, doi: 10.1177/02557614221087343.
- [28] H. Grewal, "Bridging Indigenous Knowledge and Western Science: Co-Creating Best Practices for Collaborative Environmental Research," Master of Science, School Of Earth, Environment & Society, McMaster University, 2023. [Online]. Available: Unpublished Thesis
- [29] "Centering Indigenous Intellectual Traditions," in *Read, Listen, Tell: Indigenous Stories from Turtle Island*, S. McCall, D. Reder, D. Gaertner, and G. L. H. Hill Eds. Waterloo, Canada: Wilfrid Laurier University Press, 2017.

5. Conclusions and Recommendations

The work covered in the previous chapters holds significance across diverse academic disciplines. In Chapter 2, zwitterionic polymer coatings were synthesized for future use in marine antifouling (AF) applications. Oxygen permeability tests showed that the application of these coatings does not pose a barrier to oxygen transfer across PTFE barriers, which realizes the further potential use of zwitterionic coatings for AF applications. The creation of these multilayered coatings in a non-traditional LOC device may obviate the need for more expensive methods of determining the gas permeability of manufactured solids for benchtop use, given the obtained PTFE mass transfer parameters corresponded well with literature values. It is additionally suspected that the void fraction of PTFE plays a key factor in the speed of mass transfer. In Chapter 3, the development and implementation of water quality monitoring systems (WQMSs) for use in a rural sensing environment clearly showed viable data collection for use in CBPR activities. Once developed and troubleshooted, these co-created systems can be a tool for promoting Indigenous sovereignty in the SNGR community and beyond, as described in Chapter 4.

There are many sections of this work which require future study. While zwitterionic coatings have been routinely demonstrated to work in the lab and environmental fouling conditions, it will be useful to ensure that any series of zwitterionic coatings are able to possess good AF properties while not being fabricated in such a manner as to slow oxygen permeability significantly. Electrical impedance spectroscopy, for example, may be used to assess coating degradation or the accumulation of biofouling [1]. As coated AF materials are subject to abrasion or delamination, begetting further fouling, there may be a need to incorporate AF materials directly into the PTFE membrane itself. This will prove more difficult compared to working with other polymers, given the low temperature at which PTFE decomposes [2]. The addition of electrically conductive AF

fillers, such as carbon nanotubes or reduced graphene oxide, may allow for improved AF performance without sacrificing gas transfer [3]. The utilization of AF fillers also has the potential to mitigate the need for periodic disposal of the delicate DO membrane, allowing for manual cleaning. Should further studies be conducted with the materials utilized previously, the source of mass transfer delay at the sublayer interfaces should be investigated, as well as how to minimize the exhibited bias further. Regardless of the AF strategy pursued, a consistent method of fabrication should take place to allow for consistent characterization of void fraction, and the method of fabrication should be relatively homogenous so as not to propagate further void fraction due to mechanical stressors.

Implementing zwitterionic coating technologies onto other water quality sensors will prove much more challenging than with DO. In contrast to DO probes, pH and conductivity probes inherently detect charge disparities due to their operational principles. Given the bias present in DO probes with the application of an AF coating, this bias is expected to be exacerbated with a similar treatment for pH and conductivity probes. Obtaining turbidity measurements may be easier, but the necessity of recurrent recalibration arises unless uniform coating thicknesses are consistently achieved. Optical DO sensors may be considered due to their small data drift, but they are much more expensive than Clarke-type sensors. Nitrate, nitrite, or phosphate sensors should be included, as the land surrounding SNGR is predominantly agricultural, allowing for pronounced runoff effects. While the current WQMS system is capable of reading and relaying sensor data, its size and shape make it ineffective for wide distribution. A smaller, less energy intensive design is currently in development, capable of fitting into lightweight plumbing piping. The re-addition of a solar panel to the final design should be considered to compensate for power losses. There may be interest in establishing a live monitoring station by the GRCA at the terminus of the McKenzie-

Boston subwatershed. While this would undermine the development of an autonomous water quality network on SNGR as outlined above, the proper functioning of existing operational monitoring stations in the area, coupled with a dedicated maintenance team, might offer more effective means of providing the community with enhanced water quality insights.

5.1. References

- [1] N. Zhang, H.-J. Lee, Y. Wu, M. A. Ganzoury, and C.-F. de Lannoy, "Integrating biofouling sensing with fouling mitigation in a two-electrode electrically conductive membrane filtration system," *Separation and Purification Technology*, vol. 288, 2022, doi: 10.1016/j.seppur.2022.120679.
- [2] "PTFE Film (.002 to .025 thick)." Professional Plastics: The Leader in Plastic Sheets, Rods, Tubing, Profiles, & Components. https://www.professionalplastics.com/PTFE_FilmTeflon (accessed March 8, 2023).
- [3] Q. Zhou, P. Zhao, R. Xu, Z. Wang, W. Song, and X. Wang, "Porous graphene oxide surface-coated thin-film composite membrane for simultaneously increasing permeation performance and organic-fouling migration capacities," *Journal of Membrane Science*, vol. 661, 2022, doi: 10.1016/j.memsci.2022.120942.

Appendix A: Supplemental Information

Appendix A.1: Chapter 2 Supplementary Information

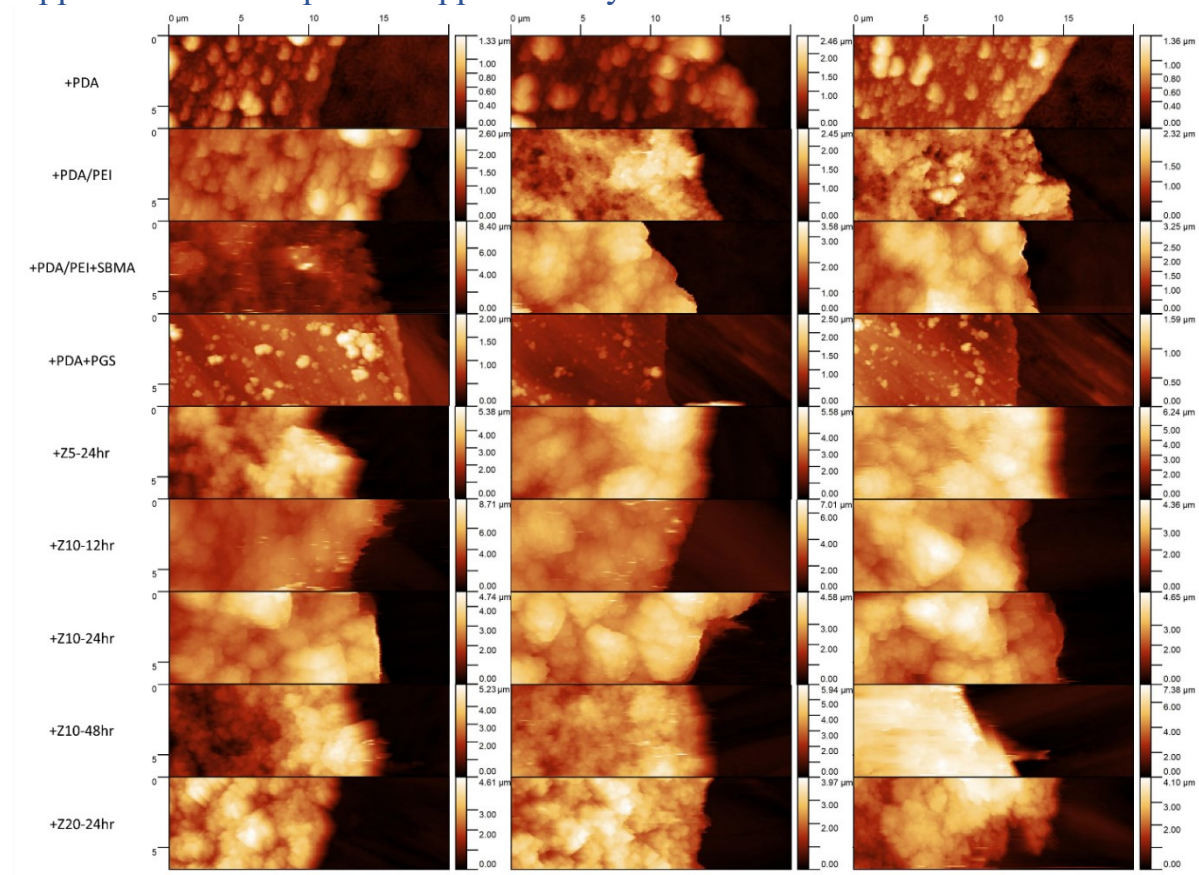


Figure A.1. Triplicate AFM scans for all coated samples.

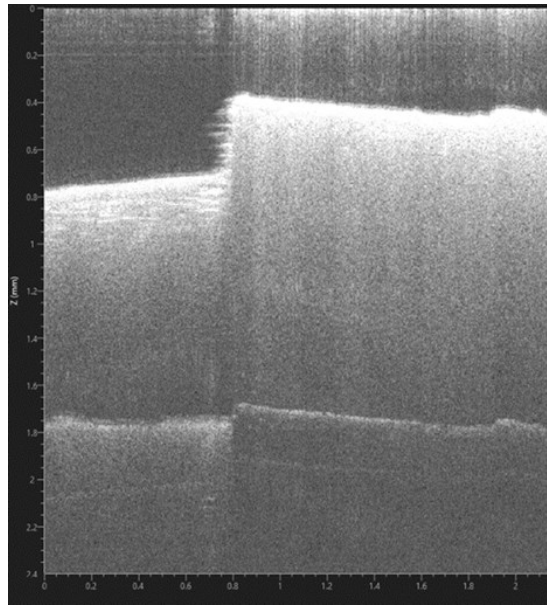


Figure A.2. Example OCT scan of an uncoated sample (left) with +Foul60 (right).

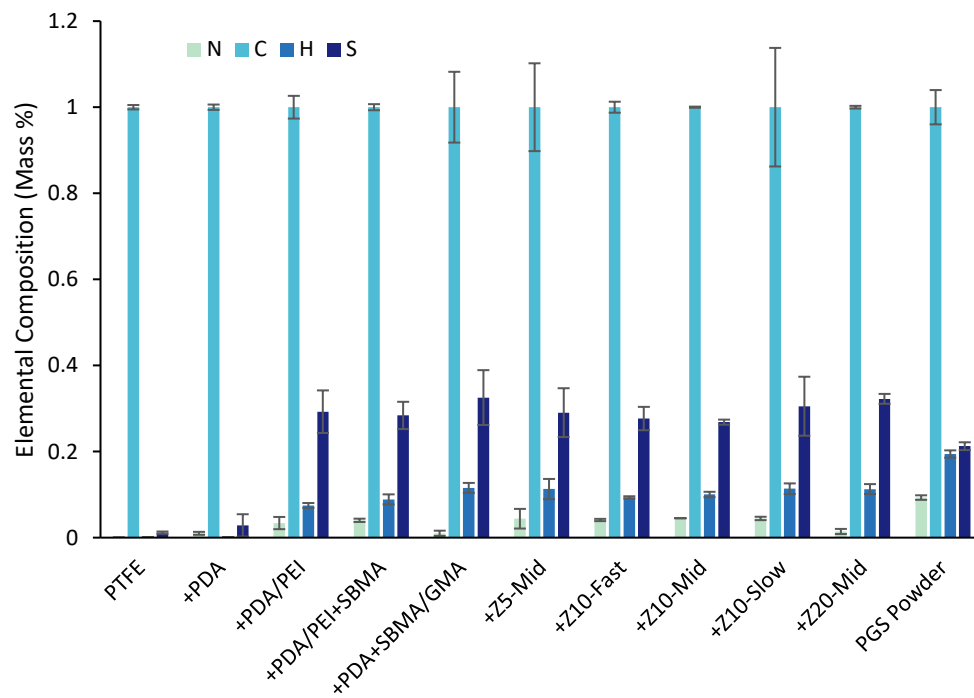


Figure A.3. Mass % Normalized to C.

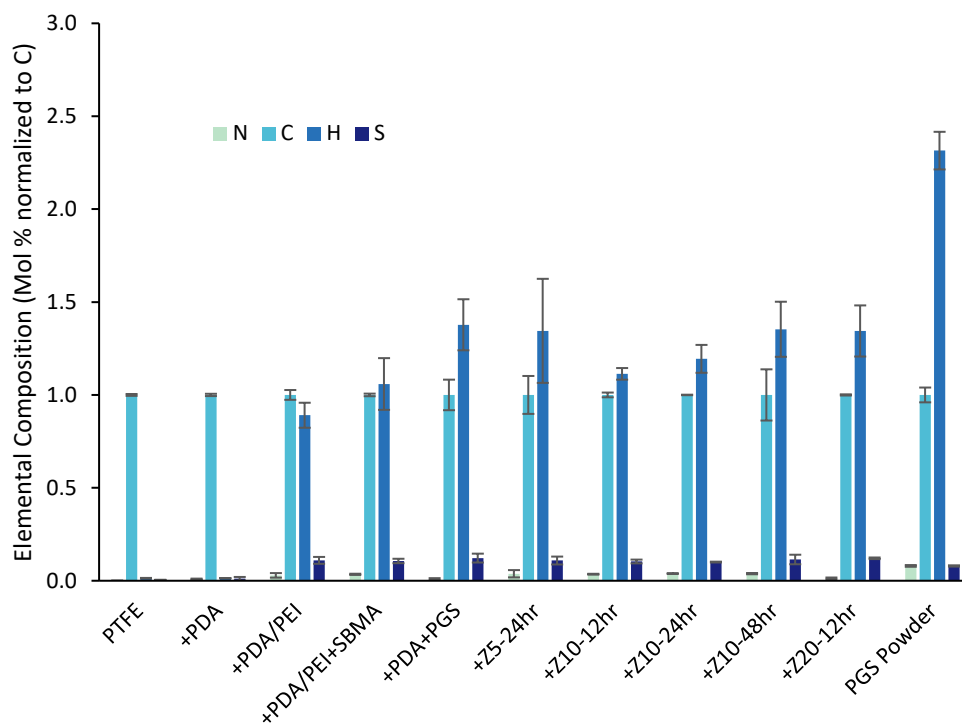


Figure A.4. Mol composition as normalized to carbon.

Table A.1. Original relative elemental percentage concentrations of bare PTFE, coated PTFE, and PGS powder samples as determined by XPS.

	C 1s	F 1s	N 1s	O 1s	S 2p	Si 2p
PTFE	32.76	67.24	-	-	-	-
+PDA	71.93	-	7.30	20.59	-	0.18
+PDA/PEI	68.04	2.02	14.77	15.18	-	-
+PDA/PEI+SBMA	67.52	-	11.29	20.16	1.03	-
+PDA+PGS	58.12	7.82	4.65	23.75	2.28	3.38
+Z5-24hr	65.60	-	7.84	23.57	3.00	-
+Z10-12hr	62.67	3.94	7.78	22.92	2.7	-
+Z10-24hr	64.99	-	8.09	23.86	2.74	0.32
+Z10-48hr	63.73	3.21	7.92	22.44	2.70	-
+Z20-24hr	64.93	-	6.79	24.51	3.78	-
PGS Powder	64.26	-	4.19	25.84	4.95	0.75

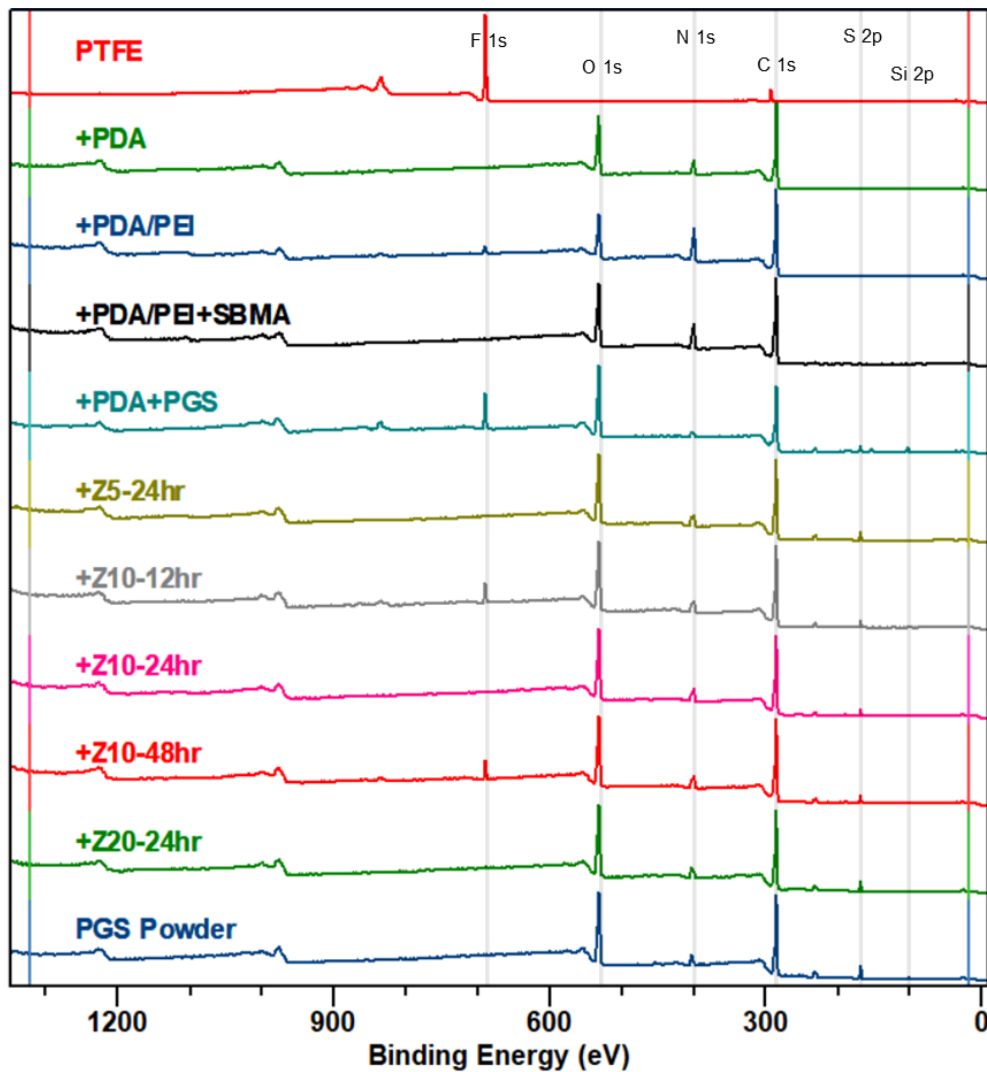


Figure A.5. Normalized XPS survey spectra for all samples.

Table A.2. Carbon XPS position data.

	C-Si	C-C	C-S	C-N	C-O	C=N	C=O	N-C-(CO) ₃	O-C=O	π - π	C-F
Mean	284.03	284.58	284.92	285.51	286.39	287.44	287.50	288.51	288.81	290.57	292.28
Standard Deviation	0.12	0.12	0.15	0.12	0.09	0.10	0.19	0.26	0.08	0.10	0.08

Table A.3. Fluorine XPS position data.

	F-C	CF ₂ - - (O,N)
Mean	689.53	690.87
Standard Deviation	0.12	0.47

Table A.4. Nitrogen XPS position data.

	-N=	-NH-	-NH ₂	N+	NO _x , π-π
Mean	398.87	399.88	401.96	402.34	405.56
Standard Deviation	0.19	0.11	0.48	0.04	0.00

Table A.5. Oxygen XPS position data.

	O=C	O-C	SO ₃ ⁻	C-O-C=O
Mean	531.03	532.47	532.88	533.43
Standard Deviation	0.13	0.47	0.17	0.50

Table A.6. Relative percentages of carbon bonds.

	C-Si	C-C	C-S	C-N	C-O	C=N	C=O	N-C-(CO) ₃	O-C=O	π-π	C-F
PTFE	-	-	-	-	-	-	-	-	-	-	100.00
+PDA	-	45.90	-	21.82	18.06	4.05	3.98	3.55	-	2.65	-
+PDA/PEI	-	29.52	-	35.67	21.43	4.00	4.13	4.01	-	-	1.23
+PDA/PEI+SBMA	-	25.04	3.14	29.39	25.03	4.90	4.32	2.62	4.90	0.64	-
+PDA+PGS	3.64	32.21	5.47	23.74	21.71	-	3.04	-	6.24	-	3.97
+Z5-24hr	-	24.91	4.95	28.05	27.18	3.74	3.16	-	8.01	-	-
+Z10-12hr	-	22.66	6.80	29.22	25.88	2.55	3.61	-	7.47	-	1.81
+Z10-24hr	1.08	22.63	6.21	28.16	26.48	4.11	3.36	-	7.97	-	-
+Z10-48hr	-	25.50	5.90	27.08	26.68	3.06	3.08	-	7.42	-	1.29
+Z20-24hr	-	26.66	6.07	26.71	28.29	2.12	1.62	-	8.52	-	-
PGS Powder	1.18	34.27	5.57	22.10	27.43	-	-	-	9.46	-	-

Table A.7. Relative percentages of fluorine bonds.

	CF ₂	CF ₂ -- (O,N)
PTFE	100.0	-
+PDA	-	-
+PDA/PEI	74.62	25.38
+PDA/PEI+SBMA	-	-
+PDA+PGS	88.59	11.41
+Z5-24hr	-	-
+Z10-12hr	84.71	15.29
+Z10-24hr	-	-
+Z10-48hr	88.70	11.30
+Z20-24hr	-	-
PGS Powder	-	-

Table A.8. Relative percentages of nitrogen bonds.

	-N=	-NH-	-NH ₂	N+	NO _x , π-π
PTFE	-	-	-	-	-
+PDA	8.88	79.63	10.24	-	1.26
+PDA/PEI	9.67	84.87	5.46	-	-
+PDA/PEI+SBMA	13.71	71.80	-	14.49	-
+PDA+PGS	10.11	41.39	-	48.51	-
+Z5-24hr	21.98	38.86	-	39.16	-
+Z10-12hr	18.26	45.11	-	36.62	-
+Z10-24hr	19.55	45.13	-	35.32	-
+Z10-48hr	20.61	43.86	-	35.52	-
+Z20-24hr	19.07	28.84	-	52.09	-
PGS Powder	3.17	-	-	96.83	-

Table A.9. Relative percentages of oxygen bonds.

	O=C	O-C	SO ₃ ⁻	C-O-C=O
PTFE	-	-	-	-
+PDA	32.87	67.13	-	-
+PDA/PEI	56.30	43.70	-	-
+PDA/PEI+SBMA	54.61	27.54	5.44	12.41
+PDA+PGS	31.59	47.51	7.59	13.31
+Z5-24hr	47.94	26.68	7.55	17.84
+Z10-12hr	46.44	25.77	9.59	18.20
+Z10-24hr	46.86	18.68	6.56	27.90
+Z10-48hr	47.57	26.77	7.94	17.71
+Z20-24hr	48.11	28.13	7.92	15.85
PGS Powder	45.13	30.45	7.01	17.40

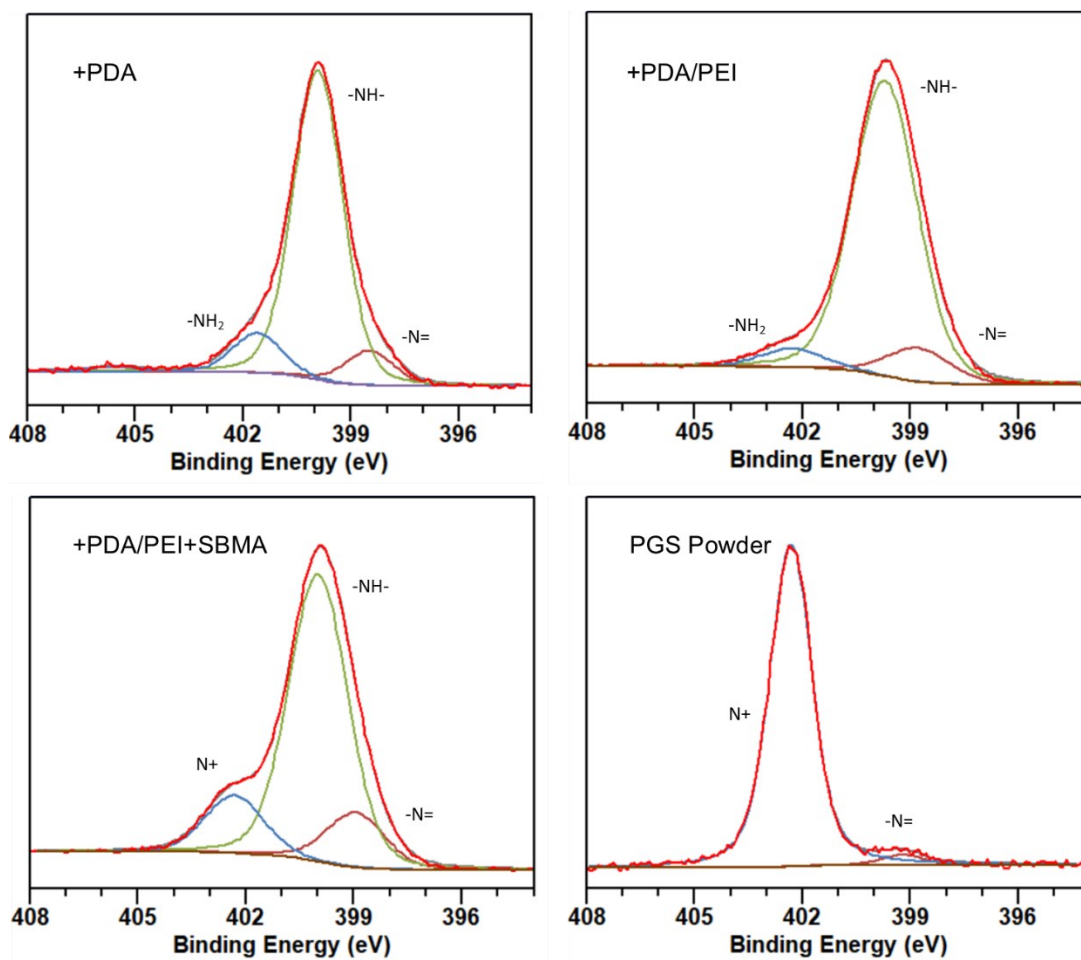


Figure A.6. N 1s spectra of +PDA, +PDA/PEI, +PDA/PEI+SBMA, and PGS powder.

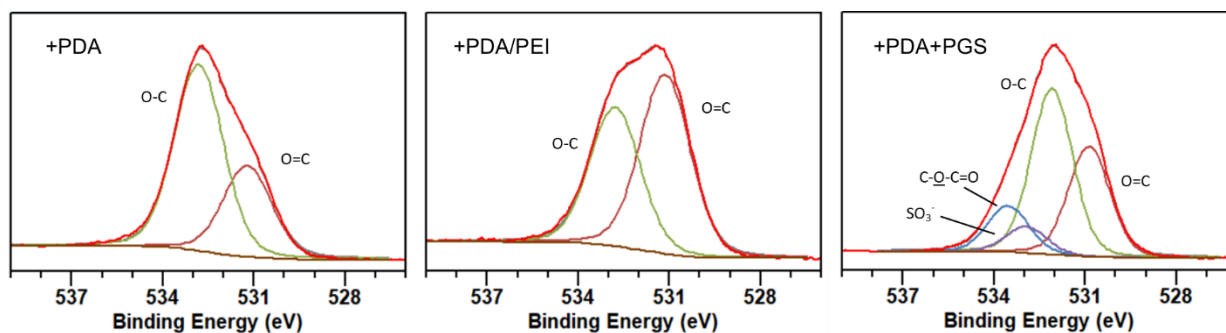


Figure A.7. O 1s spectra of +PDA, +PDA/PEI, +PDA+PGS samples.

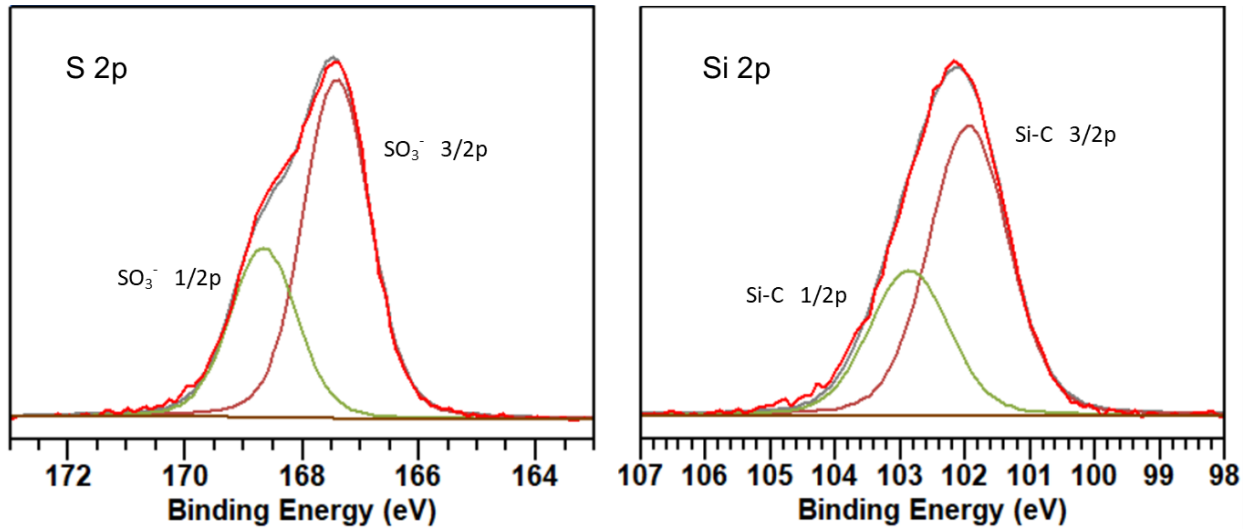


Figure A.8. Typical presentations of sulfur 2p and silicon 2p.

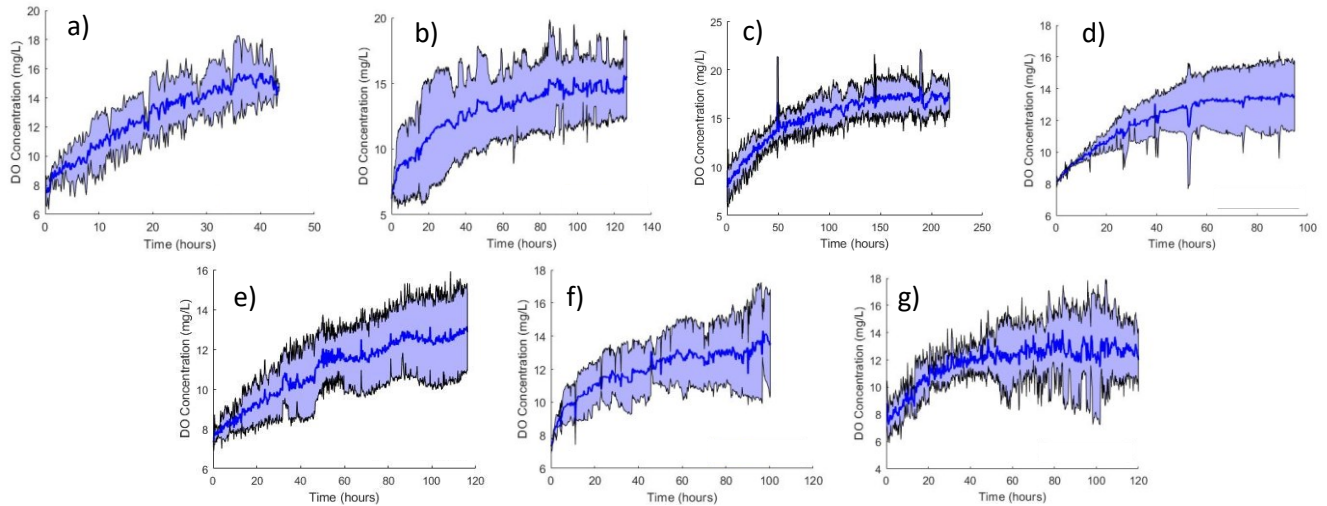


Figure A.9. Additional individual LOC tests not shown in Figure 17: a) +Foul14, b) +Foul60, c) +Z10-12hr, d) +Z10-48hr, e) +Z20-24hr, f) +Foul14, g) +Foul60. Shaded area represents standard deviation of three trials.

Table A.10. Model constants for concentration profile over time in OP tanks (time in hours).

	PTFE	+Foul14	+Foul60	+PDA	+PDA/PEI	+Z5-24hr	+Z10-12hr	+Z10-24hr	+Z10-48hr	+Z20-24hr
α	10.05093	10.22112	8.324725	12.51797	11.48199	6.955037	6.892914	6.394792	5.526088	6.246412
β	0.101057	0.040564	0.028851	0.020299	0.018347	0.031848	0.016776	0.034976	0.032939	0.048352
γ	0.099942	0.091838	0.095902	0.195968	0.200156	0.173929	0.098952	0.097827	0.099081	0.097352
δ	15.38652	17.06829	14.96718	16.33773	17.43699	13.89277	13.75508	12.34831	13.40687	12.80189

Table A.11 Model constants for concentration profile over time in OR tanks (time in hours).

	PTFE	+Foul14	+Foul60	+PDA	+PDA/PEI	+Z5-24hr	+Z10-12hr	+Z10-24hr	+Z10-48hr	+Z20-24hr
α	-6.6648	-9.59356	-9.12025	-7.21208	-12.244	-7.16659	-12.6688	-15.603	-11.4454	-7.60699
β	0.056989	0.047788	0.017404	0.016652	0.002638	0.021591	0.011843	0.009602	0.017125	0.042931
γ	0.122837	0.119615	0.120093	0.121243	0.118148	0.140863	0.173556	0.095899	0.112349	0.123698
δ	26.12106	24.21608	24.81323	24.69256	21.19768	24.07912	20.76022	19.09224	22.08885	27.32962

Table A.12. Gas permeation results as originally tested at 30°C.

Sample ID	Q, mol/m/s/Pa	D, m ² /s	S, mol/m ³ /Pa	Samp. thickness, mm
PTFE	$7.47 \times 10^{-16} \pm 1.20 \times 10^{-17}$	$3.14 \times 10^{-11} \pm 1.99 \times 10^{-11}$	$2.96 \times 10^{-5} \pm 1.84 \times 10^{-5}$	0.80
+PDA	$3.81 \times 10^{-16} \pm 5.09 \times 10^{-17}$	$3.15 \times 10^{-11} \pm 2.08 \times 10^{-11}$	$1.61 \times 10^{-5} \pm 1.23 \times 10^{-5}$	0.79

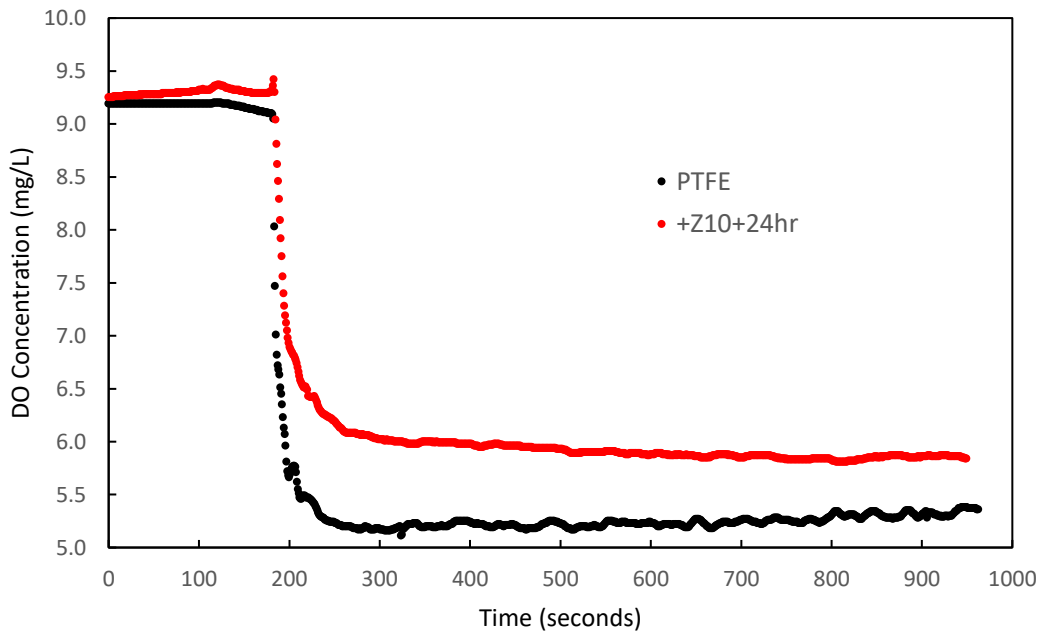


Figure A.10. Concentration profiles monitoring a sudden change in DO for modified and unmodified PTFE.

Table A.13. The following code produces the 2D and 3D concentration profiles shown in Figure 19.

```

clc;
clear all;
close all;

% Initial parameters
L_foul = 2e-6; % foulant layer thickness (m)
L_zwit = 1e-6; % zwitterion layer thickness (m)
L_graft = 2e-6; % PDA/PEI grafting layer thickness (m)
L_PTFE = 10e-6; % PTFE thickness in (m)
L_total = L_foul + L_zwit + L_graft + L_PTFE; % total length (m)
dx = 1.0e-7; % spatial step size (m)
dt = 1.0e-4; % time step size (s)
D_foul = 9.7e-12; % diffusivity of foulant (m^2/s)

```

```

D_zwit = 9.16e-12; % diffusivity of zwitterion (m^2/s)
D_graft = 5.1e-13; % diffusivity of PDA/PEI (m^2/s)
D_PTFE = 1.404e-11; % diffusivity of PTFE (m^2/s)
t_final = 50; % simulation end time (s)
alpha_low = 10.0509326153689; % model parameters for OP tank conc
vita_low = 0.101056641139388;
gamma_low = 0.0999418583778373;
delta_low = 15.3865196478933;
alpha_high = -6.66480317020079; % model parameters for OR tank conc
vita_high = 0.0569894881405939;
gamma_high = 0.12283651999359;
delta_high = 26.1210586059882;

% Spatial & time grids
x = 0:dx:L_total;
N = length(x);
t = 0:dt:t_final;
M = length(t);

% Initial conditions (in mg/L)
C_left = -alpha_high*exp(-vita_high*t/3600-gamma_high)+delta_high; % left wall concentration profile (OR)
C_right = -alpha_low*exp(-vita_low*t/3600-gamma_low)+delta_low; % right wall concentration profile (OP)
C_0 = -alpha_low*exp(-gamma_low)+delta_low; % initial concentration throughout membrane

% Initialize concentration matrix
Conc = ones(N, M) * C_0;

% Initial concentration
Conc(1, :) = C_left;
Conc(N, :) = C_right;

% BCs at interface of foulant and zwitterion layers
i_interface = round(L_foul/dx);
if L_foul == 0
else
    Conc(i_interface, :) = (D_zwit*Conc(i_interface-1, :) + D_foul*Conc(i_interface+1, :)) / (D_zwit + D_foul);
end

% BCs at interface of zwitterion and grafting layers
j_interface = round((L_foul + L_zwit)/dx);
if L_zwit == 0
else
    Conc(j_interface, :) = (D_graft*Conc(j_interface-1, :) + D_zwit*Conc(j_interface+1, :)) / (D_graft + D_zwit);
end

% BCs at interface of grafting layer and PTFE
k_interface = round((L_foul + L_zwit + L_graft)/dx);
if L_graft == 0
else
    Conc(k_interface, :) = (D_PTFE*Conc(k_interface-1, :) + D_graft*Conc(k_interface+1, :)) / (D_PTFE +
D_graft);
end

% Solving Fick's Law using forward difference in time and central difference in space
for j = 1:M-1
    for i = 2:N-1

```

```

if i == i_interface
    Conc(i, j+1) = (D_zwit*Conc(i-1, j) + D_foul*Conc(i+1, j)) / (D_zwit + D_foul);
    continue % skip first interface
elseif i == j_interface
    Conc(i, j+1) = (D_graft*Conc(i-1, j) + D_zwit*Conc(i+1, j)) / (D_graft + D_zwit);
    continue % skip second interface
elseif i == k_interface
    Conc(i, j+1) = (D_PTFE*Conc(i-1, j) + D_graft*Conc(i+1, j)) / (D_PTFE + D_graft);
    continue % skip third interface
end
if i < i_interface
    alpha = D_foul;
elseif i < j_interface
    alpha = D_zwit;
elseif i < k_interface
    alpha = D_graft;
else
    alpha = D_PTFE;
end
Conc(i, j+1) = Conc(i, j) + alpha*dt/dx^2 * (Conc(i+1, j) - 2*Conc(i, j) + Conc(i-1, j));
end
end

% Concentration profile at 't_final' seconds
figure;
plot(x, Conc(:, end));
set(gcf, 'color', 'w');
axis([0 L_total C_0-1 inf])
xlabel('Distance (m)');
ylabel('Concentration (mg/L)');
title("Concentration profile at "+t_final+" seconds");

% 3D plot of concentration profile as it changes over time
[X, Y] = meshgrid(x, t);
figure;
mesh(X, Y, Conc'); % surf if edges are desired
set(gcf, 'color', 'w');
xlabel('Distance (m)');
ylabel('Time (s)');
zlabel('Concentration (mg/L)');
title("Concentration profile over from 0 to "+t_final+" seconds");

```

Appendix A.2: Chapter 3 Supplementary Information

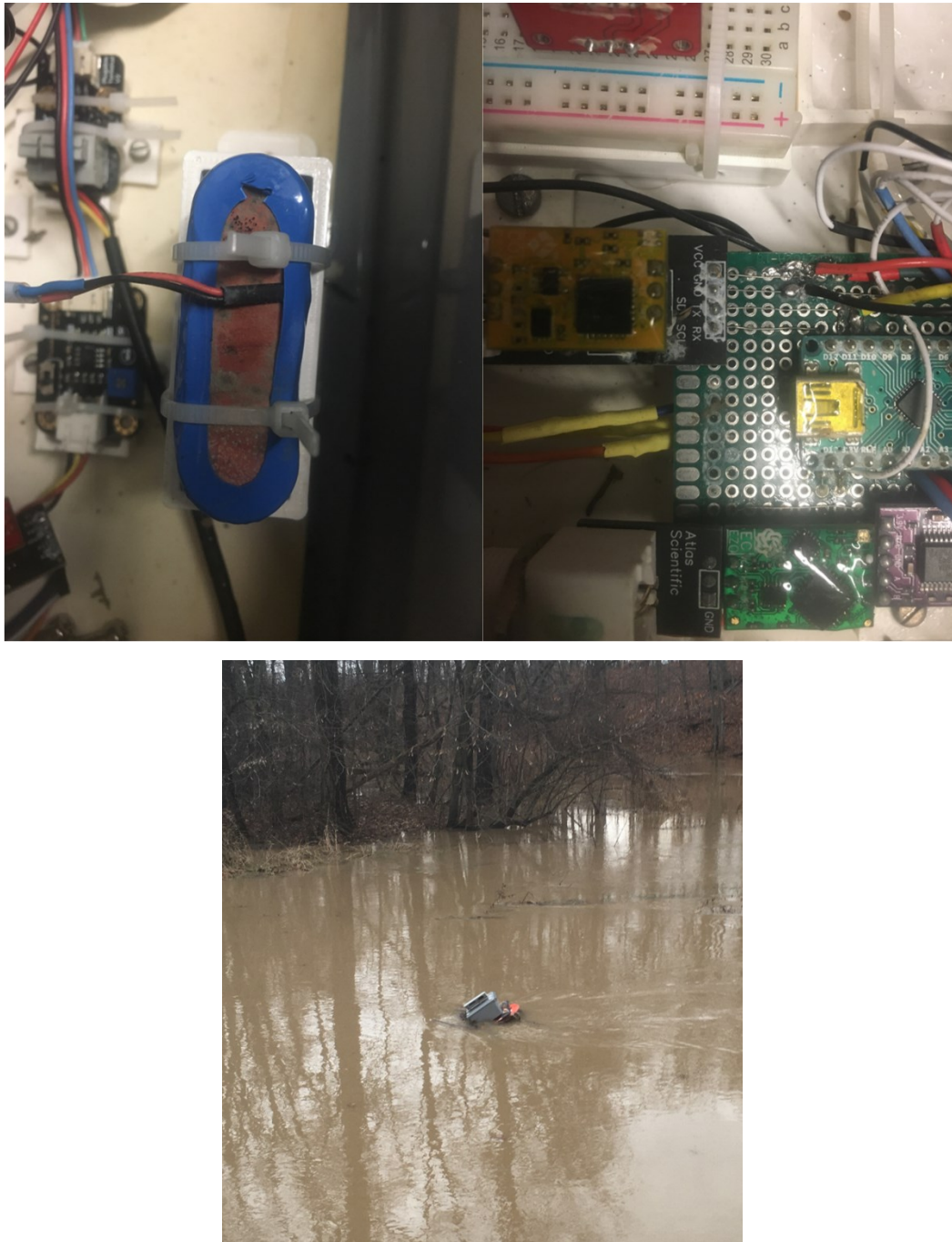


Figure A.11. Component damage due to high humidity conditions within WQMS, high creek flow conditions which may have caused water to seep into the WQMS.

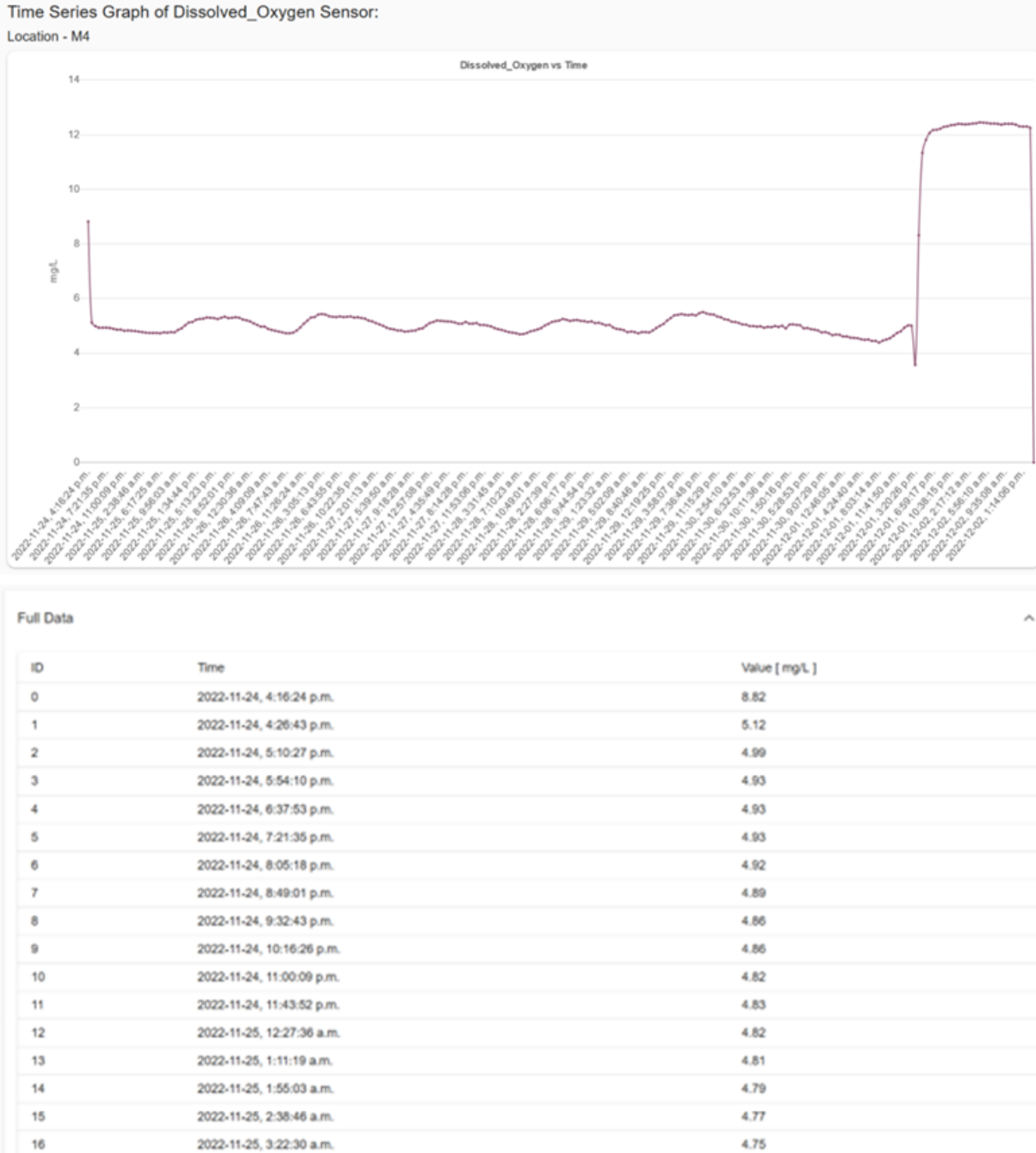


Figure A.12. Example DO data from site M4 over a period from November 24 to December 2, 2022 (top), with a selection of data that can be easily exported for community members of the curious public.

Note that in Figure A.12, the drop in DO on the 24th is caused by installation of the WQMS, and the final 25 hrs of data between December 1st and 2nd were taken after retrieving the WQMS. This shows that the DO probe behaves differently when immersed in water compared to when it is inactive in air. Also note that the O₂ concentration in air is different compared to what would

be expected (275 mg/L at 22°C) due to differences in calibration, as gaseous oxygen probes also use PTFE as a working membrane.

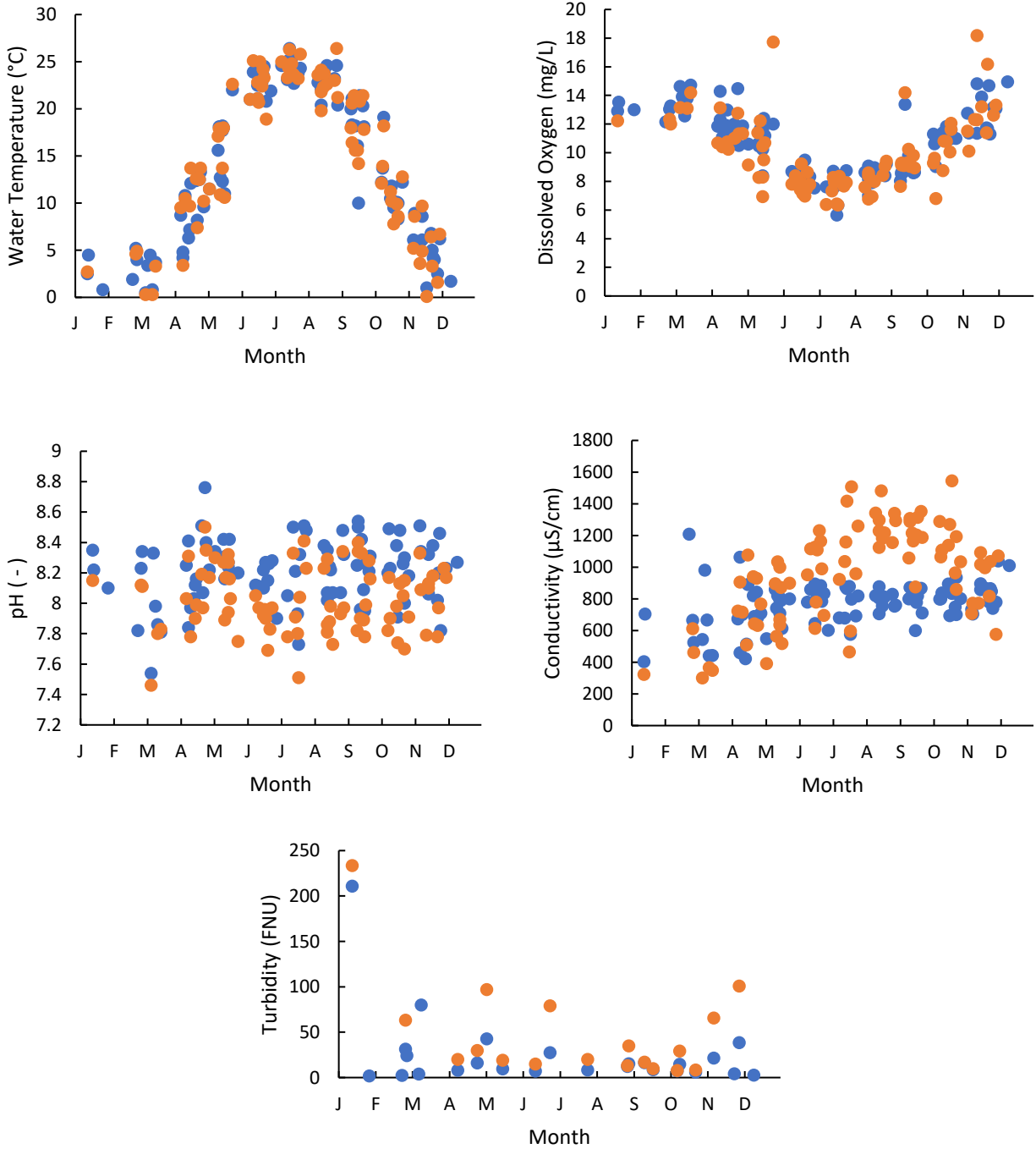


Figure A.13. PWQMN grab sample sites for conductivity, DO, pH, turbidity, and temperature from 2010-2021. McKenzie Creek samples (crossing Haldimand Road 9, MOE ID: 16018412902) are in orange and York samples (at York Bridge, MOE ID: 16018409202) are in blue [1].

The McKenzie sampling station, located on the McKenzie Creek, is located 2.4 km north of the confluence of the McKenzie Creek and Grand River, while the York sampling station, located on the Grand River, is located 300m north of the confluence [2]. Samples were taken from 10 AM to 3 PM, while grab samples in this work were obtained in the late afternoon. Temperature and DO data correlate well. Average pH values are slightly higher in the Grand River (8.20) compared to the McKenzie Creek (8.03). Conductivity data from the McKenzie shows seasonal periodicity, where this is not apparent in the Grand River. Although the McKenzie is smaller, it does not heat up faster than the Grand, so seasonal temperature changes do not play a role in seasonal conductivity change. Increased conductivity is more likely to be derived from increased effects of localized agricultural runoff, given the peak near the end of harvesting season, whereas the Grand River has a much larger volume to mitigate runoff effects. Turbidity data here uses FNU, compared to NTU used elsewhere in this work and are differentiated by the measurement light source. They are not identical but are similar enough for the purposes of this work.

Table A.14. *E. coli* and TCF data obtained from M5. * indicates RDL of 100 CFU/100mL, ** indicates RDL of 2 CFU/100mL.

Units: CFU/100mL	<i>E. coli</i>	TCF	<i>E. coli</i> /TCF
Oct 6*	500	1600	0.31
Oct 20*	300	400	0.75
Nov 17**	32	102	0.31
Dec 1**	38	70	0.54

Table A.15. Anion data obtained from M5. * indicates RDL of 0.05 mg/L, ** indicates RDL of 0.1 mg/L.

Units: mg/L	Nitrate*	Phosphate**	Fluoride*	Chloride**	Nitrite*	Bromide*	Sulfate**
Oct 6	<0.05	<0.1	-	-	-	-	-
Oct 20	<0.05	<0.1	<0.05	39.1	<0.05	<0.05	117
Nov 17	0.17	<0.1	<0.05	36.4	<0.05	<0.05	109
Dec 1	0.58	<0.1	<0.05	41.0	<0.05	<0.05	113

Appendix A.3: Appendix References

- [1] *Provincial (Stream) Water Quality Monitoring Network*, Environmental Monitoring and Reporting Branch. [Online]. Available: <https://data.ontario.ca/dataset/provincial-stream-water-quality-monitoring-network>
- [2] "GRCA Web-GIS Application." Grand River Conservation Authority. <https://maps.grandriver.ca/web-gis/public/> (accessed May 15, 2023).